Jordan Journal of Mechanical and Industrial Engineering (JJMIE)

JJMIE is a high-quality scientific journal devoted to fields of Mechanical and Industrial Engineering. It is published by The Jordanian Ministry of Higher Education and Scientific Research in corporation with the Hashemite University.

SUBMISSION ADDRESS:

Prof. **Mousa S. Mohsen**, Editor-in-Chief
Jordan Journal of Mechanical & Industrial Engineering,
Hashemite University,
PO Box 330127, Zarqa, 13133 , Jordan

E-mail: jjmie@hu.edu.jo

Hashemite Kingdom of Jordan

Hashemite University

Jordan Journal of Mechanical and Industrial Engineering

JJMIE

An International Peer-Reviewed Scientific Journal

http://jjmie.hu.edu.jo/

ISSN 1995-6665

Jordan Journal of Mechanical and Industrial Engineering (JJMIE)

JJMIE is a high-quality scientific journal devoted to fields of Mechanical and Industrial Engineering. It is published by The Jordanian Ministry of Higher Education and Scientific Research in corporation with the Hashemite University.

Intruduction: The Editorial Board is very committed to build the Journal as one of the leading international journals in mechanical and industrial engineering sciences in the next few years. With the support of the Ministry of Higher Education and Scientific Research and Jordanian Universities, it is expected that a heavy resource to be channeled into the Journal to establish its international reputation. The Journal's reputation will be enhanced from arrangements with several organizers of international conferences in publishing selected best papers of the conference proceedings.

Aims and Scope: Jordan Journal of Mechanical and Industrial Engineering (JJMIE) is a refereed international journal to be of interest and use to all those concerned with research in various fields of, or closely related to, mechanical and industrial engineering disciplines. Jordan Journal of Mechanical and Industrial Engineering aims to provide a highly readable and valuable addition to the literature which will serve as an indispensable reference tool for years to come. The coverage of the journal includes all new theoretical and experimental findings in the fields of mechanical and industrial engineering or any closely related fields. The journal also encourages the submission of critical review articles covering advances in recent research of such fields as well as technical notes.

Guide for Authors

Manuscript Submission

High-quality submissions to this new journal are welcome now and manuscripts may be either submitted online or mail.

Online: For online submission upload one copy of the full paper including graphics and all figures at the online submission site, accessed via E-mail: jjmie@hu.edu.jo. The manuscript must be written in MS Word Format. All correspondence, including notification of the Editor's decision and requests for revision, takes place by e-mail and via the Author's homepage, removing the need for a hard-copy paper trail.

By Mail: Manuscripts (1 original and 3 copies) accompanied by a covering letter may be sent to the Editor-in-Chief. However, a copy of the original manuscript, including original figures, and the electronic files should be sent to the Editor-in-Chief. Authors should also submit electronic files on disk (one disk for text material and a separate disk for graphics), retaining a backup copy for reference and safety.

Note that contributions may be either submitted online or sent by mail. Please do NOT submit via both routes. This will cause confusion and may lead to delay in article publication. Online submission is preferred.

Submission address and contact:

Prof. **Mousa S. Mohsen**, Editor-in-Chief
Jordan Journal of Mechanical & Industrial Engineering,
Hashemite University,
PO Box 330127, Zarqa, 13133 , Jordan
E-mail: jjmie@hu.edu.jo

Types of contributions: Original research papers

Corresponding author: Clearly indicate who is responsible for correspondence at all stages of refereeing and publication, including post-publication. Ensure that telephone and fax numbers (with country and area code) are provided in addition to the e-mail address and the complete postal address. Full postal addresses must be given for all co-authors.

Original material: Submission of an article implies that the work described has not been published previously (except in the form of an abstract or as part of a published lecture or academic thesis), that it is not under consideration for publication elsewhere, that its publication is approved by all authors and that, if accepted, it will not be published elsewhere in the same form, in English or in any other language, without the written consent of the Publisher. Authors found to be deliberately contravening the submission guidelines on originality and exclusivity shall not be considered for future publication in this journal.

Supplying Final Accepted Text on Disk: If online submission is not possible: Once the paper has been accepted by the editor, an electronic version of the text should be submitted together with the final hardcopy of the manuscript. The electronic version must match the hardcopy exactly. We accept MS Word format only. Always keep a backup copy of the electronic file for reference and safety. Label the disk with your name. Electronic files can be stored on CD.

Notification: Authors will be notified of the acceptance of their paper by the editor. The Publisher will also send a notification of receipt of the paper in production.

Copyright: All authors must sign the Transfer of Copyright agreement before the article can be published. This transfer agreement enables Jordan Journal of Mechanical and Industrial Engineering to protect the copyrighted material for the authors, but does not relinquish the authors' proprietary rights. The copyright transfer covers the exclusive rights to reproduce and distribute the article, including reprints, photographic reproductions, microfilm or any other reproductions of similar nature and translations.

PDF Proofs: One set of page proofs in PDF format will be sent by e-mail to the corresponding author, to be checked for typesetting/editing. The corrections should be returned within 48 hours. No changes in, or additions to, the accepted (and subsequently edited) manuscript will be allowed at this stage. Proofreading is solely the author's responsibility. Any queries should be answered in full. Please correct factual errors only, or errors introduced by typesetting. Please note that once your paper has been proofed we publish the identical paper online as in print.

Author Benefits

Page charge: Publication in this journal is free of charge.

Free off-prints: Three journal issues of which the article appears in along with twenty-five off-prints will be supplied free of charge to the corresponding author. Corresponding authors will be given the choice to buy extra off-prints before printing of the article.

Manuscript Preparation:

General: Editors reserve the right to adjust style to certain standards of uniformity. Original manuscripts are discarded after publication unless the Publisher is asked to return original material after use. If online submission is not possible, an electronic copy of the manuscript on disk should accompany the final accepted hardcopy version. Please use MS Word for the text of your manuscript.

Structure: Follow this order when typing manuscripts: Title, Authors, Affiliations, Abstract, Keywords, Introduction, Main text, Conclusions, Acknowledgements, Appendix, References, Figure Captions, Figures and then Tables. For submission in hardcopy, do not import figures into the text - see Illustrations. For online submission, please supply figures imported into the text AND also separately as original graphics files. Collate acknowledgements in a separate section at the end of the article and do not include them on the title page, as a footnote to the title or otherwise.

Text Layout: Use double spacing and wide (3 cm) margins. Ensure that each new paragraph is clearly indicated. Present tables and figure legends on separate pages at the end of the manuscript. If possible, consult a recent issue of the journal to become familiar with layout and conventions. All footnotes (except for table and corresponding author footnotes) should be identified with superscript Arabic numbers. To conserve space, authors are requested to mark the less important parts of the paper (such as records of experimental results) for printing in smaller type. For long papers (more that 4000 words) sections which could be deleted without destroying either the sense or the continuity of the paper should be indicated as a guide for the editor. Nomenclature should conform to that most frequently used in the scientific field concerned. Number all pages consecutively; use 12 or 10 pt font size and standard fonts. If submitting in hardcopy, print the entire manuscript on one side of the paper only.

Corresponding author: Clearly indicate who is responsible for correspondence at all stages of refereeing and publication, including post-publication. The corresponding author should be identified with an asterisk and footnote. Ensure that telephone and fax numbers (with country and area code) are provided in addition to the e-mail address and the complete postal address. Full postal addresses must be given for all co-authors. Please consult a recent journal paper for style if possible.

Abstract: A self-contained abstract outlining in a single paragraph the aims, scope and conclusions of the paper must be supplied.

Keywords: Immediately after the abstract, provide a maximum of six keywords (avoid, for example, 'and', 'of'). Be sparing with abbreviations: only abbreviations firmly established in the field may be eligible.

Symbols: All Greek letters and unusual symbols should be identified by name in the margin, the first time they are used.

Units: Follow internationally accepted rules and conventions: use the international system of units (SI). If other quantities are mentioned, give their equivalent in SI.

Maths: Number consecutively any equations that have to be displayed separately from the text (if referred to explicitly in the text).

References: All publications cited in the text should be presented in a list of references following the text of the manuscript.

Text: Indicate references by number(s) in square brackets in line with the text. The actual authors can be referred to, but the reference number(s) must always be given.

List: Number the references (numbers in square brackets) in the list in the order in which they appear in the text.

Examples:

Reference to a journal publication:

[1] M.S. Mohsen, B.A. Akash, "Evaluation of domestic solar water heating system in Jordan using analytic hierarchy process". Energy Conversion & Management, Vol. 38, No. 9, 1997, 1815-1822.

Reference to a book:

[2] Strunk Jr W, White EB. The elements of style. 3rd ed. New York: Macmillan; 1979.

Reference to a conference proceeding:

[3] B. Akash, S. Odeh, S. Nijmeh, "Modeling of solar-assisted double-tube evaporator heat pump system under local climate conditions". 5th Jordanian International Mechanical Engineering Conference, Amman, Jordan, 2004.

Reference to a chapter in an edited book:

[4] Mettam GR, Adams LB. How to prepare an electronic version of your article. In: Jones BS, Smith RZ, editors. Introduction to the electronic age, New York: E-Publishing Inc; 1999, p. 281-304

Free Online Color: If, together with your accepted article, you submit usable color and black/white figures then the journal will ensure that these figures will appear in color on the journal website electronic version.

Tables: Tables should be numbered consecutively and given suitable captions and each table should begin on a new page. No vertical rules should be used. Tables should not unnecessarily duplicate results presented elsewhere in the manuscript (for example, in graphs). Footnotes to tables should be typed below the table and should be referred to by superscript lowercase letters.

JJMIE

Jordan Journal of Mechanical and Industrial Engineering

JJMIE

Volume 2, Number 4, December. 2008
ISSN 1995-6665
Pages 169 - 174

Jordan Journal of Mechanical and Industrial Engineering

Improving the Performance of Two Stroke Spark Ignition Engine by Direct Electronic CNG Injection

S. Kumarappa [a,*], G.P. Prabhukumar [b]

[a] Bapuji Institute of Engineering and Technology, Davangere, Karnataka, India
[b] Acharya Institute of Technology, Bangalore, Karnataka, India

Abstract

Two stroke spark ignition engines have high exhaust emissions and low brake thermal efficiency due to the short circuiting losses and incomplete combustion, which occur during idling and at part load operating conditions. To eliminate the short circuiting losses, direct injection has been developed. Electronic CNG injection system was developed for better fuel economy and reduced emissions. The fuel and time maps were generated for the various operating conditions of the engine using an electronic system. For the mapping, the visualization tool was used to estimate the fuel injection time and delivery quantity for required running conditions of the engine. Experiments were carried out at the constant speed of 3500 rpm with a compression ratio of 12:1. The performance and emission characteristics of direct CNG injection system and carbureted engine are described. The above studies indicate the improvement in brake thermal efficiency from 15.2% to 24.3%. This is mainly due to significant reduction in short circuit loss of fresh charge and precise control of air fuel ratio. The pollution levels of HC and CO were reduced by 79.3% and 94.5% respectively compared to a conventional carbureted engine.

Keywords: Two-stroke spark ignition engine; direct injection; CNG; microcontroller;

1. Introduction

In developed and developing countries considerable emphasis is being laid on the minimization of pollutants from internal combustion engines. A two-stroke cycle engine produces a considerable amount of pollutants when gasoline is used as a fuel due to short-circuiting. These pollutants, which include unburnt hydrocarbons and carbon monoxide, which are harmful to beings. There is a strong need to develop a kind of new technology which could minimize pollution from these engines. Direct fuel injection has been demonstrated to significantly reduce unburned hydrocarbon emissions by timing the injection of fuel in such way as to prevent the escape of unburned fuel from the exhaust port during the scavenging process.

The increased use of petroleum fuels by automobiles has not only caused fuel scarcities, price hikes, higher import bills, and economic imbalance but also causes health hazards due to its toxic emissions. Conventional fuels used in automobiles emit toxic pollutants, which cause asthma, chronic cough, skin degradation, breathlessness, eye and throat problems, and even cancer.

In recent years, environmental improvement (CO_2, NO_x and Ozone reduction) and energy issues have become more and more important in worldwide concerns. Natural gas is a good alternative fuel to improve these problems because of its abundant availability and clean burning characteristics.

1.1. The objectives of present study are:

To compare the performance of a carbureted and injected engine at constant speed.

Direct injection system was developed which eliminates short circuiting losses completely and injection timing was optimized for the best engine performance and lower emissions.

In a lean burn engine, air fuel ratio is extremely critical. Operation near the lean mixture limit is necessary to obtain the lowest possible emission and the best fuel economy. However, near the lean limit, a slight error in air-fuel ratio can drive the engine to misfire. This condition causes drastic increase in hydrocarbon emission; engine roughness and poor throttle response [2-4]. A reliable electronic gaseous fuel injection system was designed and built in order to control the engine and also for the evaluation of control strategies. The electronic control unit is used to estimate the pulse width of the signal that would actuate the fuel injector and the start of fuel injection. The experiments were carried out on the engine using state-of-art instrumentation.

* Corresponding author. e-mail: kumarappa_sdvg@yahoo.com

2. Fuel Induction Techniques

The performance characteristics of an engine and the concentration level of the exhaust emissions depend, to a large extent, on the combustion pattern. It directly depends on fuel system, which provides an appropriate mixture of fuel and air to the engine at the appropriate point in the cycle. The fuel air mixture must be in right proportion as per the condition of the speed and load on the engine. The overall engine behavior depends upon the fuel induction mechanism. Introduction of a CNG kit to the existing gasoline engine hardware does not involve any substantial modifications except inducting the mixture into the intake manifold. However, in spite of the excellent characteristics and various advantages of CNG as a fuel in vehicles, it has certain problems, when used in vehicles, like backfiring during suction, knocking at higher compression ratio with advanced spark timing; these problems are due to inappropriate technology used for the formation of the mixture.

In consideration of the inherent constraints in the design of carburetor, the engine manufacturers and automobile industries now are switching over to fuel injection system. The mode of fuel injection from an injector plays a critical role in determining the performance characteristics of an engine. The lean burn for the engine operation can be easily achieved with this technique. Keeping in view the requirement of the CNG fuel, an electronic direct CNG injection system was designed and developed in the present experimental work.

3. New Direct CNG Injection System

The short-circuiting losses of the two-stroke engine can be eliminated by directly injecting the fuel into the cylinder after the closure of the exhaust port. This requires the development of an electronically controlled direct fuel injection system fitted with suitable modification to the engine.

The Figure 1 shows the cylinder wall injection, with an injection nozzle installed in the cylinder wall. The injection nozzle was tilted by 40^0 from the horizontal and injects the fuel upward, different from the method of injecting the fuel at a right angle to the cylinder axis as employed by Vieillendent [5], Blair [6], etc. The spray would be concentrated on the upper position of the combustion chamber near the spark plug. The location of the nozzle on the cylinder was determined from the pressure crank angle diagram corresponding to an in-cylinder pressure of 2 bar attained after the closure of the exhaust port. Corresponding to this crank angle a hole is drilled in the cylinder bore at an inclination of 40^0 from horizontal. A water-cooled adaptor was designed for cooling the injector to prevent excess heating of the injector.

4. Experimental Test Setup

A 98 cc, two-stroke spark ignition engine was used in this study. Table 1 gives the engine specification of the engine.

Table 1 : Specifications of the engine

Make	*Yamaha*
Bore	*50 mm*
Stroke	*50 mm*
Max. Power	*8 kW @ 7500 rpm*
Displacement	*98 cc*
Ignition timing	*30^0 BTDC*

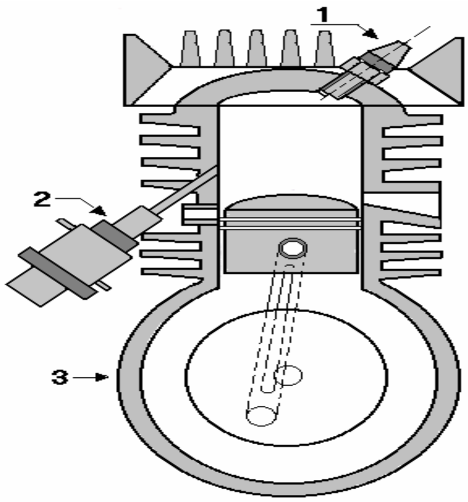

1. Spark plug,
2. Electronic CNG injector with water-cooled adaptor,
3. Crankcase.

Figure 1: Schematic diagram of direct cylinder wall injection system

The Figure 2 shows the schematic diagram of experimental setup and the engine instrumentation. The fuel system consists of high-pressure storage cylinders with a filling pressure of about 22 MPa, a regulator to reduce the line pressure to 200 kPa and a high-pressure line for connecting the cylinder to the regulator. An injection system controller was used to control the pulse width of the injector. The engine was connected to brake dynamometer for loading purposes. Fuel consumption is measured using weighing machine and rotameter. Air consumption is measured by an air flow meter.

A pressure transducer in conjunction with a charge amplifier was used to measure the cylinder pressure. The transducer was mounted in the cylinder head. Signals of crankshaft angle were derived from a shaft encoder rigidly attached to the engine crankshaft. The top dead center (TDC) signal of the encoder was checked with the engine TDC, under dynamic conditions. The encoder provides the necessary signals for the data acquisition system to collect cylinder pressure at every degree during engine cycle. The exhaust emissions of HC and CO are measured with an exhaust gas analyzer. The performance testing of the engine is carried out at constant speed.

5. Results

5.1. Performance of Direct CNG Injection

The performance of the direct injection system was tested at 3500 rpm. The injection timing was initially set such that the start of injection takes place immediately after the closure of exhaust port (250^0 ATDC). The crank position sensor sends a signal corresponding to the closure of the exhaust port and then the injection is immediately started. The injection timing was optimized for the best engine performance and emissions. Any further advancement of the injection timing above the optimum injection angle results in poor performance and higher emissions as short-circuiting losses predominate. The performance of direct injection system with the optimized injection advance angle is compared with carbureted engine at a compression ratio of 12:1.

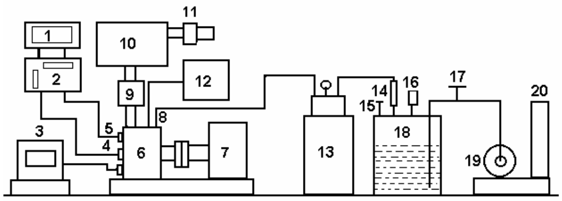

1. Computer *2. Signal analyzer*
3. Exhaust gas analyzer *4. TDC pickup*
5. Pressure pickup *6. Engine*
7. Dynamometer *8. Gas injector*
9. Air filter *10. Surge tank*
11. Air flow meter *12. Fuel injection system*
13. Stabilizing tank *14. Gas rotameter*
15. Safety valve *16. Pressure gauge*
17. Expansion valve *18. Flame trap*
19. CNG Cylinder *20. Weighing machine*

Figure 2: Schematic diagram of experimental setup

5.2. Brake Thermal Efficiency

The Figure 3 shows the variation of brake thermal efficiency with brake mean effective pressure (BMEP) at 3500 rpm. The maximum brake thermal efficiency of the direct injection mode (DI) is 24.3% at BMEP of 3.5 bar compared to carbureted engine mode (CE) is 15.2% at BMEP of 2.8 bar. This is due to reduction in short-circuiting losses and increase in air–fuel ratio. This indicates that the engine can operate in leaner air-fuel ratios without loss of power. This is achieved because of the precise timing and metering of the fuel by the microcontroller fuel injection system.

Figure 4 shows the variation of brake thermal efficiency with equivalence ratio. The maximum brake thermal efficiency of direct injection mode is 24.3% at an equivalence ratio of 0.88 where as in carbureted mode is 15.2% at an equivalence ratio of 0.99. Brake thermal efficiency increases from lean to rich and starts decreasing at engine rich mixtures. For the same equivalence ratio, the carbureted engine gives lesser brake thermal efficiency compared to the injected engine. This is due to incomplete combustion of the charge due to mixture limit inside the combustion chamber at a given compression ratio. Hence, the amount of fuel charge to give the mechanical power gets reduced and thus reduces the brake thermal efficiency.

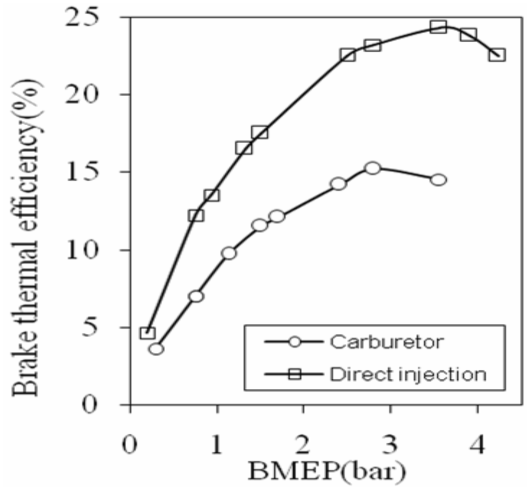

Figure 3: Variation of break thermal efficiency with BMEP at 3500 rpm

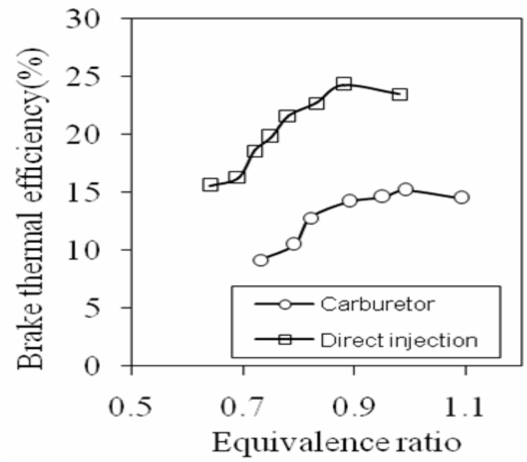

Figure 4: Variation of break thermal efficiency with equivalence ratio at 3500 rpm

5.3. Carbon Monoxide Emissions

The Figure 5 shows the variation of CO with equivalence ratio at 3500 rpm. Carbon monoxide being the product of incomplete combustion, therefore it is totally dependant on the air fuel ratio. Owing to the gaseous nature of compressed natural gas, it easily mixes with air because of diffusivity at high pressure. CO emissions with lean mixture are reduced because of CO getting converted into CO_2 with surplus amount of oxygen. In injection mode, significant lower concentration of CO is observed over entire range of operation.

The maximum reduction of CO emissions in direct injection system compared to carbureted engine is 94.5% at an equivalence ratio of 1.2. This reduction is due to leaner air fuel ratio mixtures and elimination of short circuiting losses.

5.4. Hydrocarbon Emissions

The Figure 6 shows the variation of HC emissions with equivalence ratio at 3500 rpm. The main source of hydrocarbons is due to the composition and patchy combustion occurring due to uneven mixture formation.

The maximum reduction of HC emissions in direct injection system compared to carbureted engine is 79.3% at an equivalence ratio of 0.63. This reduction is due to elimination of short-circuiting losses and precise control of air fuel ratio.

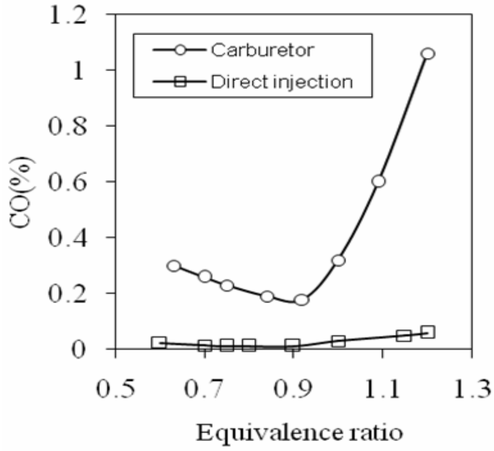

Figure 5: Variation of CO emissions with equivalence ratio at 3500 rpm

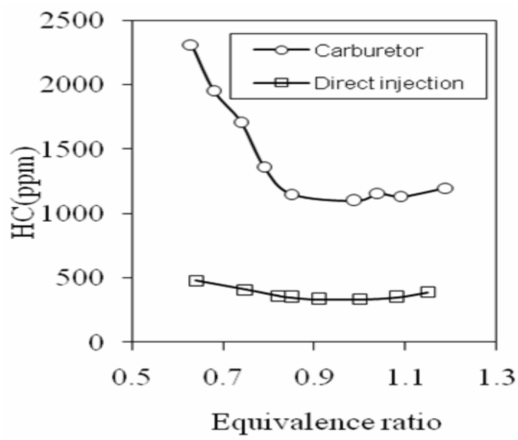

Figure 6: Variation of HC emissions with equivalence ratio at 3500 rpm

5.5. Coefficient of Variation of Peak Pressure

Figure 7 shows the variation of C.O.V. of peak pressure with BMEP for direct injection system and carbureted engine. The C.O.V of peak pressure of the direct injection system is lower than the carbureted engine at tested speed and loads. The reduction in C.O.V. peak pressure of the direct injection system compared to carbureted engine at minimum loads(BMEP of 0.75 bar) is 81.25%, whereas at maximum loads(BMEP of 4 bar), the reduction of C.O.V of peak pressure is 83.8%.

5.6. Coefficient of Variation of Indicated Mean Effective Pressure

Figure 8 shows the variation of C.O.V. of IMEP with BMEP for direct injection system and carbureted engine. The C.O.V of IMEP of the direct injection system is lower than the carbureted engine at tested speed and loads. The reduction in C.O.V. of IMEP of the direct injection system compared to carbureted engine at minimum loads (BMEP of 0.75 bar) is 73.9%, whereas at maximum loads (BMEP of 4 bar), the reduction of C.O.V of IMEP is 71.4%. At light loads, the C.O.V of IMEP of engine combustion increases rapidly. This reveals that the phenomena of mixture misfiring at light loads. The comparison between the C.O.V of IMEP for carburetor type engine and direct injection engine indicates that the fuel injected CNG engine is much more stable engine due to the better control of air fuel ratio.

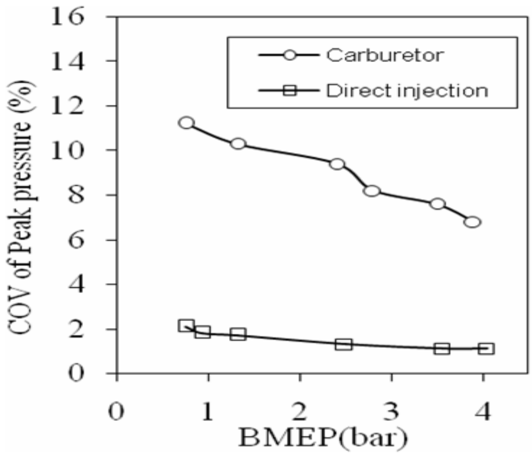

Figure 7: Variation of COV of peak pressure with BMEP at 3500 rpm

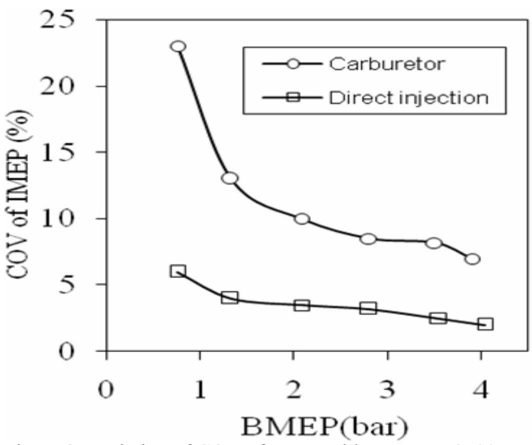

Figure 8: Variation of COV of IMEP with BMEP at 3500 rpm

5.7. Rate of Heat Release

The rate of heat release of the direct injection system is higher than the carbureted engine. The maximum increase in the rate of heat release compared to the carbureted engine as shown in Figure 9.

The increase in rate of heat release of the direct injection engine compared to carbureted engine is 38.1% at 3500 rpm. The increase in rate of heat release indicate that the combustion in the direct injection is faster than the carbureted engine due to the combustion of the relatively lean air fuel mixtures and reduction of short-circuiting loss of fresh charge through the exhaust port.

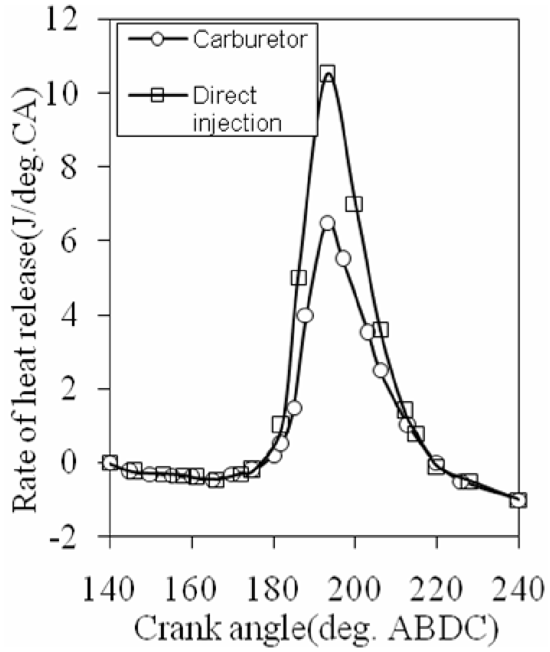

Figure 9: Variation of heat release with crank angle at 3500 rpm

6. Effect of Fuel Injection Timing on Engine Load

Fuel injection timing has a strong influence on the mixing process. In homogeneity in the cylinder charge creates limitations in the optimization of natural gas engines. It has been demonstrated, that poor mixture distribution increases the level of cycle-to-cycle combustion variability [7-8]. Mixture formation in a direct injected gasoline fueled engine is largely dependent on the atomization and evaporation of the fuel. While this complexity is not present in gaseous-fueled engines since the mixing process is far from trivial. Due to the lower momentum of injected fuel, the degree of mixing in the region of the jet is lower in the gaseous case than in the liquid case. For this reason, it is important to utilize the timing of the fuel injection event to optimize the mixing process [9].

In the present direct CNG injection system, the injection timing was optimized for the best engine performance and low emissions. Any further advancement of the injection timing above the optimum injection angle results in poor performance and higher emissions as short-circuiting losses predominate. The software of the control system was modified so that the injection timing and injection duration could be varied from TDC to any crank angle.

The Figure 10 shows that the performance of the direct injection with the injection advance angle of 250^0, 237^0 and, 233^0 after top dead center (ATDC). The maximum brake thermal efficiency with 250^0 advance angle is 20% at BMEP of 3.36 bar. When injection is advanced gradually, the performance of the engine was found to improve. At 237^0 injection advance angle, the maximum brake thermal efficiency is 24.3% at BMEP of 3.55 bar. This is due to increase in the time available for mixture formation. Any further increase in the injection advance angle of 233^0 results in reduction in maximum brake thermal efficiency is 22.1% at BMEP of 3.45 bar. This is due to the fact that the exhaust gases may carry a small fraction of injected fuel while scavenging.

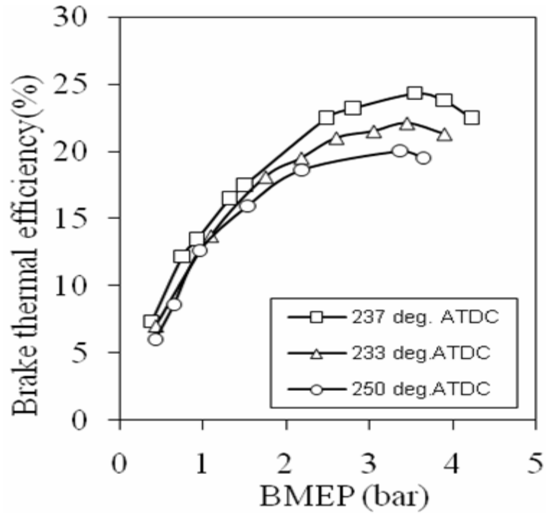

Figure 10: Variation of break thermal efficiency with BMEP at 3500 rpm

Variation of CO and HC emissions with equivalence ratio for different injection advance angle of 250^0, 237^0, and 233^0 ATDC are shown in Figures 11 and 12.

The CO and HC emissions are higher for 250^0 advance angle due to the reduction in mixture formation time and CO and HC emissions are higher for injection advance angle of 233^0 due to short-circuiting. CO and HC emissions are minimum with injection advance angle of 237^0. Hence, the optimum injection advance angle is 237^0 at 3500 rpm.

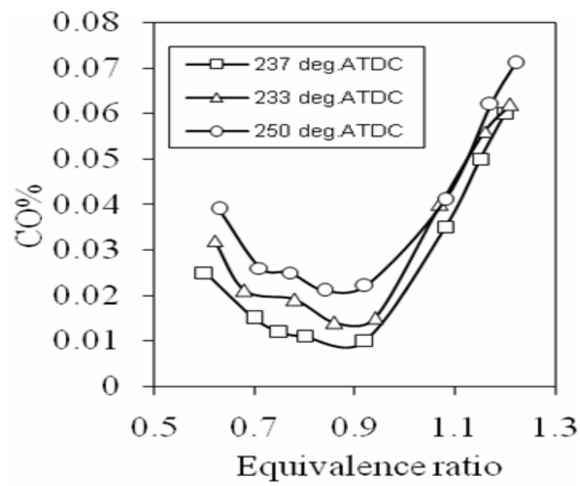

Figure 11: Variation of CO emissions with equivalence ratio at 3500 rpm

7. Conclusions

The following are the important conclusions based on the experimental analysis of the electronic CNG injected two-stroke spark ignition engine.

1. The maximum brake thermal efficiency of the direct injection engine is 9.1% more than the carbureted engine at 3500 rpm.

2. There is 79.3% reduction in the unburnt hydrocarbon with electronic fuel injection at 3500 rpm.
3. The CO emission is 94.5% less in the injected engine compared to the carbureted engine at 3500 rpm.
4. The maximum value of brake thermal efficiency of 24.3% is achieved at compression ratio of 12 with a spark timing of 30 ^{0} before top dead center.
5. With the on-line injection timing control the injection advance angle is optimized to 237^0 after top dead center at 3500 rpm.

References

[1] N.John Beck, W.P.Johnson, and S.H. Patterson, "Electronic fuel injection for two-stroke cycle gasoline engines". SAE paper No. 861242

[2] Cornel Stan, Jean-Louis Lefebvre, "Development of a direct injection concept for two wheelers equipped with two stroke engines". SAE paper No. 1999-01-1248.

[3] M.J. Pipho, D.B.Kiltelson, "Closed loop digital electronic of diesel engine timing". SAE paper No. 830579.

[4] P. William Johnson, P. Gregory Wiedemeier, Kresimir gebert, "Electronic direct fuel injection for two stroke engines". SAE paper No. 1999-01-3312.

[5] R.Douglas. G.P.Blair, "Fuel injection of a two stroke cycle spark ignition engine". SAE paper No. 820952.

[6] Edmond Vieillednt. "Low pressure electronic fuel injection system for two stroke engines". SAE paper No. 780767.

[7] M. Gupta, S.R. Bell, S.T. Tillman, "An investigation of lean combustion in a natural gas fueled spark ignited engine". Journal of energy resources technology, June 1996.

[8] David gimbres, Jacques boree, Rudy bazile, Georges charnay, "Effect of air pulsed flow on the mixture preparation for the optimization of Natural gas SI engine". SAE paper No. 1999-01-2905.

[9] Joel Hilter, Mohammed Samim**,** "The impact of injection timing on In-cylinder fuel distribution in a natural gas powered engine". SAE paper No. 971708.

JJMIE

Volume 2, Number 4, December. 2008
ISSN 1995-6665
Pages 175 - 182

Jordan Journal of Mechanical and Industrial Engineering

Fuzzy Genetic Prioritization in Multi-Criteria Decision Problems

Ahmed Farouk Abdul Moneim *

College of Engineering, Arab Academy of Science and Technology, Egypt

Abstract

A new method is presented to derive a priority vector $W = (w_1, w_2, \ldots w_n)^T$ defining the ranking of competing alternatives and factors or criteria from fuzzy pairwise judgments. The pairwise comparisons are accepted as linguistic evaluations or assessments expressing relative importance of pairs (i , j) .These evaluations are quantified in the form of trapezoidal fuzzy numbers expressed as quadruples (a_{ij}, b_{ij}, c_{ij}, d_{ij}) in order to model the vagueness and imprecision in linguistic evaluations. The problem of finding components of priority vector W, given n (n-1) / 2 quadruples (a_{ij}, b_{ij}, c_{ij}, d_{ij}) is formulated in an optimization model with a newly introduced objective function. The problem is solved by means of a genetic algorithm. The complications and inappropriateness in finding inconsistencies of fuzzy pairwise comparisons, as presented in existing literatures, are treated and resolved in the present work by introducing ratios of inconsistency index to index of inconsistency of random fuzzy comparisons. The proposed method is illustrated by numerical examples and compared with some of the existing methods in literatures.

Keywords: priority vector, trapezoidal fuzzy numbers, genetic algorithm, pairwise comparisons, inconsistency ratio.

Nomenclature

a_{ij}, b_{ij}, c_{ij}, d_{ij}	: a trapezoidal fuzzy number expressing linguistic pair-wise Judgment relating alternatives i to j
EV i j	: pair wise comparison judgments comparing i with j.
ICI	: Inconsistency Index
ICR	: Inconsistency Ratio
l i j, m i j, u i j ,	: triangular fuzzy number expressing linguistic pair-wise Judgment relating alternatives i to j
n	: size of the pairwise comparisons (reciprocal) matrix
RI	: Random Index
W	: (w1 , w2 , …. w n)T a priority vector giving weight of importance w i to each

Competing Alternative

δ_A	: Indicator function
$\delta_A = 1$	: when event A occurs
$\delta_A = 0$	: otherwise
λ	: a variable denoting to the degree of membership of the ratio w_i / w_j
$\mu_{ij}(w_i / w_j)$	: membership functions of fuzzy ratios w_i / w_j of relative importance

1. Introduction

Selecting the optimum alternative in multi-criteria decision problems is one of the most crucial challenges facing decision makers in engineering and management in different industries and businesses. These challenges are:

1. The natural limitations of human capability to compare or to decide on among more than two factors or alternatives. It becomes more intricate if the comparison is made on the basis of multiple criteria.
2. To capture and assess possible inconsistencies in comparison judgments of more than two factors or alternatives for the purpose of discarding heavily inconsistent judgments.
3. The uncertainty, imprecision and vagueness of human comparison judgments.

Over the last thirty years, numerous valuable contributions to the study and analysis of these problems were elaborated. These endeavors started with the development of Analytical Hierarchy Process (AHP) by T.L. Saaty [12] as a mathematical model built to derive priority vectors, which arrange competing alternatives, factors and/or criteria from pair-wise comparison judgments. The process of deriving an analytical hierarchy starts usually with forming a pair-wise comparison matrix with elements a_{ij} $(i < j)$ carrying values of relative importance of alternative (factor, criterion) ***i*** as compared to alternative (factor, criterion) ***j***. The number of elements necessary and sufficient to form a pairwise comparison matrix of size ***n*** is equal to *n (n-1) / 2,* since elements a_{ij} equal to $1/a_{ji}$.

* Corresponding author. e-mail: mail@ahmedfarouk.net

AHP uses a 9 point scale of importance in finding a_{ij}. After building a reciprocal matrix, AHP proceeds further to show that priority vector $W = (w_1, w_2, \ldots w_n)^T$ is the principal eigenvector of the reciprocal matrix. The corresponding Eigen value is shown to be equal to ***n*** in case of perfectly consistent pair-wise comparison judgments.

For nearly consistent and inconsistent judgments, Eigen values are larger than ***n.*** Other methods of deriving priorities are considered in several literatures. Direct Least Square (DLS) method [5] and Logarithmic Least Square method (LLS) [6] formulated the problem of deriving priorities in the form of nonlinear programs. DLS and LLS methods have drawbacks - they have multiple solutions, and they lack explicit measures of inconsistency of pair-wise comparison judgments similar to that clearly adopted in the AHP.

The possibility of having inconsistent judgments is a pivotal issue calling for serious concerns since the validity and the credibility of prioritization are, to a great extent, dependant on consistency of decision maker's judgments. Decision makers, usually, express their relative evaluations linguistically rather than in exact numbers given by a nine-point scale in the standard AHP. Linguistic evaluations such as: extremely important, moderately important and more or less of the same importance are characterized by inherent uncertainty, imprecision, and vagueness. T. L. Saaty and L. Vargas [13] treated the problem of uncertainty and its effect on the stability of rank order of competing alternatives. They considered pair-wise comparison estimations and the resulting priorities as random variables with given probability distributions. However, these quantities are extremely subjective; and differ from person to another and therefore they cannot be considered random, and cannot be treated statistically by collecting data and deriving probability distributions describing the behavior of their populations.

Fuzzy numbers are considered as the most appropriate model to express uncertainty, imprecision, and vagueness of decision makers' judgments. First approaches to solving the problem of fuzzy prioritization are given in Van Laarhoven et al [14], J. Buckley [2], C. Boender et al [1] and others.

These approaches followed similar procedures as adopted in the standard Eigen Vector method developed by Saaty [12] in the standard AHP. However, performing multiple arithmetic operations such as addition, multiplication, and division on fuzzy numbers result in fuzzy priorities with wide spreads due to propagation of fuzziness. Obtained fuzzy priorities have almost no practical meaning and sometimes they are irrational (Mikhailov [10]). Researches who tried to follow similar procedures as in standard AHP fit in the work of D.Y. Chang [4].

Chang determined crisp priority vector by performing fuzzy ordering and evaluating the truth value of the assertion that a fuzzy number I is greater than fuzzy number J. The error in this approach is that components of a priority vector may have zero values, which may result in infinite relative importance. This is in a total contradiction with assumed finite scale of relative importance upon which the problem is formulated and solved. Chang's approach does not permit evaluations of inconsistencies of pair-wise judgments. This is why Erensal et al [7] did not detect this high inconsistency; and proceeded to find a hierarchy; and reached to a conclusion which is naturally questionable. To overcome such complications, Mikhailov [10] proposed two approaches: 1) Fuzzy Preference Programming (FPP) and 2) Modified Fuzzy Preference Programming (MFPP). In the first approach (FPP), the defuzzification technique known as α – cuts is used. Crisp priorities rather than fuzzy priorities are derived from interval judgments corresponding to different α – cut levels. Priorities of the same alternative (factor or criterion) at different α – cut levels are then aggregated to obtain resultant priority. In the second approach (MFPP), a nonlinear optimization model has been obtained, and thereby avoiding the need for using α – cuts which requires a great deal of computations. The MFPP model formulates the problem in a nonlinear program given as follows:

Maximize λ Subject to:

$$\left(m_{ij} - l_{ij}\right)\lambda\, w_j - w_i + l_{ij} w_j \le 0$$
$$\left(u_{ij} - m_{ij}\right)\lambda\, w_j + w_i - u_{ij} w_j \le 0$$
$$\sum_{i=1}^{n} w_i = 1 \tag{1}$$

(i = 1, 2,…..*n*-1), (j = 2,3,……*n*)

The optimum solution of the above nonlinear program (1) is a vector W*, represents the optimum priority vector that leads to a maximum possible degree of membership λ*. As indicated by L. Mikhailov [10], λ* is the degree of satisfaction and is a natural indicator of the inconsistency of decision makers' judgments. But however, since λ* may accept negative values as well as positive values, it becomes inappropriate to act as a natural indicator of the inconsistency and to measure the degree of satisfaction. In order to render λ* positive for inconsistent ratios as well, Mikhailov proposed to introduce tolerance parameters - thus complicating problem.

The rationality and tangibility of inconsistency ratio (ICR) as adopted by T.L. Saaty in the standard AHP disappear when replaced by the indicator λ. The absence of a reference to measure relatively how severe inconsistency is in pair-wise comparisons adds to the inappropriateness of λ. The formulation in (1) is a nonlinear program which can be solved numerically by commercial software such as "Lingo" with declaration of λ as an unrestricted variable. But however this formulation is not amenable to direct application of nontraditional optimization techniques, for instance, Genetic Algorithms since the objective (fitness) function λ is an implicit function of the decision variables (w_1 , w_2 , …. w_n). Recently, these nontraditional optimization techniques, like Genetic Algorithms, are widely used because of their simplicity, ease of their implementations, capability to deal with nonlinearities, scalability, and their proven validity. The present work is mainly concerned with overcoming the above-mentioned complications and shortcomings in deriving priority vectors from fuzzy pair-wise comparison judgments. This, in principle, will be accomplished by:

1. Reformulating the problem by introducing an explicit objective function and using trapezoidal fuzzy numbers.
2. Solving the reformulated problem by use of one of the most powerful search techniques- Genetic Algorithms.
3. Determining inconsistency index RI for different sizes of pair-wise comparisons matrices.

Reformulating the problem enables the writer to restore back the concept of inconsistency ratio *ICR* with reference to inconsistencies of random fuzzy pair wise comparisons.

2. Problem Statement and Mathematical Formulation

Given **n (n-1)/ 2** pair-wise comparison judgments EV_{ij} of the relative importance of n alternatives, factors or criteria named afterwards as factors. The pair-wise comparison judgments are linguistic. It is required, at first, to prioritize these n factors and determine priority vector $W(w_1, w_2, \ldots w_n)^T$ and then to evaluate the relative inconsistency ICR of judgments of each decision maker (DM).

2.1. Modeling of Linguistic Judgments

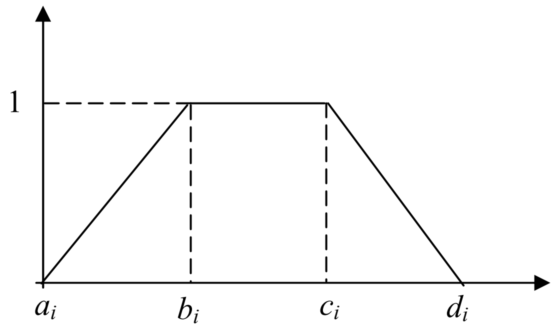

Figure 1: A membership function of a trapezoidal fuzzy number

Linguistic evaluations are usually characterized by their vagueness, imprecision, and uncertainty. They cannot be expressed by crisp numbers as already adopted in standard AHP. Random numbers are also not the proper model because of subjectivity of judgments and absence of statistical data necessary to derive probability distributions describing uncertainty. Fuzzy numbers are the most appropriate model to quantify linguistic judgments. Quantification of linguistic judgments is necessary for proceeding further with the solution of the stated problem and finding the weights w_i of the n competing factors. Fuzzy numbers are normal convex fuzzy sets first introduced by L. Zadeh [15]. Membership functions are used to express the degree of belonging of each element to the fuzzy set. Membership functions of fuzzy numbers may be taken as triangular or trapezoidal. In the present work, trapezoidal membership functions are considered as shown in Figure 1 - since triangular are special cases of the trapezoidal. Usually, trapezoidal fuzzy numbers are given in the form of quadruples $EV_{ij}\,(a_{ij}, b_{ij}, c_{ij}, d_{ij})$. EV_{ij} is evaluating the importance of factor *i* relative to factor *j* as judged by a decision maker *DM*. A scale quantifying linguistic judgments into trapezoidal fuzzy numbers is given in the following table 1.

Table 1: Scale translating linguistic judgments into fuzzy numbers

Linguistic judgments When i compared with j	Fuzzy numbers			
	a_{ij}	b_{ij}	c_{ij}	d_{ij}
Extremely Important	7	8	9	10
Moderately Important	5	6	7	8
Important	3	4	5	6
Slightly Important	1	2	3	4
Nearly of Equal Importance	1/2	1	1	3/2

Since $EV_{ij} = 1 / EV_{ji}$ the matrix of pair-wise comparisons is sufficiently defined by *n (n-1)/ 2*, which are the number of the elements in the upper triangle of the matrix for which (i < j), (i = 1,2,…, n-1), (j = 2,3,…n).

2.2. Mathematical Formulation

2.2.1. Decision Variables:

w_i - weight of importance of factor i (i = 1,2,…. n), ($0 < w_i < 1$)

Our objective is to find values of weights w_i similar to values of their ratios w_i / w_j, which will be maximizing their membership in corresponding fuzzy sets EV_{ij}. Maximum contributions to the value of the objective or the fitness function occur when ratios w_i / w_j lie in the interval from b_{ij} to c_{ij}. On the other hand, contributions diminish as ratios w_i / w_j get values less than b_{ij} or greater than c_{ij}. Negative contributions to the objective function or fitness function occur as ratios w_i / w_j take values less than a_{ij} or greater than d_{ij}. Next function **G** ($w_1, w_2, \ldots w_n$) is introduced in the present work, to represent the behavior of the fitness of a solution $w_1, w_2, \ldots w_n$.

2.2.2. Fitness function(expression 2), Where (expression 3):

Conditions $a_{ij} < b_{ij}$ and $c_{ij} < d_{ij}$ are necessary to render the fitness function $G(w_1, w_2, \ldots w_n)$, which is finite. Triangular membership functions could be accepted as special cases where, $b_{ij} = c_{ij}$.

$$G(w_1, w_2, \ldots, w_n) = \underset{i<j}{Min}\left(\mu_{12}, \mu_{13}, \ldots, \mu_{ij}, \ldots, \mu_{(n-1)n}\right) \quad (2)$$

$$\mu_{ij} = \frac{w_i / w_j - a_{ij}}{b_{ij} - a_{ij}}\,\delta_{(w_i/w_j) < b_{ij}} + \delta_{b_{ij} < (w_i/w_j) < c_{ij}} + \frac{d_{ij} - w_i / w_j}{d_{ij} - c_{ij}}\,\delta_{(w_i/w_j) > c_{ij}} \quad (3)$$

In these Special cases the indicator functions:

$$\delta_{b_{ij} < (w_i / w_j) < c_{ij}} = 0$$

Fitness function :

G(w_1 , w_2 , …. w_n) as given in (2) and (3) is obviously nonlinear function in decision variables

w_i (i = 1, 2, …..n). Therefore, the problem of deriving a priority vector W $(w_1 , w_2 , …. w_n)^T$ from pair-wise comparison judgments are expressed in the form of $n (n-1)/ 2$ trapezoidal fuzzy evaluations

EV_{ij} (a_{ij}, b_{ij}, c_{ij}, d_{ij}) and can be readily given in the following form:

Maximize G (w_1, w_2, w_n)

Subject to

$$\sum_{i=1}^{n} w_i = 1 \qquad (4)$$

Where G (w_1, w_2, …. w_n) is completely defined by expressions (2) and (3).

3. Solution of The Formulated Problem by a Genetic Algorithm

The optimization problem formulated in (4) could be effectively and efficiently solved by applying one of the most powerful search techniques- Genetic Algorithms (*GA*) originally developed by J.H. Holland [9] and later refined by D.E. Goldberg [8] and others. *GA* outperforms Directed Search Techniques because of their capability to explore wider spaces of feasible solutions aiming at a global optimum solution and thus have higher effectiveness. *GA* also outperforms methods of Random Search since they exploit obtained good solutions to arrive at better solutions and thus they are more efficient. *GA* starts with devising a special coding set of decision variables known as chromosomes as inspired by theories of evolution and genetics in biology. Each chromosome represents a solution to the problem by coding all variables of decision. The chromosome representation, as shown in **Error! Reference source not found.**, consists of *n* boxes (genes). Each gene carries a value for one of the *n* decision variables w_i . An initial population of 30 to 50 chromosomes is randomly generated. The fitness of each *feasible* chromosome (solution in which the *n* decision variables sum to one) is evaluated by (2) and (3). Consecutive generations are evolved from the initial population by applying *GA* operators: crossover, mutation, and copying. In biological systems, nature mercilessly selects only the fittest for longer lives and further reproduction. In a similar manner, chromosomes are selected for crossover and copying in accordance with and proportional to their fitness values. Crossover of two parent chromosomes is operated aiming at having better offspring. Crossover is generally operated with a predetermined probability P*xov*er raging from 90% to 95%. Copying is a complementary with crossover event having probability of 5% to 10% and is operated with the purpose of enriching the population with good solutions.

Mutation is a random change of gene values in order to widen the exploration front. This operator is necessary to avoid premature convergence and falling into a local optimum. However, it is recommended to apply mutation with low probability **P*mut*** from 1% to 10% in order to preserve the exploitation capability of *GA,* and not becoming just random searches. The Genetic Algorithm adopted in the present work, named as *Fuzzy Genetic Prioritization* (***FGP***), is described in the following steps:

w_1	w_2			w_i			w_n

Figure 2: A chromosome of n genes carrying values of n decision variables

1. Build a chromosome, by generating ***n*** random numbers uniformly distributed between 0 and 1, and normalize these ***n*** random numbers to render them - summing to one. These ***n*** normalized random numbers represent one of the feasible solutions.
2. Substitute for the values of the priorities w i , where(i = 1,2,….n) in (2) by the values of n normalized random number obtained in step 1 in order to evaluate the fitness of the chromosome.
3. Repeat steps 1 and 2 until having an initial population of 30 chromosomes (feasible solutions).
4. Decide on probabilities of crossover Pxover and mutation Pmut to start reproduction.
5. Select two chromosomes from the population by giving higher chances to those Chromosomes with higher fitness
6. Generate **y** - a continuous random number [0,1] uniformly distributed. If y <= **P*xov*er**. Then the next operation will be crossover, otherwise it will be copying. In case of having crossover apply steps 7 and 8, otherwise skip them and go directly to 9.
7. In case of having crossover operation, uniform crossover is applied since it is found more suitable for the problem at hand. In uniform crossover, each two corresponding genes in the two selected in step 5 parent chromosomes will exchange their values with 50% probability. Thereby two new child chromosomes are formed.
8. Generate **z** – a continuous random number [0, 1] uniformly distributed. If z <= **P*mut***, then perform mutation in the first gene in one of the parents, otherwise skip and take next gene. Repeat this step for all genes of the two child chromosomes. Normalization of the set of newly obtained gene values after crossover and mutation should be restored back and then one evaluates the fitness of each new child. Go to step 10.

9. Copying, in the present algorithm, is performed simply by replacing the two worst chromosomes having least fitness by the two selected in step 5 chromosomes.
10. By completing the above steps, a new generation is already obtained. Go to step 5 for further reproduction.
11. Repeat until convergence is obtained or reaching at a given terminating signal.
12. The solution is then reached by taking values of the genes of the fittest chromosome in the last generation.

The described algorithm is illustrated in Figures 3, 4 and 5 and then implemented in Visual Basic forApplication (VBA) under Excel.

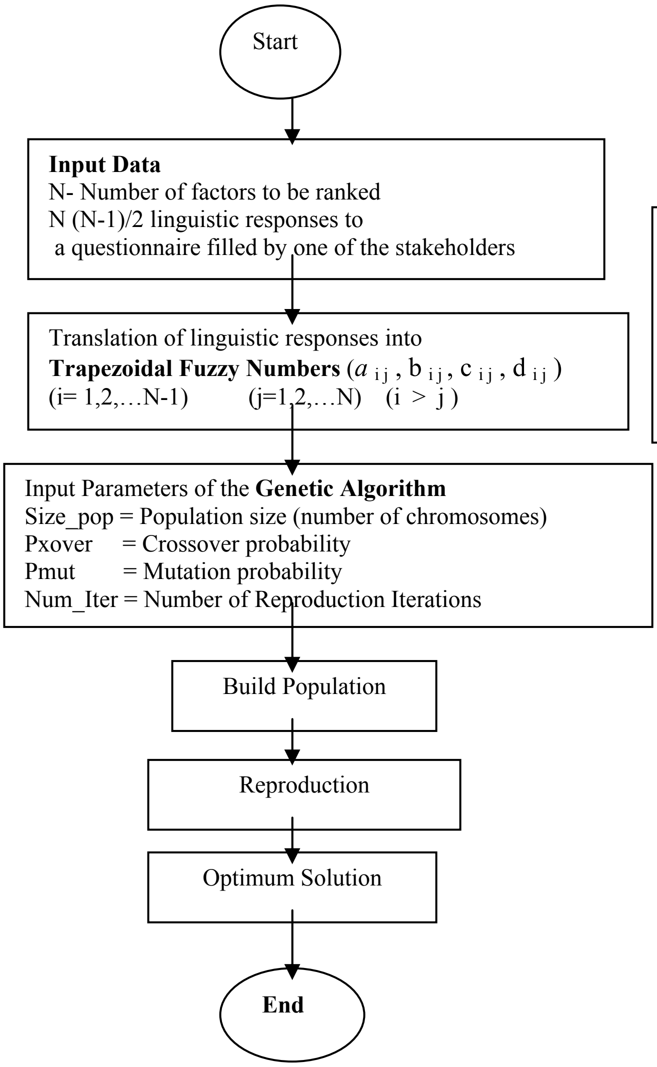

Figure 3: Main Block diagram of the Fuzzy Genetic Prioritization (FGP) Model

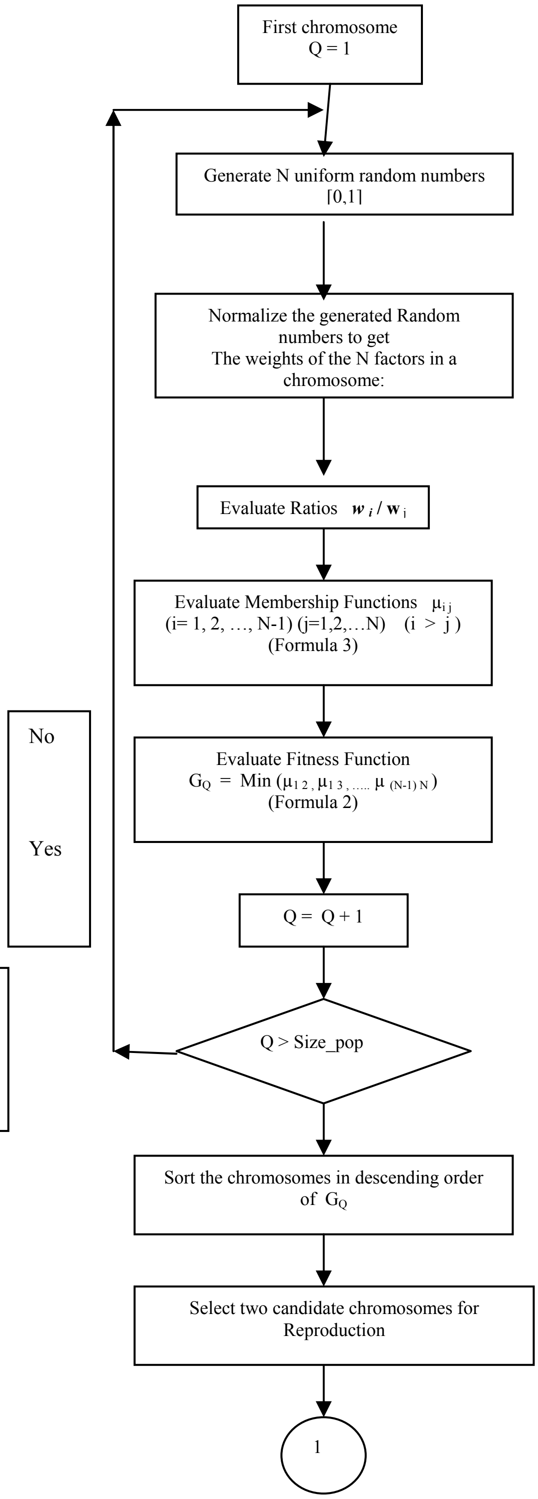

Figure 4: Flow Chart for Build Population Procedure

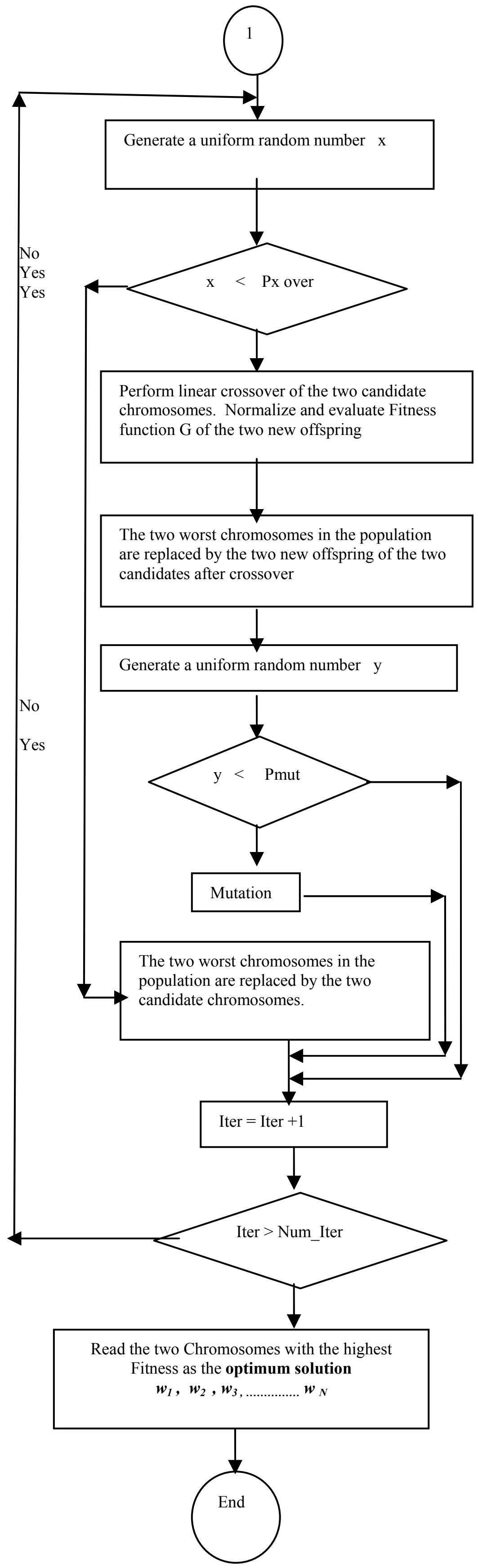

Figure 5: Flow chart for Reproduction and Optimum solution procedure

4. Evaluating Inconsistency of Fuzzy Pairwise Comparison

When constructing a judgment matrix for more than two competing factors or alternatives for the purpose of their ranking, there is a possibility of being inconsistent in decision making *DM* pair-wise comparisons.

For example comparing factor *A* with factor *B*, it is found that *A* is more important than *B* (*A* > *B*). Similarly comparing *B* with *C*, it is found that (*B*>*C*). To be consistent *A* should be rather more important than *C*. But for any reason, *DM* may enter a wrong entry (*A* < *C*). The comparison judgment becomes severely inconsistent. If the entry is correct, without appropriate evaluation of the relative importance, inconsistent comparisons are also obtained and to a lesser degree. Inconsistency increases as the number of factors to be compared and ranked. T.L. Saaty proposed a method to evaluate inconsistency in judgments; and showed that the judgment is perfectly consistent if the maximum eigen value of the reciprocal matrix is equal to the matrix size *n*. Note that the inconsistency index *ICI* is equal to (Max. eigen value – matrix size) / (matrix size – 1). In order to take a decision to discard one of *DM* matrices or not, *ICI* should be compared with the value of *ICI* of a completely random judgment *RI*. Saaty [12] evaluated *RI* for matrices of different sizes. The ratio of *ICI* of any *DM* judgment to *RI* gives the inconsistency ratio (*ICR*). Based on the value of *ICR*, it can decide whether to discard a *DM* judgment, depending on the number of available *DM* s and the criticality of the decision making problem. Acceptable values of *ICR* may take values ranging from say 0.01 to 0.1. Method of T.L. Saaty [12] is applicable only to case of *DM* comparison judgments represented by crisp (single) values.

It cannot be applied directly to the case of fuzzy representations. As already stated in the introduction, one of the main concerns of the present work is to extend the method of finding *ICR* s in the standard AHP to cover cases of fuzzy judgments. This is to overcome complications and inconveniences produced in existing methods that is adopted for evaluation of inconsistency in case of fuzzy judgments.

It is easy to show that fitness function G(w_1 , w_2 , …. w_n) in (2) has the upper bound of unity in case of perfectly consistent judgments for which $b_{ij} <= w_i / w_j <= c_{ij}$. As ratios w_i / w_j get values less than b_{ij} or greater than c_{ij}, the value of fitness function decreases. This behavior of G (w_1, w_2, …. w_n) proposes the following expression to evaluate the inconsistency index ICI as follows:

$$ICI = 1 - G\left(w_1, w_2, ... w_n\right) \geq 0 \tag{5}$$

As in the standard AHP, inconsistency measure becomes more tangible if the index *ICI* is related to a random index *RI*. Next, values of *index RI* for different matrix sizes (n = 3 to 9) have been computed by solving the problem formulated in (4) with random fuzzy judgments.

The inconsistency ratio is given as:

$$ICR = \frac{ICI}{RI} \qquad (6)$$

5. Evaluation of the Random Index (*RI*)

Fuzzy numbers $(a_{ij}, b_{ij}, c_{ij}, d_{ij})$ are generated randomly. The *GA* described in section 3 is run for seven values of n (n = 3, 4,…, 9). For each value of n, the *GA* is run 100 times in order to take an average for the fitness function $G(w_1, w_2, \ldots w_n)$ Having $G(w_1, w_2, \ldots w_n)$, *ICI* can be calculated by (5). In case of randomly generated fuzzy pairwise judgment, *RI = ICI.* In table 2, results of these computations are given.

Table 2: Random Index RI for different sizes n of fuzzy pairwise judgment matrices

n	3	4	5	6	7	8	9
RI	2.62	4.74	6.18	7.2	7.9	9.62	11.28

6. Numerical Examples

The first example to be considered is that presented several times by L. Mikhailov and P. Tsvetnov [11]. The pair-wise comparison judgment matrix is given in table 3.

Table 3: Pairwise comparison (reciprocal) matrixwith triangular fuzzy judgments taken from L. Mikhailov et al [11]

	A	B	C
A	1	(2, 3, 4)	(1, 2, 3)
B	(1/4, 1/3, 1 / 2)	1	(1/3, 1 / 2, 1)
C	(1/3, 1 / 2, 1)	(1, 2, 3)	1

The solution obtained by applying Fuzzy Genetic Prioritization (*FGP*), and developed in the present work, and that is obtained by (MFPP), and is developed by Mikhailov is presented in the following table 4

Table 4: Priority vector derived by FGP of the present work and MFPP of Mikhailov et al [11]

	Present work (*FGP*)	MFPP
w_1	*0.53749*	*0.538*
w_2	*0.17*	*0.17*
w_3	*0.2925*	*0.292*
$G(w_1, w_2, \ldots, w_n)$	*0.83757*	$\lambda = 0.838$
ICI	*0.1624*	
RI	*2.62*	
ICR	*0.062*	

The comparison in table 4 reveals coincidence of solutions obtained from the two approaches. This evidently proves validity of the proposed Fuzzy Genetic Prioritization (*FGP*) as developed in the present work. The inconsistency ratio *ICR*, as proposed in the present work, gives a value of 0.062, which is low, and gives a tangible measure of consistency of pair-wise comparison given in table 3 rather than that of λ = 0.838 used in [11].The second example is considered by Erensal et al [7]; and is solved by the method of D. Chang [4]. As already stated in the introduction, method of Chang belongs to a category of works that extend the approach of standard AHP to be applied directly to fuzzy pair-wise comparisons. However, Chang derived a crisp priority vector by evaluating the truth value of the assertion that a fuzzy number (I) is greater than a fuzzy number (J) as pointed out in the introduction. The priority vector, derived from reciprocal matrix in table 5 given by Erensal et al [7] applying Chang's method, is given in table 6. The same example, as given in table 5, is solved by the Fuzzy Genetic Prioritization *FGP* of the present work; and is also solved by the Modified Fuzzy Preference Programming MFPP developed in [10]. The comparison of the results of the three approaches reveals the following:

- The solution of Erensal et al [7] is not an optimum solution since better solutions have been obtained by both *FGP* and MFPP for the same reciprocal matrix.
- The inconsistency ratio *ICR* as obtained by the present work for the optimum solution is 0.341. This ratio is high; and assures that pairwise judgment in table 5 is inconsistent. This result is confirmed by the findings of MFPP for which λ has negative value ($\lambda = -1.06$).

Table 5 : Pair-wise comparison reciprocal matrix with triangular fuzzy evaluations , from Erensal et al [7]

	Cost	Price	Quality	Flexibility	Time
Cost	1	1/5,1/3,1	1/7,1/5,1/3	1/5.1/3,1	1/7,1/5,1/3
Price	1,3,5	1	1/9,1/7,1/5	0.5,1,1.5	1/5,1/3,1
Quality	3,5,7	5,7,9	1	1/7,1/5,1/3	0.5,1,1..5
Flexibility	1,3,5	0.9,1,1.1	3,5,7	1	1/7,1/5,1/3
Time	3,5,7	1,3,5	0.9,1,1.1	3,5,7	1

7. Findings and Conclusions

7.1. The extension of the standard AHP method, as introduced by T.L. Saaty, in which the pairwise comparisons are given by crisp values, to be applied directly to cases of having fuzzy pair-wise judgments is not valid; and leads mostly to irrational and inconsistent solutions.

7.2. The proper handling of problems of deriving priorities from fuzzy pair-wise judgments is to formulate them as optimization problems. Fuzzy Preference Programming developed by Mikhailov [10] is the first trial in this concern.

7.3. Expressing objective functions explicitly, in optimization models, is an important prerequisite to rendering the nonlinear programs amenable to applications of the effective and widespread nontraditional search techniques such as Genetic Algorithms.

Table 6: Priority vector derived by three methods FGP of the present work, Chang [4] applied by Erensal et al [7] and MFPP of Mikhailov [10] for the pair-wise comparisons matrix given in table 5

	Present work (FGP)	Chang method applied by Erensal et al [11]	MFPP by Mikhailov Using Lingo 8
w_1	*0.0473*	*0.00*	*0.0447*
w_2	*0.0282*	*0.12*	*0.03188*
w_3	*0.1223*	*0.31*	*0.1224*
w_4	*0.2602*	*0.25*	*0.2578*
w_5	*0.542*	*0.32*	*0.54314*
G	*-1.107*	*-6.8*	$\lambda = -1.06$
ICI	*2.107*	*7.8*	
ICR	*0.341*	*1.262*	

7.4. It has been demonstrated that Genetic Algorithms can be easily and transparently applied to solve the formulated optimization models for deriving priorities from fuzzy pair-wise judgments after modification of the objective (fitness) function and making it explicit function of decision variables w_i. The coincidence of results obtained from the application of the developed, in the present work, Fuzzy Genetic Prioritization FGP and solutions obtained from MFPP by Mikhailov is clearly demonstrated by the two provided numerical examples.

7.5. Modeling of linguistic judgments in the form of trapezoidal fuzzy numbers is sought to be more realistic and capable of capturing fuzziness of comparisons.

7.6. To have ICR as a tangible measure of inconsistency of pair-wise judgments is crucial for making rational decisions. The measure ICR acts as a screening element by means of which seriously inconsistent responses of DM to questionnaires could be discarded. This screening is mandatory prior to getting geometric means in case of having group of decision makers. The computations of the random indexes RI for matrices of different sizes with random fuzzy entries, as elaborated in the present work, made it possible to evaluate ICR s

REFERENCES

[1] Boender C., De Graan and Lootsma F. "Multi criteria decision analysis with fuzzy Pair-wise comparisons", Fuzzy Sets and Systems, Vol. 29, 1989, 133-143.

[2] Buckley J., "Fuzzy Hierarchical analysis", Fuzzy Sets and Systems, Vol. 17, 1985, 233 – 247.

[3] Brazili L. A., "Deriving Weights from pairwise comparison matrices", Journal of Operational Research Society, Vol. 48, 1997, 1226-1232.

[4] Chang D., "Application of the extent analysis method on fuzzy AHP", European Journal of Operational Research, Vol. 95, 1996, 649-655.

[5] Chu A. , Kalaba R. Springarm K., "A comparison of two methods for determining the weights of belonging to fuzzy sets", Journal of Optimization Theory and Application, Vol. 7, 1979, 531-541.

[6] Crawford G. and Williams C., "A note on the analysis of subjective judgment Matrices", Journal of Mathematical Psychology, Vol. 29, 1985, 387-405.

[7] Erensal Y. C., Oncan T. and Demircan M. , "Determining Key Capabilities in Technology of Management Using Fuzzy Analytic Hierarchy Process: A case study of Turkey", Journal of Information Science, Vol. 176, 2006, 2755-2770.

[8] Goldberg D.E., "Genetic Algorithms in search optimization and machine Learning", Addison- Wesley, Mass, 1989.

[9] Holland J.H., "Adaptation in natural and artificial systems", University of Michigan Press, Ann Arbor, Michigan, 1975.

[10] Mikhailov L., "Deriving priorities from fuzzy pairwise comparison Judgments", Fuzzy Sets and Systems, Vol. 134, 2003, 363-385.

[11] Mikhailov L. and P.Tsvetinov, "Evaluation of services using a fuzzy Analytic hierarchy process", Applied Soft Computing, Vol. 5, 2004, 23-33.

[12] Saaty T.L. "A Scaling method for priorities in hierarchical structures", Journal of Mathematical Psychology, Vol. 15, 1977, 234-281

[13] Saaty T.L. and Vargas L. G. , "Inconsistency and Rank preservation", Journal of Mathematical Psychology, Vol. 28-2, 1984

[14] Van Laarhoven P. and Pedrycz W., "Fuzzy Extensions for Saaty's priority Theory", Fuzzy Sets and Systems, Vol. 11, 1983, 229-241.

[15] Zadeh L. A., "The concept of linguistic variable and application to Approximate reasoning", ERL-M411, Berkeley, California, 1973

JJMIE

Volume 2, Number 4, December. 2008
ISSN 1995-6665
Pages 183 - 190

Jordan Journal of Mechanical and Industrial Engineering

Human Error Control in Railways

Amit Kumar [a*], P.K.Sinha [b]

[a] Mechanical Engineering Department, National Institute of Technology, Patna-800005(BIHAR),India
[b] Mechanical Engineering, National Institute of Technology, Patna - 800005 (BIHAR), India

Abstract

Humans are the weakest link in any embedded system. Failure rates for humans as system components are several orders of magnitude higher than other parts of the system. Railway operation system requires involvement of a large number of persons. This results in more human errors and hence disastrous consequences. The paper presents general theory of human errors; and stresses the need to adopt optimization in railway operations to the maximum possible extent; and to develop a continuous monitoring system for physical and psychological status of the workers.

Keywords: Human error, Railways, Railway Operational System, Attention Subsystem, Automatic Subsystem, Schemata, Absolute Block System.

1. Introduction

All systems have a human component. Even the most highly automated systems are designed, installed, and maintained by people. To err is human. Human error plays a part in most accidents, if not all.

In critical systems like transport systems, safety measures against human errors play a substantial role. Human error can be committed in different phases of life cycle, namely, during system specification and development; and in the longest phase of the life-cycle during operation. In railway operation, several safety-critical tasks are assigned to the operators and are not controlled by signaling and interlocking systems. Many tasks are necessary in situations occurring very rarely. Since these situations are unfamiliar to the operators and demand of good interaction is high, pre-training is necessary to provide information and practice to solve these situations [1].

The European standards concerning railway safety - leading with EN50126, about the specification and demonstration of railway reliability, availability, safety and maintainability - forces the efforts of training and retraining of operational personnel. The main equipment for training of railway signaling personnel has become computer-based interlocking, signaling, and traffic simulation systems [2-3]. It is desirable that operators and the maintenance personnel possess necessary knowledge of equipment from the first moment of its operation. This is indispensable to an untroubled, smooth, and safe traffic operation. In case of extraordinary and troubled situations, rapid recognition and solution of the given problem is required to avoid accidents. Computer-based simulation systems are capable to help in the above-mentioned tasks.

A scenario, which represents a sequence of actions/operations, can involve human agents (H) and machine agents (M). A human agent may communicate with another human agent, and a machine may pass information to another machine in a distributed system. The minimum set of interactions between H and M are: H, M, HM, HH, and MM. Each interaction pattern, in this set, can lead to an inappropriate or undesired system performance. Based on this set of possible interactions, five types of errors may be identified; (i) human error, (ii) machine error, (iii) error resulted from human-machine interaction, (iv) errors related to machine-machine communication, and (v) errors attributable to human-human communication. Apart from these five types, a sixth type may be identified and included, i.e. organizational errors, which are caused by organizational structure or social conditions [4].

A human agent, as an integral component in the social environment of a system, takes decisions, performs actions, etc. During these interactions, deviation of normal behavior of a human agent may result in inappropriate system performances. The causes of deviations in the actions or behaviors of human agent are called human errors. Human errors may occur because of inadequate knowledge, memory lapses, incorrect mental model, etc.

Design errors, or non-adherence to user interface guidelines, etc. may give rise to situations where a human agent is unable to make a decision or to diagnose a problem when interacting with machines.This results in an undesirable system performance. Such errors are labeled as human- machine interaction mismatches. These may arise due to usability problems, poor feedback mechanisms, or inadequate error- recovery mechanisms [5]. When a

* Corresponding author.; e-mail:amitnidhi31@yahoo.com.

human agent is not able to communicate appropriately, or as desired, to another human agent via any media; and which may cause an unacceptable system performance, then such factors are called human-human communication errors. Errors due to human-human communication may be linked to communication mismatch between fellow workmen as a result of ambiguous task allocation or lack of co-ordination at management level. A situation may arise when a machine is unable to communicate correctly to another machine in a network or a distributed system. This may be caused by machine- machine miscommunication [6].

The occurrence of one error may give rise to another and hence triggering a chain of non-normative events leading to an undesirable or inappropriate system performance. An attempt has been made to illustrate these causal relations of problem errors leading to an unplanned behavior through the following example.

Consider the case when an operator of a control system is not able to optimally control certain parameters (human errors) like when an operator does not have the access rights for some function/information of the machine, or is not trained enough to perform an allocated responsibility. This actually reflects on structure and planning of the organization (organization error). The human error caused by the cumulative effect of human and organization errors may lead to malfunctioning of the control system (machine errors) and ultimately result in a system breakdown.

The example is not to demonstrate a generic path for causal relations errors causing the problem, but to illustrate the occurrence of interaction between different types of errors responsible for the problem. The example has two important messages: First, if error is known, the requirements engineer can explore its effect(s) on the system behavior by exploiting these causal relations to simulate the causal chain of events in the normal task-flow. on the other hand, if consequences are known from any previous histories of undesirable system behavior, the requirements engineer can start from the consequences to determine the cause(s) or errors by following the causal path of events. These techniques of forward and backward searches can be integrated in the method of scenario analysis. This approach of causal analysis is very similar to hazard analysis techniques, for instance, HAZOP in safety engineering.

2. Human Error

It has been estimated that up to 90 % of all workplace accidents exhibit human errors as a cause [7]. Human error was a factor in almost all the highly publicized accidents in recent memory including the Bhopal pesticide plant explosion, Hillsborough football stadium disaster, Paddington and Southall rail crashes, capsizing of Herald of Free Enterprise, and Challenger Shuttle disaster.

In order to address human factors in workplace safety settings, peoples' capabilities and limitations must first be understood. The human characteristics that can lead to difficulties interacting with the working environment are the following:

2.1. Attention

The modern workplace can 'overload' human attention with enormous amount of information, besides of that encountered in the natural world. The way in which we learn information can help reduce demands on our attention, but can sometimes create further problems.

The Automatic Warning System installed on all passenger trains in U.K is an example of a system that is designed without considering limitations of human attention in mind. It is a device fitted in the train cab and based on the current obsolete mechanical system of signaling which is used to signal either STOP or PROCEED. It sounds a bell when a clear (green) signal is passed and a buzzer when caution or danger is signaled. If the buzzer is not acknowledged by the press button, then the train begins to stop automatically. In commuter traffic, most signals are at the 'caution' aspect, and given the frequency of signals (spaced 1 km apart), most drivers will face two signals per minute. Given the tendency for the attention system to automate highly repetitive behavior, many drivers lose focus on the reasons for carrying out this repetitive task, and act in reflex whenever the buzzer sounds.

The ultimate result is that drivers often hear the buzzer and press the button reflexively without actively thinking about the train speed and location.

2.2. Perception

In order to interact safely with the world, we must correctly perceive it and recognize the dangers it holds. Work environments often challenge human perception systems and information can also be misinterpreted.

2.3. Memory

Our capacity for remembering things and imposing methods upon ourselves to access information often put excessive pressure on us. Increasing knowledge about a subject or process allows us to retain more information relating to it.

2.4. Logical Reasoning

Failures in reasoning and decision-making can have severe implications for complex systems such as railway operations, chemical plants, and for tasks like maintenance and planning.

Under optimum field conditions and with the best of intentions, a human being is likely to commit error now and again. Human operators are one of the biggest sources of errors in any complex system. Human errors are dependent on many factors [10] as indicated in Table 1.

To reduce the extent and consequences of human errors in railway operation, automation is quite helpful. A well-designed human-computer interface (HCI) is an essential requirement of automation [8]. However, human beings are often needed to be the fail-safe in other automated system. Even the most highly trained and alert operators have a tendency to monotony when they are usually not needed for normal operation. They panic when an unusual situation occurs, and stress levels are raised, and lives are at stake. The HCI must give appropriate feedback to the operator to allow him/her to make well-informed decisions based on the latest information of the state of the system.

High false alarm rates will make the operator ignore a real alarm conditions. Automated systems are extremely good at repetitive tasks. However, if an unusual situation occurs and corrective action must be taken, the system usually cannot respond well.In this situation, a human operator is needed to handle an emergency.

Humans are much better than machines at handling novel occurrences, but cannot perform repetitive tasks well. Thus, an operator is left to passively monitor the system when there is no problem; and is only a fail-safe in an emergency.

Table 1: Human errors factors

CATEGORY	SOURCES OF ERRORS
Physiological	(1) Work Environment- Noise, lighting, work timings, shift arrangements, temperature, ventilation, etc. (2) Stress- Reaction to stress. (3) Attention capacity- over attention or inattention, perceptual confusion. (4) Adoption-reaction to changes in system and environment. (5) Mental Load-tired, stressful.
Anatomical	Physical Health-disability, age, sick or injured, poor physical co-ordination.
Social & Personal	Distress to family member(s). Strained relationship between Two/more family members. Social disharmony /distressful situation.

This is a major problem in HCI design because when the user is not routinely involved in the control of the system, they will tend to become bored and be lulled into complacence (9). This is known as operator drop-out. Since the user's responsiveness is dulled, in a real emergency situation, he or she may not be able to recover as quickly; and will tend to make more mistakes.

Stress is also a major factor to human error. Stressful situations include unfamiliar or exceptional occurrences, incidents that may cause a high loss of money, data, life, and time critical tasks. Human performance tends to decline when stress levels are raised. Intensive training can reduce this affect by turning unusual situations into familiar scenarios via drills. However, cases where human beings must perform at their best to avoid hazards are often the cases of most extreme stress and worst error rates. The failure rate can be as high as thirty percent. Unfortunately, the human operator is our only option, since a computer system usually cannot correct unique situations and emergencies.

3. Classification of Human Errors

Better training or supervision can prevent errors but most effective action can be taken to reduce opportunities for error, or minimize their effects, by changing designs or methods of work. Human errors are committed due to different reasons and it requires different actions to prevent or reduce the different sorts of errors [10]. They are:

3.1. Those That Occur Because One Does Not Know What to Do.

The intention is wrong. They are usually called mistakes.Some of these errors are due to a lack of the most basic knowledge of the properties of materials or equipment handled or to lack of sophisticated knowledge and other errors may be caused by following the rules when flexibility was needed. However, many written rules cannot handle every situation that might arise and people should therefore be trained to diagnose and handle unforeseen problems. Sometimes people are given contradictory instructions or instructions with implied contradictions.

3.2. Those That Occur Because Someone Knows What to Do but Decides not to do.

They are usually called violation or non-compliance. Many accidents have occurred because operators, maintenance workers or supervisors did not carry out procedures that they considered troublesome or unnecessary. If the wrong method is easier than the correct method, people are tempted to use the wrong one.

3.3. Those That Occur Because the Task is Beyond the Physical or Mental Ability of the Operator.

They are called mismatches, few accidents occur because individuals are unsuitable for a job. More occur because people are asked to carry out tasks, which are difficult or impossible for anyone, physically or, more often, mentally.

3.4. The Errors Due to a Slip or a Momentary Lapse of Attention.

The intension is correct but it is not carried out.

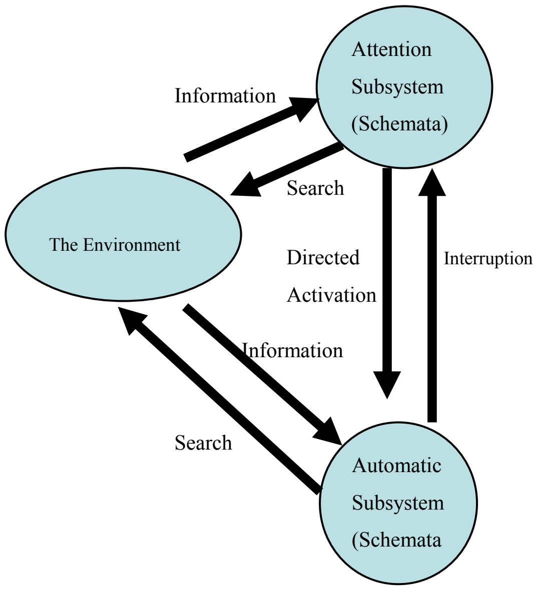

Figure 1: Three Interacting Sub-Systems.

4. General Theory of Human Error

An adequate theory of human action must account not only for correct performance, but also for the more predictable varieties of human error. Perhaps the most important convergence in human error research is responsible for the development of a partial model of human cognition. Figure 1 illustrates the basic elements of this emerging model as drawn from Reason's [11] Generic Error-Modeling System (GEMS).

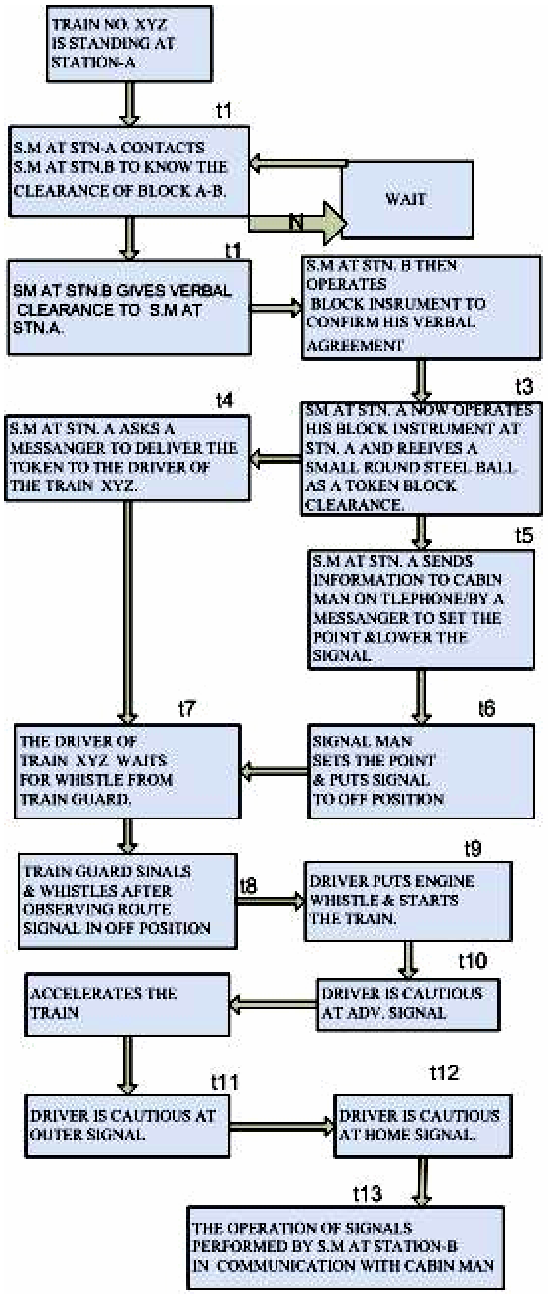

Figure 2: Flow chart for movement of trains

Figure 1 has three interacting subsystems. One is the Automatic subsystem that works below the level of consciousness. Research indicates the automatic subsystem schemata (organized collections of information) and response patterns within a person. When the proper conditions exist, a schema is activated. There are two core mechanisms for selecting schemata to be activated. The first mechanism is pattern matching and the second is frequency gambling.

The second subsystem is Attention subsystem (consciousness). The attention system has powerful logical capabilities. According to Reason [8], this mode is "limited, sequential, slow, effortful, and difficult to sustain for more than brief periods.

The automatic and Attention subsystems do not work independently. The attention subsystem holds goals. These goals influence the activation of automatic subsystem nodes. When the attention subsystem loses its goal, the entire cognitive system is likely to err. However, the limited attention resources must also be allocated to planning for future actions and dealing with unexpected conditions.

The third subsystem is the environment. Human cognition is not merely internal. It is situated in the environment surrounding it. Sellen and Norman stresses that the integration with the environment takes place continuously as we plan and execute an action. First, we form a high-level intention. When we execute it, we constantly adjust our action through feedback with environment. This adjustment takes place without burdening our limited attention system in most cases. In addition, once the adjustment begins, it takes on a life of its own. Sometimes it goes in unforeseen directions.

5. Human Involvement in Railways

With the advancement of civilization and as a result of globalization of business, travel and transport sector are still in a period of major growth. The challenge is to manage this growth with a commensurate increase in safety. As a response to this, railways are expanding throughout the world.

Many workers are required for system design, operation, and maintenance of the railways. Most of rail accidents are attributed to human error. In engineering, an error is a difference between desired and actual performance of a system or object/man. One type of error is human error, which includes cognitive bias. Human errors are predictable, and thus can be prevented by changing the design of a system. Psychologists use their knowledge of human perception, response time, and cognition to predict and prevent possible errors.

Any organization that professes to have a safety culture should treat human behavior as an important issue.

5.1. Dependencies between Human Actions

One human error may make other more likely. A mistake by an operator that results in a hazardous situation may cause them to be more stressed, impairing their thought processes and making further errors is more expected. An inadequate understanding of dependencies between human actions can lead to a significant underestimation of risk.

5.2. Indian Railways

In India, more than 90% of train movements are being controlled by "Absolute Block" system. This system requires a large number of manpower for operation control, which is evident from the flow chart shown in figure2.

In the flow chart, t_1 to t_{13} are the times consumed by the persons concerned with train movement. It also depends on the I.Q., efficiency, skill, age, and health status of individuals concerned.

Moreover, physical environment will vary from individual to individual. At busy railway stations, a number of incoming and outgoing trains have to be handled simultaneously. The manual of such situations becomes quite complex, and probability of human errors is higher (12).

In addition, huge manpower is engaged in works like, track maintenance, cabin management, station administration, workshops, etc. Such a sizable involvement of manpower in railway operating system makes it prone to human errors and consequent accidents.

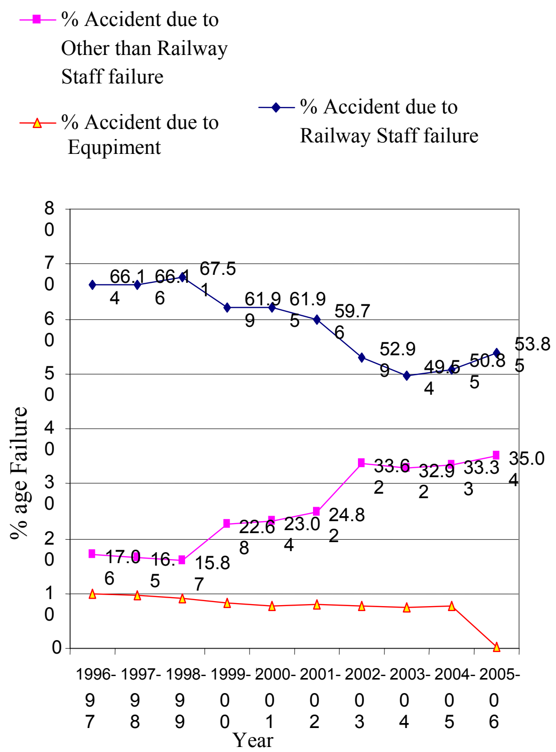

Figure 3: Responsibility wise Analysis during 1996-97 to 2005-06 on Indian Railway

Amitabh Agarwal, Ministry of Railways, Government of India, reports that in last ten years (1996- 2006), 59% of the accidents on Indian Railways have been caused by failure of Railway staff, and 25.5% have been caused by failure of other than Railway staff. Failure of equipments has contributed 6.5% and 9% by balance. From the break-up it is more than evident that human error has been the major factor in causing accidents on Indian Railways. Figure 3 represents responsibility-wise analysis during this period (13, 14, and 15).

5.3. Case Study

Head-on collision of 9112 Dn Jammu Tawi Ahmedabad Express with JMP Diesel Multiple Unit Passenger train between Bhangala and Mirthal stations of Northern Railway on fourteenth of December.2004 happened, where 38 persons lost their lives and many were injured.

The present case study was undertaken by officials of Indian Railways, Ministry of Railways, and Government of India.

5.3.1. Cause of the Accident

The two Station Masters did not exchange messages properly on VHF sets. This resulted in dispatching trains in the same block section from opposite directions on a single line section.

5.3.2. Key Observations

1. Quad cable supporting the block circuits was damaged due to construction activity in the section causing failure of Block instruments and block phones at both stations 24 hours prior to the accident.
2. Trains between Mirthal and Bhangala were being worked on paper line clear (PLC) 24 hours prior to the accident.
3. This is a saturated section handling both passengers and traffic to full capacity. It is quite demanding to operate even under normal circumstances.
4. Both Station Masters dispatched trains from their respective stations towards each other in the same block section by granting "line clear" on VHF sets exchanging private numbers and issuing PLC.
5. Poor supervisory and managerial interventions were continuing in this most unsafe and accident-prone conditions.
6. Work of locating and rectifying the fault was not undertaken on emergency basis.

5.3.3. Human Errors Involved

5.3.3.1. Human errors were manifested by vulnerable functioning after the technical failure i.e. the cutting of quad cable supporting control circuits during excavation of earth.

5.3.3.2. Both station masters adopted the least cumbersome process of granting "line clear" after failure of Block instruments and Block phones i.e. VHF communication over controller communication being easy to use. Despite VHF communication being more vulnerable to outside interference, the prescribed safeguard for ensuring that reply to the line clear inquiry is emanating from the authorized person competent to grant "line clear" was not adopted by Station Masters.

5.3.3.3. Though the practice of granting "line clear" using VHF communication had been going on for about 24 hours for several trains in both directions. By this time abnormal working had lost its alert value in the minds of individuals and a lapse was bound to take place at the level of Station Masters.

All the above lapses manifested in the form of dreaded head-on collision with the last string of frontline action coming from the two Station Masters. Role of maintenance agencies cannot be overlooked in causing the vulnerable situation of train operation for prolonged period which ultimately was manifested into the accident.

REMARK: All the above lapses resulted in the form of dreaded head-on collision with the last string of frontline action coming from the two Station Masters. Role of maintenance agencies cannot be overlooked in causing vulnerable situation of train operation for prolonged period, which ultimately manifested into this accident.

6. Remedial Approach to Railway Operation System

The basic approach towards reducing human errors in railway operations may be listed as follows:

6.1. *Reduction In Man-Power Requirement:*

This requires adoption of automation to the maximum possible extent. A variety of software packages should be available or can be indigenously developed for Centralized Railway Traffic Control System and Automatic Railway Traffic Control System. The proper selection of structure and basic function pools achieve an optimal relation between monetary requirement and performances in the above mentioned operation systems [16].

6.2. The Basic Characteristics of the Function Pool are:

(a) Effective support of operator's supervision of routes and traffic.
(b) Train number following and corresponding support functions of passenger informing, traffic disposition, and automatic control.
(c) Effective support for automatic following of traffic running and registration.
(d) Effective support for administrative activities.
(e) Automatic programmable traffic control on train number and timetable basis with the support of alternative solution in the case of conflicting states.
(f) Automatic programmable control of shunt routes.
(g) Possibility of direct manual control of routes and interlocking equipment.
(h) Special system support of "off-line" maintenance and browsing of timetable base and automatic control programs.
(i) Flexible interfaces between interlocking equipment and CTC system.
(j) Spontaneous diagnosis and centralized information of errors and self-documentation of CTC system operation.

6.3. *Selection of Necessary Man-Power*

Even after adoption of automation in railways, a reasonable number of human-related requirements would be indispensable. This makes it essential to recruit only competent and well-qualified staff for different jobs. Consequently, carefully considered standards stating qualifications and expertise for each category of employees are to be prepared and updated frequently. These standards should be adhered to since any slight deviation may result in accidents leading to loss of human lives.

6.4. Indoctrinating new Recruits

New employees should be familiar with the new work conditions, work environment, and potential work hazards. Thus, a well-planned training program for new recruits before involvement is essential. Its high effectiveness will ensure less of human errors. Continuous modifications and updating of training programs are predicated to make the whole process effective.

6.5. Refresher Training Programs:

Refresher training programs are necessary at regular intervals for all working personnel to keep them responsive to safe working conditions and practices. Such programs also provide a platform for interaction between workers and top management.

6.6. Periodical Health Check-Ups and Psychological Fitness Tests

Human errors are also dependent on health and psychological status of the employees concerned. Hence, regular health check-up and psychological fitness camps should be organized regularly. If health and psychology of employees are not suitable for a job, they should not be allowed to continue - for humanitarian considerations.

6.7. Identifying Hazards, Assessing, and Reducing Risk

Railway organization must make a systematic and vigorous attempt at regular interval to identify any possible hazards that may result in an accident at any time. The process of human error identification should be integrated with the general process of hazards identification within the system.

7. Conclusions

1. In any complex system such as railway operation, most errors and failures in the system can be traced to human errors. Humans have higher failure rates under high stress levels. Yet, they are more flexible in recovering from emergent situations and consequent potential disasters.
2. New technology always requires new safety challenges and thus entails more intricate training and retraining of the workers periodically.
3. Human involvement can be minimized if automation in railway operation is adopted, and thus lowering the probability of human errors and its consequences.
4. A high-quality system should impose accountability. This may sound obvious, but system design is carried out in the absence of feedback from its potential users, which increases the chance that the users will not be able to interact correctly with the system.
5. Continuous monitoring for physical and psychological status of employees involved in railway operations is likely to diminish the human errors.
6. Unsuitable workers in a railway job are more likely to err; and thus must be suspended immediately as soon as they are identified.

References

[1] Aranyosi. Z, L.Mosoczi, G. Racz, G. Tarnai, "Training the Personnel Using Simulator and Training System", World

Congress on Railway Research WCRR,'97 Proceedings, 1997.

[2] Baranyi. A, G. Racz, B. Saghi, "Application of Simulation Systems in planning and Training of Railway Operation: Formal Methods for Railway Operation and Control Systems", Proceedings of Symposium FORMS2003, L'Harmattan, Budapest, 2003.

[3] Dobrosi. A, I. Hrivnak, R. Schwendke, "Multifunction Simulator Developed For amburg/Simulation Based Training and Planning Systems for Railway Technology", International Railway Journal, U.K, 1999, 25-27.

[4] Neil Maiden, Shailey Minocha, Michele Ryan, Keith Hutchings and Keith Manning, "A Cooperative Scenario Based Approach to Acquisition and Validation of Systems Requirements: How exceptions can help?" Workshop on Human Error and Systems Development, Scotland, 1997.

[5] Burns. A, "The HCI component of dependable real-time systems." Software Engineering Journal, Vol. 6, No. 4, 1991, 168-174.

[6] Kirwan, Barry, "a Guide to Practical Human Reliability Assessment", London: Taylor & Francis Ltd, 1994.

[7] Feyer, A. M, and A. M. Williamson, "Human factors in accident modeling". In: Stellman, J.M. (Ed.), Encyclopaedia of Occupational Health and Safety, Fourth Edition, Geneva: International Labour Organisation, 1998.

[8] Reasons. James, "Human Error", Cambridge, U.K, Cambridge University Press, 1990.

[9] Charles. P. Shelton, "Human Interface/ Human Error", http:// www.ece.cmu.edu/~koopman/des-s99/human/index.html. 1999,

[10] Kletz. T. A, "An Engineer's View of Human Error", 3rd edition, (Institutio of Chemical Engineers, Rugby) 2001.

[11] Dr. Raymond R. Panko, "Theories of Human Error", http: // panko.cba. Hawaii. Edu/human err/theory, htm.

[12] Kumar Amit, Ph.D Thesis entitled "Development of a System for regulatin Traffic of Indian Railways Based on the principle of Automated Guided Vehicles", Patna University, 2007.

[13] Amitabh Agarwal, Director (safety), Ministry of Railways, Government of India, "Human Interface in Railway Safety – A New Dimension", http://panko.cba.hawaii.edu /humanerr/Theory.htm, 2007.

[14] Government of India, Ministry of Railways, "Indian Railways Corporate Safety Plan" ,2003.

[15] Agarwal Amitabh, "Rail Accidents due to Human Errors-Indian Railways Experience", International Railway Safety Conference, Cape Town, South Africa, 2005.

[16] Railway Central Traffic Control System (APIS-90/CTC), Institute for Process Automation, Stegne 21, SI-1000 Ljubljana, Slovenia.

JJMIE

Volume 2, Number 4, December. 2008
ISSN 1995-6665
Pages 191 - 200

Jordan Journal of Mechanical and Industrial Engineering

An Investigation into Plastic Pipes as Hot Water Transporters in Domestic and Industrial Applications

M. H. Zgoul* , S. M. Habali

Mechanical engineering Department,, Faculty of Engineering and Technology, University of Jordan,, Amman, 11942 Jordan

Abstract

This work discusses convenience of thermo-pipes as compared to traditional steel and copper pipes when used for transporting hot water in domestic and industrial applications. Comparison is made here between thermo pipes and steel pipes regarding strength, material properties, corrosion resistance, aging effect, energy saving, electrical properties, and workability. Tensile tests were conducted in this research for two types of thermo pipes: Cross-Linked Polyethylene (Thermopex) and Polypropylene Random Copolymer (PPRC). The tests were conducted by computer labs of Royal Scientific Society. A lot of material properties (E, σ_y, σ_f, u_r, u_t, B, e%, a%) were gained from these tests, which are in good agreement with the values given by the manufacturer. The results show, that both types of thermo-pipes (polyethylene and polypropylene) are more convenient for heating purposes, corrosion resistance, and easier workability than traditional materials like steel and copper. Thermo-pipes materials behave satisfactorily when subjected to thermal stresses for long periods of time (aging effect). Also, they possess low thermal and electrical conductivities with lower melting points than steel. Therefore, they exhibit higher energy conservation and safety than steel pipes do.

Keywords: Thermo-pipes, plastics, water heating transportation, thermal stresses, aging effect, thermal and electrical conductivities.

Nomenclature

σ_y	: Yield stress, MPa
σ_f	: Fracture stress, MPa
u_r	: Modulus of resilience, MPa
u_t	: Modulus of toughness, MPa
e%	: Percent elongation,
a%	: Percent reduction in area
PPRC	: Thermopipe Polyproylene Random Copolymer
CLPE	: Cross Linked Polyethylene = Thermopex = Pex
DSC	: Differential Scanning Calorimetry
σ_{avg}	: Average tensile stress
B	: Bulk modulus
u_r	: Modulus of resilience
u_t	: Modulus of toughness
e%	: Percent elongation
a%	: Percent area reduction

1. Introduction

The development of efficient thermo pipes since the mid of 1980s resulted in a worldwide rapid increasing use of these pipes for domestic and industrial applications. This requires studying their properties and behavior when subjected to high temperature and pressure, trying to improve their quality for future applications.

Two types of thermo pipes are investigated in this work:

1.1. Polypropylene Random Copolymer (PPRC) Thermo-pipes have proved to be deal for plumbing, heating, air conditioning, and for a wide range of industrial and medical uses. PPRC system has been improved with the additional of a full range of PPRC fittings that can be poly-welded to thermo-pipe system creating fully watertight systems even under most severe conditions of use, [1].

1.2. Cross-linked Polyethylene (Thermopex) thermo pipes are capable of handling a wide variety of materials in industrial and domestic applications including water, fluid waste, gas, and chemicals. Furthermore, piping systems can be manufactured for electrical installations, [2].

Thermo pipes are made of high quality raw materials using some of the most advanced production techniques in the world. Also, engineers are required to develop piping systems for special needs.

The workability of these pipes, due to lightness (low density ρ = 898 kg/m, ρ = 7850 kg/m) and flexibility (1/E, E = 2.1-3.4, GPa = 200GPa) is fast and easy. Together with its wide range of fitting, lightness and flexibility of thermo pipes permit an easy, stable, and fast construction of hydro thermo sanitary installations compared to conventional pipes of steel or copper. The fitting used for the pipes are brass fittings. There are some installation

* Corresponding authore-mail: m.zgoul@ju.edu.jo.

instructions that must be taken into consideration when installing pipes, [1] and [2]. Pipes and fittings should not be directly exposed UV radiation. Ultimately, this will lead to crystallization of its material, [1].

When using thermo pipes in space heating, hot water of changeable temperature flows within pipes; and hence raises their temperature. The temperature variations occur in longitudinal and radial directions with destroying effect on the pipes. Because such a distribution leads to local deformations and stress concentrations, cracks will initiate at such locations. In other words, local temperature gradients will result in generating thermal stresses in the pipe. Pipe aging and pipe failure can be considered as a direct result of thermal stresses.

The effect of this phenomenon on pipe properties and materials will be studied in this research - focusing on material properties taken from tensile and fatigue tests, temperature effect, variation of melting point, and thermal and electrical conductivities.

Heating systems are one of the most important applications at homes, companies, school, universities, and other facilities. Best materials for space-heating pipes are Polypropylene Random Copolymer (PPRC) and Cross-Linked Polyethylene (PEX). These two types of thermo pipes are widely used in heating systems due to convenient properties.

Thermo pipes reach their operating temperature much faster than metal pipes, because of dissipated energy of thermo pipes. Since low thermal conductivity is less than thermal conductivity of metal pipes. This indicates that less energy is wasted by heating pipes and less insulation is needed, too. Table 1 includes some of the mechanical and thermal properties of thermo pipes. Also, high level of thermal insulation (low thermal conductivity k), ensures minimal drop in temperature of the fluid transported between the hot water source and the delivery points.

Thermo Pipes Possess Some Important Characteristics, Like:

- Low Heat Dissipation and Energy Saving:
  Due to low thermal conductivity, thermo pipe systems reach their operating temperature much faster than metal piping systems do. Thus, less energy is wasted in heating the pipes and less insulation is needed, figure 1,
- Low Friction Loss:
  The smoothness of internal surface of pipe with no porosities leads to low friction coefficient which results in low friction loss with high velocities.
- No Corrosion Resistance:
  Thermo pipes don't rust given that their chemical resistance for most chemicals and all water types,.
- Thermal Memory :
  In practice, any incorrect bend or twist can be easily rectified. If thermo pipe (CLPE) is heated to its softening temperature (135°C), it retains its original shape.

Table 1: Mechanical and thermal properties of thermo pipes [1-2].

Thermo pipe Property	Polypropylene Random Cpolymer (PPRC)	Cross-linked Polyethylene CLPE (Thermopex)
Density, ρ	895 kg/m^3	930 kg/m^3
Melting range, M_p	140-150 °C	
Yield stress, σ_y	21 MPa	
Fracture stress, σ_f	40 MPa	
Percent elongation, $e\%$	800	
Brinell Hardness, HB	40 MPa	
Mod. of elasticity, E	0.8 GPa	
Shear modulus, G, at:		
0°C	1100 MPa	
10°C	770 MPa	
50°C	180 MPa	
60°C	140 MPa	
80°C		
100°C		
Impact stress, σ_{imp}	No break at -10°C	No break at -20°C No break at +20°C
Thermal coefficient, α	1.5 x 10^4	1.4 x 10^4
Thermal conductive., k	0.24 W/mK	0.41 W/mK
Specific heat, c	2 kJ / kgK	

- Quit Water Flow And Less Noise:
  The high insulation value of CLPE reduces noise level significantly and damps water hammer. The elasticity of PPCR is 257 times higher than that of steel.

A thermo pipe system will absorb water hammers, which cause annoying vibration noise inside the building

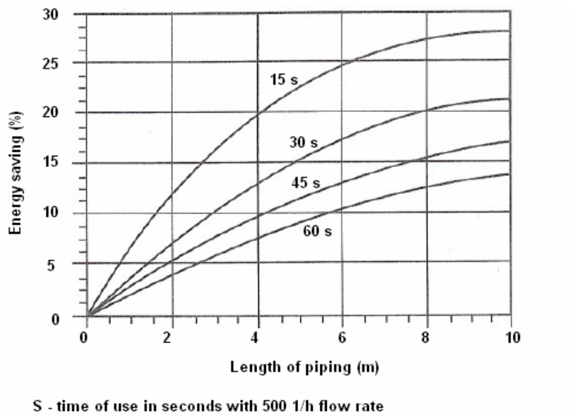

Figure 1: Percentage energy saving under transient conditions

Table 2: Operating temperature, pressure and service life for PPRC and CLPE

Operating temperature (°C)		Servicelife (year)	
PPRC	CLPE	PPRC	CLPE
20	20	50	50
40	40	50	50
60	60	50	50
-	70	-	50
80	80	50	25
-	90	-	10
95	95	50	10

Operating pressure (bar)	
PPRC	CLPE
20	12.5
20	10.4
12.6	8
-	7
7.8	6
-	5.5
5.2	5

- *Hygienic And Nontoxic*
  Thermo pipe systems are not toxic in line with current international standards, and they meet international standards for drinking water systems.
- *Frost Resistance*
  Thermo pipe will not burst in cold weather. The elasticity of thermo-pipe material allows the pipe to increase in cross-sectional diameter according to volume of the frozen material. For example the operating- temperature range is +95°C to -100 °C for CLPE
- *Long Life*
  The molecule structure of thermo-pipes material and special additives ensure a high mechanical resistance and a long life depending on operating temperature and pressure. A thermo pipe system can be expected endure for 50 years.
- *Abrasion Resistance*
  Abrasion resistance of thermo piping is four times equal to that of metal piping, allowing higher water velocities up to 7 m/s without corrosion problems.

2. Theoretical Background

2.1. Properties Of Thermo-Pipe Materials

2.1.1. Thermal conductivity k

Thermal conductivities of thermo-pipe materials are $k = 0.24$ W/mk(for PPCP) and $k = 0.41$ W/mk (for CLPE), as shown in table 1.

These values are too small compared to $k = 45$ to 60 W/mk for steel and $k = 300$ to 400 W/mk for copper.

This means that the thermo-pipe materials are of high level of thermal insulation, which guarantees low heat loss on the part of the fluid transported. This lead to minimal drop in temperature between the hot water source and the delivery points with energy saving [1].

The low thermal conductivity value of thermo-pipe materials causes strong reduction in the formation of condensation on the outside of the pipe; a phenomenon that happens frequently on metal pipes in some temperature and humidity conditions.

Due to low thermal conductivity, thermo-piping systems reach their operating temperature much faster than metal piping systems do, consequently less energy is dissipated and less Isolation is needed. The percentage of energy saving under transient conditions is shown in figure 1, where energy saving percentage (%) is drawn versus length of piping (m) for different time periods of use and with 500 l/h flow rate, [1].The thermo pipes are also very poor electrical conductor. In addition, no punctures will occur because of any stray current.

2.1.2. Hoop Stress and Internal Pressure

The relationship between the maximum operating pressure and the hoop stress of the thermo pipe is given by the following equation, [2]

$$p = 20\, t\, \sigma / (d-t) \qquad (1)$$

p = internal pressure (bar),
σ = hoop stress (MPa),
d = outside diameter of the pipe
t = wall thickness (mm)

2.1.3. Operating Temperature and Pressure

Thermopex in general can withstand on operation pressures up to 12.5 bar for 50 years of service life, also a temperature range between 95°C to (-100°).

2.1.4. Dimensions of The Thermo Pipes

Thermo pipes PPRC and CLPE are manufactured in the following dimensions according to DIN 8077 / 78 and DIN16893 standards, respectively. They are available in the following diameters as shown in tables 3.a and 3-b.

1. For fluids and gases, the required inside diameter can be calculated from the following equation [1];

$$d_i = 35.7 \sqrt{(Q/v)} \qquad (2)$$

Q = flow rate, (l/s),
v = fluid flow speed, (m/s).
Reference values for v are: 1 to 3 m/s for liquids, and, 10 to 30 m/s for gases.

2. For heating systems:

$$d_i = 0.6 \sqrt{H/(v\, \Delta T)} \qquad (3)$$

2.1.5. Total Loss of Pressure

The total system head loss in pressure is obtained by adding together continuous and localized loss of pressure [1].

$$\Delta p = L \times R + 10Z \qquad (4)$$

Δp = total pressure loss, (mm c.a.)
L = Pipe length (m),
R = continuous loss of pressure, (mm c.a./m)

Table 3-a: Thermo pipe PPRC dimensions with nominal working pressure of 20 bar (*: PN20) and of 10 bar (**: PN10)

d_o mm (in)	t mm	d_i mm
16 (3/8)	2.7 *	10.6
20 (1/2)	3.4 *	13.2
25 (3/4)	4.2 *	16.6
32 (1)	5.4 *	21.2
40 (1.25)	6.7 *	26.6
50 (1.55)	8.4 *	33.2
63 (2)	10.5 *	50
75 (2.5)	12.5 *	73.6
90 (3)	8.2 **	90
110 (4)	10 **	102.2
125 (5)	11.4 **	114.6
140 (5.5)	12.7 **	130.8
160 (6)	14.6 **	
d_o = outer diameter d_i = inner diameter t = wall thickness		

Table 3-b: Thermo pipe CLPE standards dimensions

d_o(mm)	T(mm)	di (mm)	L (m)
16	2	12	50, 100
20	2	16	50, 100
25	2.3	20	50
32	3	26	50

Z = localized pressure (mbar)

$Z = \Sigma\, r \times v \times \gamma / 2g \cong$ (5)

γ = 999,7 kg/ m = specific weight of water,

g = 9.81 m/s = gravity acceleration,

v = speed of water (m/s) in the pipe'

r = coefficients,

Figure 2 shows pressure loss Z versus flow speeds v in relation to r-1 and water temperature of 10 °C.

2.1.6. Temperature effect on thermo pipe materials

2.1.6.1. Thermal expansion (elongation) of thermo pipes

The pipe expansion ΔL can be calculated from the basic formula [1]

$\Delta L = \alpha \times L \times \Delta T$ (6)

ΔL = pipe expansion, (mm)

α = thermal expansion coefficient of Thermo pipe, $\alpha_{avg} = 0.15\ °C^{-1}$,

L = pipe length (m),

Δt = temperature difference between warm water and ambient temperature (°C).

Figure 3 shows temperature difference versus pipe expansion. Since thermo pipes can be laid in walls or under floors in direct contact with lime, gypsum or cement.

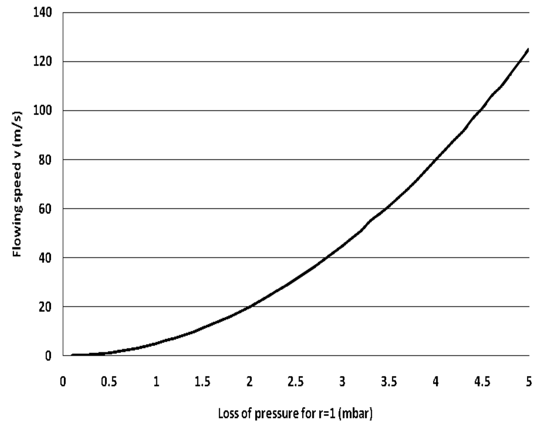

Figure 2: Loss of pressure z in relation to r=1 with water at 10 °C for various speeds v.

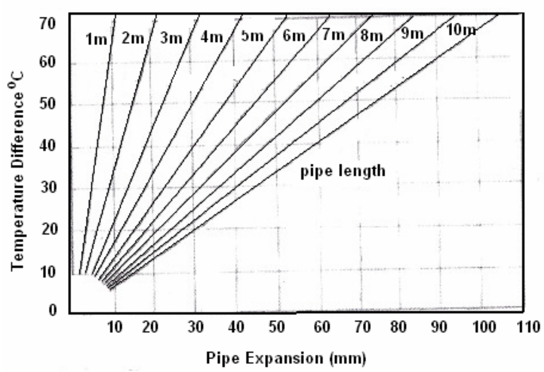

Figure 3: Pipe expansion dependence on temperature difference.

then the Previously mentioned values of ΔL and ΔT are only valid for surface mounted systems. Values are lower for pipes installed in the wall or under the floor.

2.1.6.2. Thermal Transition of Polymer

When polymer is exposed to temperature, thermal transition will occur. In other words, thermal transitions are changes that take place in polymer when it is heated. The melting of a crystallized polymer is one example on these changes. Determining the melting point of thermo pipe plastic materials is very important for this work. Differential Scanning Calorimetry (DSC) is a technique that is used to study the behavior of polymer when it is heated.

During heating, the polymer shows different characteristics:

1. *Constant Heat Flow Q/T and Heat Capacity Cp ,[1] It is:*

$(q/t)/(\Delta T/t) = q/\Delta T = C_p$, figure 4, And $q/t = f$ = heat flow (7)

2. *Glass transition temperature Tg*

Heating polymer after reaching a certain temperature will rise suddenly upward through $\Delta(q/t)$. This shifting in the heat flow means getting more heat flow and thus increasing the heat capacity of the polymer.This happens because the polymer has just gone through glass transition. Polymers have higher heat capacities than glass transition.

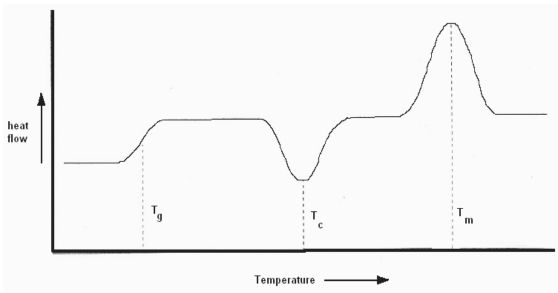

Figure 4: The whole DSC test operation.

Because of this change in heat capacity of polymers at glass transition temperature, DSC can be used to measure the polymer's glass transition temperature. Since the change in the heat flow does not occur suddenly, but over a temperature range ΔT_g, it makes picking one discrete T_g value complicated. Therefore, the middle of the incline is picked as Tg.

3. *Crystallization Temperature Tc*

Beyond glass transition, a polymer has a lot of mobility. It never stays in one position for a long time. When it reaches the right temperature, it will move into ordered arrangement (crystal arrangement). In a crystal arrangement, polymers emit heat. Drop in polymer heat can be seen as a full-size dip in the plot of heat flow q/t versus temperature T as shown in figure 4. The temperature at the lowest point of the dip is usually considered to be the polymer's crystallization T_c.

4. *Melting and Melting Point (Temperature) Tm*

Heating polymer beyond T_c will result in positive jump in the heat flow (melting transition) with melting point T_m. When the polymer reaches the melting temperature T_m, crystals start to fall apart and melt. The chains depart their ordered arrangement and start to move freely. For melting the polymer crystals, they must absorb energy (heat). Melting is a first order transition, i.e., when polymer reaches the melting temperature, the polymer's temperature will not rise until all the crystals have melted. Accordingly, the little heater under the sample pan has to supply the polymer with a lot of more heat in order to melt crystals and to keep temperature rising at the same rate as that of the reference pan. This extra-heat flow during melting displays as a peak on the DSC plot in figure 4.

3. Materials, Equipments and Experiments

3.1. Materials and Material Selection

Thermo pipes PPRC and thermopex CLPE investigated in this work are made of row materials according to international standards. Themopipes are made of polypropylene material that is randomly polymerized (PPRC) - applying European raw materials according to German DIN 8077 and DIN 8078 .Thermopex pipes are made of Poly Ethylene material that is created from European raw materials according to German DIN16892 and DIN16893.

The final product as pipes is investigated and tested. However, the chemical composition and analysis of these raw materials are beyond the scope of this research.

3.2. Tests and Equipments

The equipments include measurement tools, devices, and machines. Equipments used in this work will be discussed in sequence with the stages of their use throughout the experimental work.

Experimental work done on thermo pipes in this work includes the following:

1. tensile tests
2. differential Scanning Calorimetry (DSC) tests to determine the thermo pipe's melting point T_m and oxidation temperature T_o
3. Burst pressure tests

These tests are conducted at the RSS labs.

3.2.1. Tensile tests:

3.2.1.1. Samples Preparation:

Five almost flat samples from each thermo pipe types (PPRC and CLPE) were prepared. Each sample has the dimensions shown in figure 5. Not to forget that these samples are taken from pipes with dimensions shown in Table 3-a, therefore the samples are not perfect flat but with some curvature. Flat sheets of these materials were not available.

3.2.1.2. Calculations

The tension test is conducted by increasing changeable load at a constant strain rate to the specimen shown in figure 5, using the tensile machine AG-IS MS shown in figure 6. The purpose of this test is to obtain the stress-strain diagrams for PPRC and CLPE materials and to read mechanical properties belonging to these thermoplastic materials, such as: Young modulus E, yield stress σ_y, ultimate stress σ_u, elongation percent, area reduction percent, Poisson's ratio, fracture stress, and etc, The main relations used by tensile test to determine the mechanical properties can be summarized as follows [4]:

$$\sigma_{avg} = P/A_o \quad (8)$$

$$\varepsilon_{eng} = \delta/ L_o = (L_f - L_o)/ L_o \quad (9)$$

$$E = \sigma_y / \varepsilon_y \quad (10)$$

$$u_r = \int_0^{\varepsilon_y} \sigma \, d\varepsilon = \int_0^{\varepsilon_y} E\varepsilon \, d\varepsilon = ½ E \varepsilon^2 = ½ \sigma_y^2/ E \quad (11)$$

$$u_t = \int^{\varepsilon_f} \sigma \, d\varepsilon = 2/3\, \sigma_m \varepsilon_m \quad (12)$$

^{0}= area under the σ-ε curve up to fracture

$$B = 1/3\, E\, (1-2\nu) \quad (13)$$

$$e\% = (L_f - L_o)/ L_o * 100 \quad (14)$$

$$a\% = (A_o - A_f)/ A_o * 100 \quad (15)$$

  - Volume 2, Number 4 (ISSN 1995-6665)

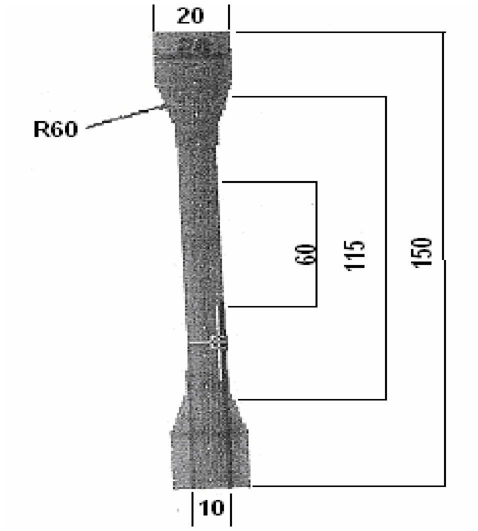

(a)

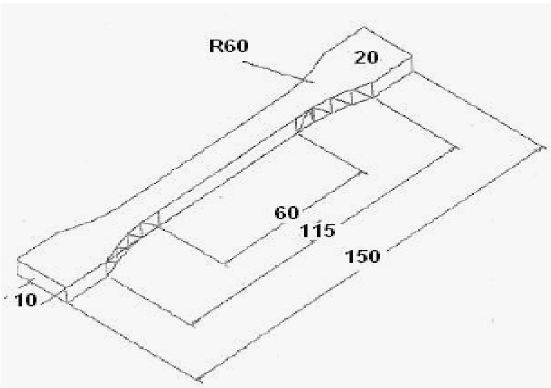

(b)

Figure 5: Polyethylene Specimen's dimension, (a), (b).

3.2.1.3. Equipments

a) Tensile Machine:

The tensile machine AG-IS MS series (table type) shown in figure 6 was used in this work.

b) Tensile Machine Camera:

Figure 7 shows the tensile machine camera used in this Work a single camera mode which uses only one camera is shown in figure 7-a. This mode was used to measure the peak-to-peak distance. The gauge length was measured as the distance between the gauge marks as shown in figures 7-b and 7-c.

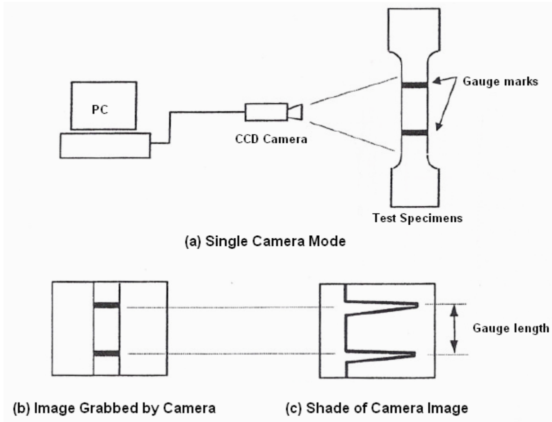

Figure 7: Tensile machine camera.

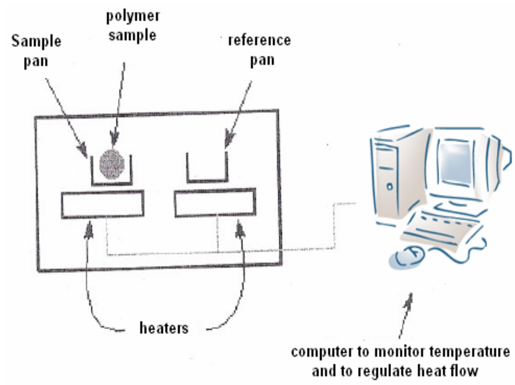

Figure 8: The DSC apparatus.

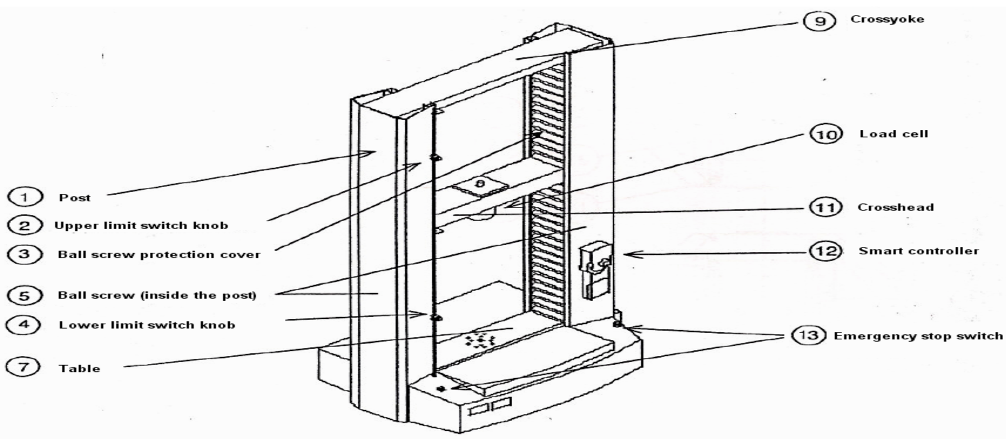

Figure 6: Main parts of the AG-IS MS series (Table-type) Mainframe [10].

3.2.2. Differential Scanning Calorimetry Test

3.2.2.1. Equipment :

DSC apparatus

Figure 8 shows the differential scanning calorimetry apparatus used in this work to measure the temperature of thermo pipes when exposed to temperature. The calorimetry is a known technique, and it is discussed in literature [4]

3.2.3. Pressure Burst Tests

3.2.3.1. Equipments:

Pressure Tester:The apparatus is a pressure tester machine with maximum pressure of 100 bars.

3.2.3.2. Samples

a) Sample a For PPRC Tests

Test conditions:

- Ambient Water Temperature = 20 °C
- Test Duration = 1 hour
- Sample Dimensions: L x d0 x t = 550 mm x 32 mm x 5.4 mm (three samples).

Table 4: Sample dimensions for the pipes PPRE and CLPE

Sample	Thickness (mm)		Width (mm)	
	PPRC	CLPE	PPRC	CLPE
1	5.66	2.07	10.073	10
2	5.76	2.01	10.20	10
3	5.63	2.02	10.167	10
4	5.77	2.10	10.20	10
5	5.60	2.13	10.18	10
Sample	Gauge length (mm)			
	PPRC	CLPE		
1	50	50		
2	50	50		
3	50	50		
4	50	50		
5	50	50		

b) For CLPE Tests

Test conditions:

- Ambient Water Temperature = 20 °C.
- Test Duration = 1 hour.
- Sample Dimensions: L x d0 x t = 500 mm x 20 mm x 2 mm (three samples).

4. Experimental Data and Results

4.1. Tensile Tests Results:

Tensile test were executed for the five specimens made of each pipe material PPRC and CLPE. The data of each sample is given in table 4.

Five stress-strain diagrams belonging to the five samples of material were obtained. Two representative diagrams for PPRC and CLPE are shown in figures 9 and 10, respectively.

Material properties obtained from these diagrams are tabulated in tables 5.

4.2. DSC Results

Melting points and oxidation temperatures were obtained from differential scanning calorimetry tests. Table 6 shows these values PPRC and CLPE pipes.

Table 7 shows some important material properties of pipes made of plastics (PPRC and CPLE), steel and copper for sake of comparison when used as hot water transporters in domestic and industrial applications.

5. Results and Discussion

- By considering the conditions when the tests were conducted at the RSS, unlike conditions followed by the *"World Plastics"*, results are in good agreement with those of the world plastics, [1-3].
- Results and materials properties given in table 6, E, u_t, ductility, costs, σ_y, thermal conductivity, melting point, oxidation temperature, and density show plastic pipes

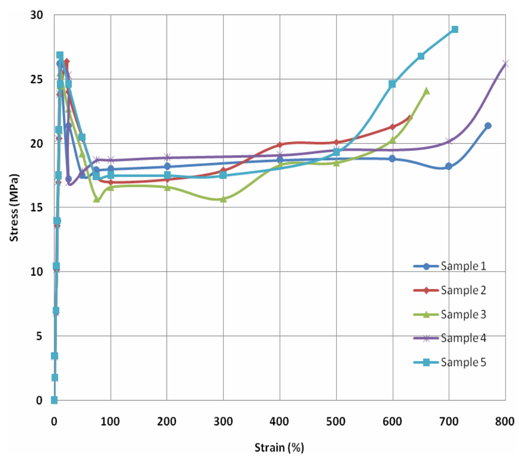

Figure 9: Stress-strain diagram for Thermo pipe (Copolymer polypropylene, PPRC).

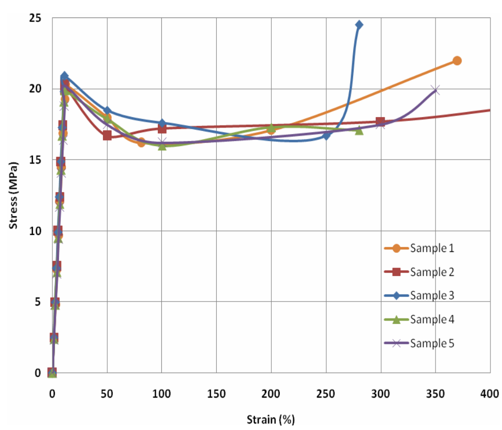

Figure 10: Stress-strain diagram for Thermopex (Cross-linked polyethylene, CLPE).

  - Volume 2, Number 4 (ISSN 1995-6665)

Table 5: Material properties of PPRC and CLPE pipe

Property	Sample 1	Sample 2	Sample 3	Sample 4	Sample 5	Average
σ_y (MPa)						
PPRC:	26.2	26.4	25.5	26.1	26.9	26.22
CLPE:	20.3	20.3	20.9	19.9	20.2	20.32
σ_f (MPa)						
PPRC:	21.4	22.0	24.1	26.2	28.9	24.52
CLPE:	22	18.7	24.5	17.1	19.9	20.44
E (MPa)						
PPRC:	238	240	231	261	245	243
CLPE:	169	185	190	181	168	178.6
u_r (MPa)						
PPRC:	1.44	1.45	1.40	1.31	1.48	1.42
CLPE:	1.22	1.12	1.15	1.09	1.21	1.16
u_t (Nmm/mm^3)						
PPRC:	109.85	92.4	106.1	139.73	136.79	116.97
CLPE :	54.27	52.36	45.73	31.92	46.43	46.14
B (N/mm^2)						
PPRC:	248.11	250	241.48	271.88	254.74	253.24
CLPE:	-375.93	-410.10	-422.22	-402.02	-374.07	-396.87
e%						
PPRC:	770	630	660	800	710	714
CLPE:	370	420	280	280	350	340
a% PPRC:	88.51	86.3	86.84	88.89	87.65	87.64
CLPE:	78.72	80.77	73.68	73.68	77.78	76.93
ε_y (mm/mm)						
PPRC:	11	11	11	10	11	10.8
CLPE:						
ε_f (mm/mm)						
PPRC:	770	630	660	800	710	714
CLPE:	370	420	280	280	350	340

Table 6: Melting-point temperature T_m and oxidation temperature T_{ox}

	Melting point Tm (°C)		Oxidation temperature T_{ox} (°C)	
	Trial 1	Trial 2	Trial 1	Trial 2
Thermo pipe PPRC	143.7	145.7	274.1	275.1
Thermo-pex CLPE	128.1	128.4	257.3	258.2

5.1. pressure burst results

Table 8: pressure burst results

Sample	Pressure (bar)		Notes
	PPRC	CLPE	
1	100	58	No burst
2	100	57.5	No burst
3	100	58.5	No burst

Table 7: Some important properties of plastic pipes (PPRC and CLPE) and metal pipes (steel and copper)

No.	Property	PPRC	CLPE	Steel	Copper
1	Service life (y)	up to 50	up to 50	up to 15	up to 20
2	Density (kg/m^3)	895	930	7850	8900
3	Workability	Easy	easy	difficult	Difficult
4	Maintenance	Easy	easy	Difficult	Difficult
5	Corrosion resistance	no corrosion	no corrosion	high corrosion	
6	Melting point (°C)	144.7	128.3		
7	Abrasion resistance	$4*A_{met}$	$4*A_{met}$	A_{met}	A_{met}
8	Fluid speed Profile	low friction loss	low friction loss	high friction loss	high friction loss
9	Frost resistance (bursting probability)	No burst	no burst	burst	burst
10	Linear thermal Coefficient at 20°C (10^{-4}/°C)	1.5	1.4- 2	0.10- 0.18	0.166-0.176
11	Specific heat at 20°C (kJ/kg.°C)	2	2.3	O.44	0.385
12	Thermal conductivity at 20°C (W/m.°C)	0.24	0.41	45- 60	300- 400
13	Costs	cheaper than CLPE	more expensive than PPRC	Expensive	Very expensive
14	Electrical Conductivity	very low	very low	high	high

- PPRC are more suitable as thermo pipes than plastic pipes CRPE.
- As a general result, plastic pipes are more suitable than steel pipe and copper pipes as thermo pipes (pipes for transporting hot water). PPRC pipes are more convenient than CRPE pipes for thermo pipes.
- The melting points of both PPRC and CRPE are so high that no fear of melting if these pipes are used for transporting hot water even when boiling point is 100°C.
- PPRC and CRPE pipes are hygienic because no possibility of oxidation of these pipes due to their high oxidation temperatures.
- Thermal conductivity of PPRC is lower than that of CRPE. This means that heat transfer rate of PPRC pipes is lower than that of CRPE pipes. PPRC can preserve the water temperature better than CRPE pipes and PPRC can achieve a longer life than CRPE, [5].

- PPRC has greater linear thermal expansion coefficient α than that of CRPE. For the same ΔT and the same length, the final length of PPRC pipe will be greater than that of CRPE pipe. [$\Delta L = L_2 - L_1 = \alpha\ \Delta T\ L_1 \Rightarrow L_2 = L_1\ (1+\ \alpha\ \Delta T) \Rightarrow L_2 > L_1$]
  CRPE is better than PPRC regarding this property since it resists thermal deformation more than PPRC does. Plastic pipes are worse concerning this property than metal pipes.
- The heat energy amount that can be stored by CRPE is higher that of PPRC. This is because of the fact that specific heat of CRPE is greater than that of PPRC, which means that CRPE possesses a greater specific heat capacity than PPRC. Again, CRPE is better in relation to this property than PPRC.
- In this research, the basic important tests such as tensile tests, differential scanning calorimetry tests, and pressure bursting tests, were conducted. As a future work, It is recommend to run the following test: bending, fatigue, torsion and shear tests.

References

[1] World Plastic for construction industries. Thermopipe Polypropylene Random Copolymer. Advanced piping system. Catalog, E-mail: wp@nol.com.jo.

[2] World Plastic for construction industries. Thermopex (cross-linked polyethylene), advanced piping systems. Catalog, E-mail: wp@nol.com.jo.

[3] Word Plastics for construction plastics. Advanced piping systems, www.advanced-piping.com

[4] Gere Jones M. "Mechanics of Material",. 6th Edition, Thomson, Brooks/Cole, 2004.

[5] Incropera Frank P, DeWitt, David P., "Heat and mass transfer", 5th Edition. Wiley, http:// www.pslc.ws/mactest/dsc.htm, 2002.

[6] Raymond A. Higgens, "Properties of Engineering Materials", 2nd. Edition, Arnold,. Royal Scientific Society Catalogs, 1992.

JJMIE
Volume 2, Number 4, December. 2008
ISSN 1995-6665
Pages 201 - 208
Jordan Journal of Mechanical and Industrial Engineering

Delineation of Frost Characteristics on Cold Walls by Using a New Formula for Psychrometrics Demarcation Boundary

Ahmed Hamza H. Ali*

Department of Mechanical Engineering, Faculty of Engineering, Assiut University, Assiut 71516, Egypt

Abstract

In this study, a direct new formula that predicts frost formation on cold walls corresponding to psychrometric-subsaturated. The new formula uses data of the entering air dry-bulb temperature and absolute humidity and absolute humidity of air at saturation corresponding to the coil surface temperature. To validate the formula, case studies of demarcation criteria for frost formation on evaporator coil using experimental measured data and on walls of cold storage freezer using measured data from literature are used. Results completely match with the graphic plot of the data on the psychrometric chart. In case of cold storage freezers, results clearly show that a greater demarcation criteria value indicates frost formation under severe condition, as snow-like with low density and thermal conductivity.

Keywords: frost formation; psychrometric-subsaturated; demarcation criteri; and Psychrometric-Supersaturated Region

Nomenclature

Alphabetic symbols

a, b and c: coefficient in equation 2
D : demarcation condition,-*
P : partial pressure, Pa
P : total pressure, Pa.
RH: relative humidity, %
T : temperature, Co
UA: total conductivity, W/ oC.
W : humidity ratio, kgH2O/kgda

Subscripts

a: air
cs: coil surface

critical: critical
da : dry air
DB : dry bulb
Dry : dry
Fr : frost
H_2O : water vapor
Ice : ice
In : entering
Load : load
Out : leaving
Ref : refrigerant
S : saturation
Scw : supercooled water
Sw : saturated water

* Corresponding author.e-mail: ah-hamza@aun.edu.eg.

1. Introduction

Frost problems often occur in cold storage freezers because of infiltration of warm humid air through access doors. When the cold storage freezer door open, air at the upper layers in the docks rushes inside freezer in order to replace ex-filtrated air and it mixes with freezer air in the upper layers of the freezer. This air mixture creates fog and ice fog crystals that deposit on the freezer walls and products. Also, as moist air is cooled by passing over evaporator coil that has surface temperature below both dew point and freezing point of the air, near the coil surface, frost forms and deposits on the coil surface. The word frost in this study refers to the formation of ice crystals in air or on surfaces, either by freezing of a dew droplet or by a phase change from water vapor to ice directly. Frost deposition on the walls of cold storage freezers and evaporator coil is usually undesirable. The main problems associated with frost growth on an evaporator coil are the decline in heat exchanger efficiency resulting from an insulating effect of the frost layer and the rising pressure drop due to a decreasing hydraulic diameter of the flow channel, which increases the energy consumption of the air-blowing fan. Whereas, in cold storage freezers, products quality suffers as frost forms on products in the freezer. For these reasons frost must be removed be means of defrost for restoring coil performance or to be removed away manually form the walls and products in cold storage freezers. The physical structure of frost layer forming on an evaporator coil depends on many factors, including the evaporator coil design and its operating temperature, entering air dry-bulb temperature and relative humidity, and face velocity of air entering the coil, Şahin [1]. Dietenberger [2] characterizes the first regime of frost formation over cold wall as follows: the initial frost layer can begin in one of two ways. In the first case, initial condensation occurs at nucleation sites on the wall resulting from a critical supersaturation. In the other case (i.e. for a very cold wall), boundary layer fogging occurs, and fog becomes the major source for water droplet condensation on the wall. For cooling of moist air at freezer temperatures, Smith [3] proposes a concept of frost formation in accordance with a graphic plot on a psychrometric chart. The concept suggests that when the line representing temperature and absolute humidity of the air cross saturation curve of the psychrometric chart (i.e., become supersaturated), the unfavorable frost formation occurs.

Once a supersaturated state exists in air, whose temperature is below freezing point, fog and ice fog are likely to form, based on operating temperatures. This formed frost under supersaturated condition has affinity to deposit on any surface in their path inside the freezer. When it is deposited over evaporator coil, it has higher impact on reduction of coil airflow rate, and it needs more energy to defrost than frost formed under less extreme conditions do.

A symptom of such frost when formed on evaporator coil is that the coil performance deteriorates rapidly and coils seemingly require near-continuous defrosting. Smith [4 and 5] discusses his concept [3] of applied psychrometrics in typical industrial freezers issues pertaining to latent heat - equipment-related loads. Sherif et al. [6], Mago and Sherif [7], and, Cleland and O'Hagan [8] experimentally confirm Smith's concept [3] by using real size evaporator coil.

Throughout the literature, it is evident that few researches (Smith, Sherif and coworkers, and, Cleland and coworkers) investigate demarcation boundary of frost formation inside cold storage freezers or real size evaporator coil, either in subsaturated or supersaturated regions with the aid of the psychrometric chart. In addition, Cleland and O'Hagan [8] publish the only available formula in literature, for delineation of the demarcation criteria that declare whether frost is formed in supersaturated and subsaturated regions, based on Smith [3] concept. They use the definition of a critical load sensible heat ratio (SHR), and they report that if the actual heat loads have a SHR, less than the critical value, then unfavorable frost will be expected to occur. Cleland [9 and 10] uses this demarcation criterion to explore aspects of refrigerated facility design and operation, and to consider the effect of infiltration air into a frozen warehouse and loading dock, respectively. Cleland and O'Hagan [8] report that data used is not of sufficient quality either to fully prove or disprove proposed transition between frost types.

For cold storage freezers, prediction of frost formation type guides refrigerating system designers in their quest for improved designs and efficient operation. Therefore, in this study, a direct formula predicting demarcation boundaries in psychrometric saturation of delineation frost formation on cold walls is presented. It indicates if frost is formed in psychrometric-subsaturated or supersaturated regions. The formula uses data of the entering air dry-bulb temperature, absolute humidity, and the absolute humidity of air at saturation correspondence to the coil surface temperature. Case studies from experimental measurements, as well as measured data from literature, are used to validate the formula. Subsequently, characteristics of frost formed on the cold walls for the studied cases are described.

2. Analysis

The following premises are applied on psychrometric chart too formulate the demarcation boundaries in psychrometric chart in order to declare whether frost formed in psychrometric-subsaturated or supersaturated regions, and to delineate the frost type formed on cold walls, using Smith (1989) concept, a straight-line path describing air-cooling process, line (C-D) in subsaturation or line (A-D) in supersaturated case as shown in Figure 1; and is plotted on the psychrometric chart. The beginning of the path line is the entering air condition, while the end-point of the path line is coil surface temperature or cold storage freezer temperature; and lies on the psychrometric saturation curve. In this step, straight-line approximation approach of Stoecker [11] and ASHRAE [12] - for cooling and dehumidification through a coil that relates the change in conditions of the air passing the cooling coil- is used.

Demarcation from subsaturated to supersaturated regions, critical condition, and lay at minimum coil refrigeration temperature correspond to the lowest coil surface temperature, which can occur without causing straight-line path to invade the supersaturated region of the chart. In the premise, line (B-D) in Figure 1 is plotted tangential to the psychrometric saturation curve at the coil surface temperature or cold storage freezer temperature.

If the air path invades the supersaturated region, the case of line (A-D) in Figure 1, frost precipitation occurs within the airstreams, and it deposits on cold walls in their path. Where the path does not invade the supersaturated region (e.g. the case of line C-D in Figure 1), the coil-frost is of ice-like quality, and formed over the cold walls.

The following points should be addressed with the premises plotted in Figure 1. The refrigerant evaporation temperature, T_{ref}, can be occasionally used instead of coil surface temperature, T_{cs} (i.e. point D' in Figure 1). Indeed, using (T_{ref}) represents a minimum border for T_{cs}, and will lead to conservative estimates of the demarcation boundaries as frost is formed in the supersaturation region. Another point is that in case of evaporator coil - as the time passes frost layer thickness increases- frost surface temperature increases. It should be used as the end-point of the straight-line approach on psychrometric saturation curve, point D'' in Figure 1. In this case, the condition for frost formation shifts the demarcation boundaries slightly into subsaturated region.

To alter the graphic concept into a formula, an equation is required to relate air absolute humidity at saturation condition with air dry-bulb temperature and psychrometrics saturation curve. The absolute humidity at saturation, $W_s(T_a)$, as function of the air dry-bulb temperature is calculated from ASHRAE [13] by:

$$W_s(T_a) = 0.622 \left(\frac{p_s(T_a)}{P_a - p_s(T_a)} \right) \quad (1)$$

Where P_a is total static pressure of the air in Pa, and $p_s(T_a)$ is the saturation vapor pressure in Pa as a function of air dry-bulb temperature, T_a, in ^oC. Magnus [14] equation, which is the fit to the Clausius–Clapeyron equation for $p_s(T_a)$ is used in this study and is given by

$$p_s(T_a) = a \quad \exp\left(\frac{bT_a}{c + T_a} \right) \quad (2)$$

The coefficients a, b and c are set, and they are obtained from correlation of measured data. Magnus [14] equation is the most widely used approximation for calculation of $p_s(T_a)$ in terms of accuracy and usability in analytical expressions.

In the literature, there are different set of coefficients for Magnus equation.

In this study, selection of such set is based on the deviations between the tabulated values in ASHRAE [13] for absolute humidity at saturation with correspondence values calculated by a set of coefficients using eqs. (1 and 2).

Set of coefficients obtained from Magnus [14], Sonntag [15], WMO [16], and Whiteman et al. [17]. Their validity temperature range are presented in Tables (1 and 2) for both saturation vapor pressure with water and ice, respectively. The calculated correspondences of deviation values to each set at certain temperature range are also shown in last rows of Tables (1 and 2). As Table 1 shows, for absolute humidity at saturation with water, the minimum deviation is obtained when using Whiteman *et al.* [17] set of coefficients.

As Table 1 shows, for absolute humidity at saturation with ice, the minimum deviations are obtained by using either WMO [16] or Whiteman *et al.* [17] sets of coefficients; and are almost equal.

Only, Whiteman *et al.* [17] presents an extra set of coefficients for saturation vapor pressure with super cooled water, the case of fog in supersaturated region. Therefore, the set of coefficients of Whiteman et al. [17] shown in Table 3 for the cases of saturation vapor pressure over water, super cooled water, and ice will be used in this study.

To calculate the demarcation boundaries that define whether the frost is formed in psychrometric subsaturated or supersaturated regions in psychrometrics saturation, the tangent line (B-D) in Figure 1, and the slope of approach line (B-D) to the psychrometric saturation curve equal the differentiation of equation 1. For this purpose, equation 1 is approximated by:

$$W_s(T_a) \approx 0.622 \left(\frac{p_s(T_a)}{P_a} \right) \quad (3)$$

The deviations among tabulated values in ASHRAE [13] for the absolute humidity at saturation with correspondence values were calculated using equation 3 in the temperature range from -40 to 0 ^oC is ranged from 0.552% to 0.991%. While, that was calculated with equation 1 as shown in Table 2. A set of coefficients of Whiteman et al. [17] ranged from 0.47% to 0.6%. Therefore, a less complicated formula of the critical demarcation boundary and the slope of the line (B-D) in Figure 1 is the differential of equation 3 at the coil surface temperature, T_{sc}, in ^oC is given by:

Table 1:Coefficients of equation 2 for saturated vapor pressure over water and deviations of W_s with ASHRAE [13] values.

	Magnus [14]	Sonntag [15]	WMO [16]	Whiteman et al. [17]
a	603.7074	611.213	611.2	610.78
b	17.1485	17.5043	17.62	17.0809
c	234.69	241.2	243.12	234.175
Valid in T_a range	-20 to 118 °C	-30 to 70 °C	-45 to 60 °C	-60 to 20°C
$\frac{W_{s,ASHRAE} - W_s}{W_{s,ASHRAE}}$	1.2% to 1.6%	0.38% to	0.38% to	0.26% to 0.44%
(T_a range 0 to 20°C)		0.59%	0.69%	

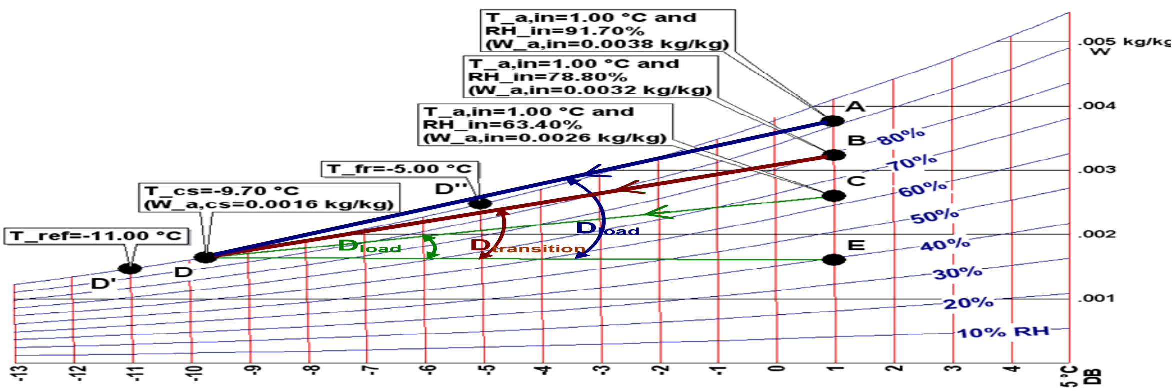

Figure 1 : Psychrometric plot of the demarcation criteria principles used to in this study.

TABLE 2: Coefficients of equation 2 for saturated vapor pressure over ice and deviations of W_s with ASHRAE [13] values.

	Sonntag [15]	WMO [16]	Whiteman et al. [17]
a	611.213	611.2	610.71
b	17.5043	22.46	22.4429
c	241.2	272.62	272.44
Valid in T_a range	-60 to 0.01°C	-65 to 0°C	-60 to 0°C
$\frac{W_{sASHRAE} - W_s}{W_{sASHRAE}}$ (T_a range -40 to 0°C)	0.4% to 0.96%	0.39% to 0.52%	0.47% to 0.6%

TABLE 3: The coefficients used in this study for equation 2 from Whiteman et al. [17].

For saturation vapor pressure	a	b	C
over water	610.78	17.0809	234.175
over supercooled water	610.78	17.8436	245.425
over ice	610.71	22.4429	272.440

$$D_{critical} = \frac{\partial W_s(T)}{\partial T} = a\left(\frac{0.622}{P_a}\right)\left(\frac{b}{T_{cs}+c} - \frac{bT_{cs}}{(T_{cs}+c)^2}\right)\exp\left(\frac{bT_{cs}}{T_{cs}+c}\right)z \quad (4)$$

While the While the slop of the load line, either (C-D) or (A-D), is shown in Figure 1 and can be calculated by:

$$D_{load} = \frac{W_{a,in} - W_s(T_{cs})}{T_{a,in} - T_{cs}} \quad (5)$$

Where $W_{a,in}$ is the absolute humidity of the air entering the coil. And $T_{a,in}$ and T_{cs} are the entering air dry-bulb temperature. And the coil surface temperature is approximated, in some cases, by the refrigerant evaporation temperature, respectively.

The Ratio of the slope of the load line, D_{load}, to the slope of the critical demarcation line, $D_{critical}$, is the criteria used in this study defining the demarcation boundaries that clarify whether the frost is formed in psychrometric-subsaturated or supersaturated regions. The Ratio is given by:

$$Ratio = \frac{D_{load}}{D_{critical}} \quad (6)$$

If the value of the Ratio is greater than 1.0, the load approach line is crossing the psychrometric saturation curve, and, in this case, frost is formed under supersaturation condition. Thus, as the air temperature falls below its dew point, it is possible for fog droplets to be nucleated, and ice fog is likely to form based on operating temperatures. If the value of the Ratio<1.0, the load approach line is completely in the psychrometric subsaturated region, and the formed frost on the cold walls is of ice-like quality.

3. Experimental Measurements

The test apparatus, experimental procedure, and data reduction techniques described in Ali and Ismail [18] are used to investigate the effect of frost formation on the evaporator coil in psychrometric-subsaturated region with minor modifications in the apparatus. The modifications are increasing the capillary tube length, and are cooling the last eight tubes in the condenser by water. However, with this apparatus and indoor environmental conditions, frost formation on the coil surface occurs at a face velocity of 0.612 m/s or less. The measurements were performed at the Heat Laboratory, Assiut University, Egypt.

4. Results and Discussion

Experimental measurements, as well as measured data from literature, are used to validate the formula for the demarcation criterion in cases of frost formation on the evaporator coil, and on the walls in cold storage freezer. Furthermore, the characteristic of the formed frost under this condition is described.

4.1. Frost Formation on the Evaporator Coil in Psychrometric-Subsaturated Region and its Characteristics

To validate the criterion of the demarcation boundaries presented in this study that declare whether the frost is formed on the coil in psychrometric-subsaturated or supersaturated regions and characteristics as well, an experiment was carried out at a higher freezing temperature with face velocity of 0.612 m/s for a number of hours. The operating conditions for this experiment, as well as the experimentally determined coil performance in terms of the ratio of the coil total conductivity (UA) under frost to dry conditions, is shown in Figure 2. The performance results shown in the figure indicate that at early stage of frost formation on the coil, the determined ratio of total conductivity at thin frost layer formation to dry coil condition, (UA_{fr}/UA_{dry}) for the presented operating conditions is 1.1. At 2.25 hours later. The frost layer thickness is increased, and consequently the ratio (UA_{fr}/UA_{dry}) is decreased to 0.86. To interpret these results, the demarcation criterion is applied to the operating condition correspondence to the points giving ratios (UA_{fr}/UA_{dry}) of 1.1 and 0.86, as shown in Figure 2 at time = 0 and 2.25 hours respectively. The plot of the operating point condition at time zero on psychrometric chart shown in Figure 3 are the points (A-A'-A"). wheras the condition at time=2.25h are points (B-B'-B"), respectively. The calculated criteria value correspondence to points (A-A'-A") is (Ratio) 0.84, while for points (B-B'-B") is 0.83, respectively. Comparing calculated criteria with plotted data on the psychrometric chart of Figure 3 indicates that they are completely matched. Clearly, with these calculated and plotted demarcation criterion values, the frost is formed on the coil during this experiment in psychrometric-subsaturated region. A photograph showing the formed frost on the coil face under this condition is also shown in the Figure 3. A close visual examination of the nature of frost formed on the coil under the aforementioned condition was found to be thin, fluffy, and dryer. This declares that the type and shape of frost crystal forms on the coil surface reflect its growth environment. Interpretation of the performance results as the ratio (UA_{fr}/UA_{dry}) was 1.1 in early stage of frost formation; and became 0.84 as frost thickness increases is explained as follows.

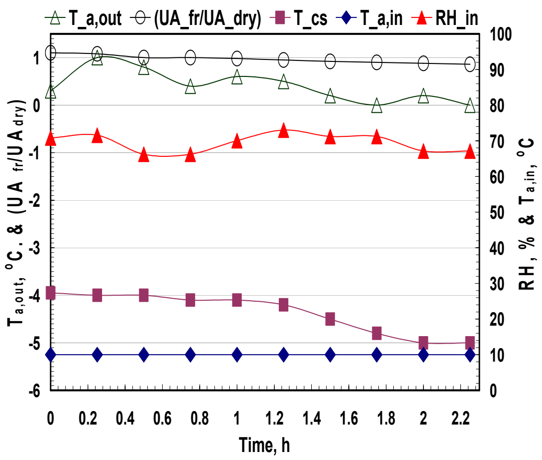

Figure 2 : Effect of formed frost at higher freezer temperature correspondence to psychrometric-subsaturated region on evaporator coil performance.

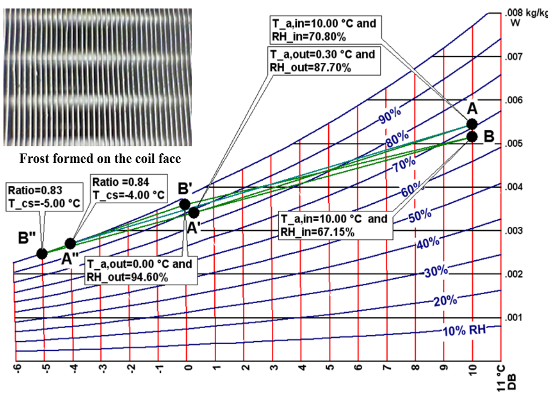

Figure 3 : Psychrometric plot of measured data to declare the demarcation criteria conditions.

For coil surface temperature range from 0 to -4 °C. And a condition of frost formation on the coil surface exists in psychrometric-subsaturated region. Under this operating condition, air temperature in near wall boundary is cold; and is having very small size moisture droplets. As these small droplets settled on the cold coil surface, it results in a formation of very light fluffy ice crystal shape made up of six sided individual ice crystals (plates) - based on Libbrecht [19] morphology diagram. These formed individual thin crystals (plates) create roughness over the coil surface that leads to this enhancement in the heat transfer coefficient i.e. the mass transfer coefficient. Moreover, a thin frost layer covering the coil surface leads to a higher driving force for mass transfer between mist droplets in the boundary layer and frost surface. The driving force is the vapor pressure difference over mist droplets and outer surface of the formed frost. This driving force is starting to exist with frost formation, see Figure 4. Figure 4 is a plot of vapor pressure difference of water (mist in subsaturated region), ice, vapor pressure difference of super cooled water (fog in supersaturated region), and ice. The pressure differences are calculated from equation 2 using the set of coefficients from Table 3. Due to the crystalline structure of ice, water molecules are not able to break free from an ice surface as easily as from a water surface.

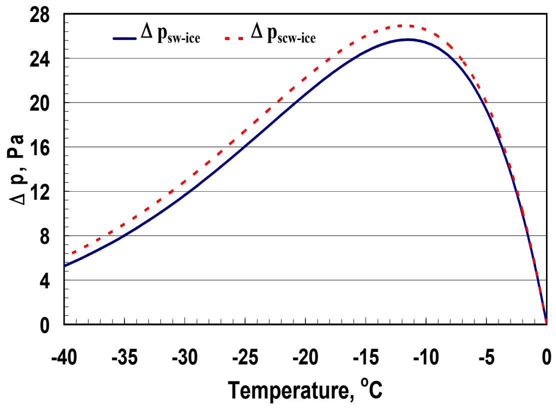

Figure 4: Vapor pressure differences of water and ice, and, super cooled water and ice as function of air dry-bulb temperature.

Thus, driving force of mass transfer toward ice surface is a consequence of ice crystals having lower saturation vapor pressures than liquid droplets do, which creates a gradient of high to low water molecules from liquid to ice that promotes ice growth based on the environmental temperature. This leads to in early stage of frost formation, and this is an enhancement in the rate of mass transfer. As mass transfer process continues, it is assumed that the part of the air water vapor content and all mist droplets in the boundary layer are transported to the frost surface; and freeze at the surface. In addition, diffused water vapor into the existing frost layer before it freezes. Therefore, as time passes, ice crystals on the coil surface join together into larger clumps consisting interlocked aggregates of thin crystals at the surface leading to the ratio (UA_{fr}/UA_{dry}) to be around unity. Under this operating condition, both frost thickness and surface temperature increase until frost surface temperature reach to 0°C. Consequently, the frost layer becomes denser and the heat transfer resistance is increased. The mentioned factors decrease heat and mass process through the frost layer. As a result, values of the ratio (UA_{fr}/UA_{dry}) are degraded to 0.86. It is worth to mention that the term favorable frost used by Smith [3], Cleland and O'Hagan [8] and Sherif et al. [8] for the frost formed correspondence to psychrometric-subsaturated region is not generally appropriate. It can be valid only at early stage of frost formation due to the enhancement in both heat transfer and mass transfer process at the evaporator coil surface. Otherwise, frost deposition on cold walls in refrigeration equipments is usually undesirable.

4.2. Case of Frost Formation on Cold Freezer Walls in Psychrometric-Supersaturated Region

The condition of frost formation inside cold storage freezers is different. It is mainly attributable to the infiltration of warm humid air into the freezer. Regarding formed frost inside cold storage freezers, data from the presentation of Simkins [20] is used to investigate demarcation criteria, and to declare whether frost is formed in either psychrometric subsaturated or supersaturated regions and the formed frost characteristics. Data from Simkins [20] on the infiltration air from docking area into the cold storage freezer and the freezer air temperature are plotted in Figure 5. In addition, data is used to calculate demarcation criteria value, which is found Ratio =3.76. From both the plot and demarcation criterion value, the frost formed on the cold storage freezer walls at this condition is correspondence to psychrometric-supersaturated region. Both the calculated criteria and the plotted data on the psychrometric chart of Figure 5 are completely matched. In addition, it can be recognized for this higher demarcation criteria value. The frost is formed under sever condition. Sever condition for frost formation due to the mixture of infiltration air and freezer air crossing the psychrometric–saturation line at temperature of 4.3 oC, straight-line approach as shown in Figure 5. As the air mixes in a supersaturated region with further cooling with the air fog, and begins to be formed in the mixture followed by formation of ice fog. The ice fog - when presented in the freezer- deposit on any surfaces inside the freezer. Characteristics and shape of ice crystal that forms in the mixed air inside the freezer depend on the environment, temperature and degree of supersaturation condition on psychrometric chart. And is explained as follows. From morphology diagram presented in Libbrecht [19] when air temperature ranges from 0 to - 4 oC. Thin plates are formed in psychrometric-subsaturated region and dendrites are formed in psychrometric-supersaturated region. If air temperature ranges from minus four to minus ten ^{o}C, columns are formed in subsaturated region and needles are formed in supersaturated region. When air temperature ranges from -10 to -22 ^{o}C, plates are formed in subsaturated region and dendrites are formed in supersaturated region. Yet, when the air temperature ranges from -22 to -35 ^{o}C, thick plates are formed in subsaturated region and columns are formed in supersaturated region. It can be concluded from the morphology diagram that when air temperature is lowered from 0 to -35 oC, the remarkable sequence of air borne ice crystal habit in psychrometric-supersaturated region. The present case of frost formed inside cold storage is dendrites-needles-dendrites-columns. Şahin [1] stated that whenever a crystal was transferred into a new environment, the continued growth assumed a new habit characteristic of the new conditions. Thus, when needles grown at temperatures between -3 and -5 ^{o}C and suddenly moved up in the chamber to about minus two ^{o}C, plates develop on their ends. In addition, when similar needles are lowered to about -14 ^{o}C, they prosuce a star shaped crystals. Such radical changes in crystal shape could not be produced by varying the supersaturation at constant temperature. But in some cases they were produced by only a degree or two changes in temperature at constant supersaturation.

The driving force of mass transfer when air temperature ranges from 0 to -40 °C is shown in Figure 4. As it is explained in previous section- It is higher in the case of saturation vapor pressure difference between super cooled water (fog) and in ice than the saturation vapor pressure difference in case of liquid water and ice at a given temperature. Therefore, when super cooled liquid water drops (fog) and ice particles co-exist in the mixed air inside the cold storage freezer, the liquid maintain a vapor pressure higher than that of the formed ice crystal tolerate. Thus, water vapor deposits on the ice particles surfaces as fast as it evaporates from the water drops. Since the air borne frost is formed in a supersaturated environment, higher mass transfer rate occurs when the mixed air inside the cold storage freezer reach temperature about -12.0 ^{o}C. At this temperature, the formed frost has a shape of dendrites that built over needles built over plates, at a temperature ranges from 0 to -10 ^{o}C. Moreover, ice crystals continue to grow in this sequence of composite dendrites-needles-dendrites-columns according to air mixed temperature, at expenses of the fog inside the freezer. Whenever, the mixed air reached to the freezer walls and stored products surfaces they deposit on them. The photograph shown in Figure 5 from the presentation of Simkins [20] shows the shape of the frost formed on the surfaces inside the cold storage freezer close to the docks door corresponding to the plotted operating condition.

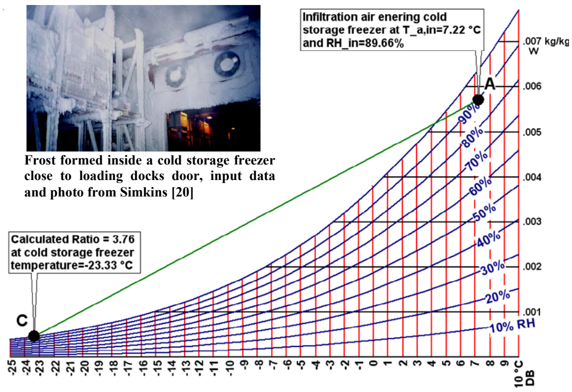

Figure 5: Psychrometric plot of a data from Simkins [20] for infiltration air from dCoking area into the cold storage.

Moreover, additional frost is formed by diffusion of water vapor from high partial vapor pressure conditions in the airstream to lower partial pressures conditions at the deposited frost surface. As shown in Figure 4, the driving force for diffusion of water vapor from high partial vapor pressure conditions in the air stream, either in subsaturation or supersaturation to lower partial pressures conditions at the frost surface is the function of air temperature. It begins at zero value at the triple point, 0.01 ^{o}C, and reaches up its maximum value at about -12 ^{o}C. In addition, it decreases again as the air temperature decreases. As the cold storage temperature is -23 ^{Co}, the diffusion portion from the air to the deposited frost is to be lowered. Consequently, this frost density and thermal conductivity are low, and the deposited frost consists of a porous structure that contains composite structural ice crystals and air pCokets. This can be recognized from the photograph of Simkins [20] shown in Figure 5.

4.3. Comparison of the Demarcation Criteria Formulas

The only available formula for delineating the demarcation criteria is published by Cleland and O'Hagan [8]. They show that the condition for the demarcation between the frost formed in supersaturated and subsaturated regions is given by the tangent line to the psychrometric saturation curve at the coil surface temperature using the definition of a critical load sensible heat ratio (SHR). They report that, if actual heat loads have a SHR less than critical value, then unfavorable frost is likely to Cocur, i.e. when the value of ($SHR_{critical}$ /SHR_{load}) is > 1.0. Their measured operating conditions are shown in Table 4, and are used in this study for validation and comparison of demarcation criteria formulas. Using Cleland and O'Hagan [8] measurement operating conditions as input to the present formula, the calculated criteria values and correspondences demarcation criteria values of Cleland and O'Hagan [8] are presented in Table 4. As shown in Table 4 few cases of demarcation criteria values agree, while most are not. To clarify which formula accurately gives demarcation criteria, plotting few data points in psychrometric chart are shown in Figure 6. The cases in which agreement of general trend of the demarcation criteria calculated by both formulas are the lines (A'-A"), (C'-C") and (D'-D") in Figure 6.

The calculated value are sometimes not as the same as shown in Table 4. In some points, Cleland and O'Hagan [8] demarcation criteria indicate that the frost is formed under critical conditions i.e. on border of psychrometric-saturation curve. The graphical plot in this case should be tangent psychrometric-saturation curve. While, when plotting this condition on psychrometric chart line (B'-B") in Figure 6 as well as the calculated demarcation criteria in this study shown in Table 4 indicates that the condition of frost formation is still in psychrometric-subsaturated region. Overall, there is no general trend of the differences between both calculated demarcation criteria values by Cleland and O'Hagan Cleland and O'Hagan [8] formula and that calculated values by this study formula, as shown in Table 4. However, as Cleland and O'Hagan [8] reported that although the concept of unfavorable frost is strongly supported, accurate measurement of coil frosting performance is difficult, and the data used here are not of sufficient quality to either fully prove or disprove the proposed transition between frost types. In addition, the calculated demarcation criteria values in this study match very well with the plotted data on the psychrometric chart. Thus, the present developed formula for calculation the demarcation criteria values are able to predict whether the frost is formed on the cold walls at certain operating condition is corresponding to either psychrometric-subsaturated or supersaturated region precisely.

5. Conclusions

A new direct formula predicting demarcation boundaries in psychrometric saturation for delineation the frost formation on cold walls is presented. The formula uses data of the entering air dry-bulb temperature, absolute humidity, the absolute humidity of air at saturation correspondence to the coil surface temperature.

TABLE 4: Comparison of the present results for the demarcation criteria with results of Cleland and O'Hagan [8]

Operating conditions of Cleland and O'Hagan (2003)			Demarcation criteria of Cleland and O'Hagan [8]	Demarcation criteria of the Present study	Plotted line in Fig. (6)
$T_{a,in}$, Co	RH_{in}, %	T_{ref}, Co			
-0.2	68	-9	0.93	0.57	
-0.4	68	-9.7	0.94	0.62	A'-A"
-1.6	72	-11.6	1	0.8	B'-B"
-0.8	83	-9.7	1	1	C'-C"
-1.6	82	-10.1	1.03	0.94	
-0.3	82	-8.4	1	0.9	
0.0	76	-10.5	1.06	0.94	
0.2	77	-10	1.04	0.93	
-0.6	78	-11.4	1.06	1.02	
-0.4	81	-10.2	1.01	1.01	
-1.4	87	-10.4	1	1.12	
-0.7	89	-8.9	1.06	1.11	
-1.8	87	-11.2	1.13	1.15	
-0.1	87	-9.1	1.17	1.11	
0.1	93	-10.5	1.17	1.39	
0.2	93	-10.6	1.17	1.41	D'-D"

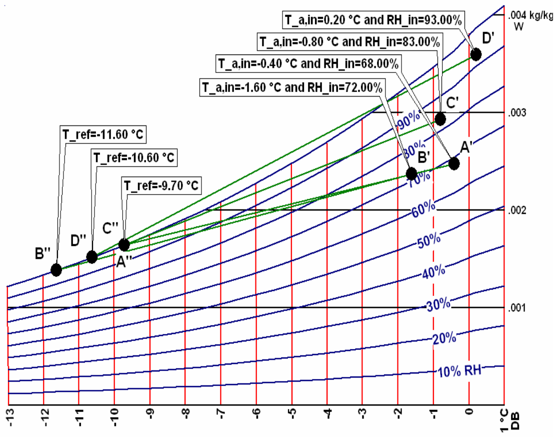

Figure 6: Psychrometric plot of data from Cleland andO'Hagan [8] to declare the demarcation criteria conditions.

The developed formula predicts either frost formation is in psychrometric-subsaturated or is in supersaturated region on the cold walls precisely. Case studies of demarcation criteria for frost formation on evaporator coil using experimental measured data and on walls of cold storage freezer using measured data from literature are used to validate the formula. The results of these studies are summarized as follows:

- The calculated demarcation criteria values in this study are complete when matched with the plotted data using the psychrometric chart. Therefore, the developed formula for calculation of the demarcation criteria values is able to predict whether the frost is formed on the cold walls at certain operating condition is corresponding to either psychrometric-subsaturated or supersaturated region.

- For an evaporator coil working at higher freezing temperature, the demarcation criteria is guided to interpret the enhancement in heat transfer and mass transfer coefficients at the operating condition. The characteristic of the frost formed on the coil under aforementioned condition was found to be thin, fluffy, and dryer. This declares that the type and shape of frost crystal forms on the coil surface reflect growth environment.
- In case of cold storage freezers, clearly a higher value of demarcation criteria is an indication that the frost is formed under severe condition. In such case, as the frost is formed corresponds to psychrometric-supersaturated region under severe condition. Its crystal composite of dendrites-needles-dendrites-columns is based on the environmental in the freezer.
- The term favorable frost used in the literature for the frost formed corresponding to psychrometric-subsaturated region is not generally appropriate. It can be valid only at early stage of frost formation due to the enhancement in both heat transfer and mass transfer prCoesses at the evaporator coil surface. Otherwise, frost deposition on cold walls in refrigeration equipments is usually undesirable.

REFERENCES

[1] Şahin, A.Z., "An analytical study of frost nucleation and growth during the crystal growth period". Heat and Mass Transfer, Vol. 30, 1995, 321-330.

[2] Dietenberger, M.A., "A Frost Formation Model and Its Validation under Various Experimental Conditions". NASA Contractor Report No.3595, 1982, 68p.

[3] Smith, G.R., "Theoretical cooling coil calculations at freezer temperatures to avoid unfavourable coil frost". ASHRAE Transactions, Vol. 95 (2), 1989, 1138-1148.

[4] Smith, G.R., "Latent heat, equipment-related load, and applied psychrometrics at freezer temperatures". ASHRAE Transactions, Vol. 98 (2), 1992, 649-657.

[5] Smith, G.R., "Coil icing and other opportunities within freezer/anteroom complexes". ASHRAE Transactions, Vol. 112 (2), 2006, 469-484.

[6] Sherif, S.A., Mago, P., Al-Mutawa, N.K., Theen, R.S., Bilen, K., "Psychrometrics in the supersaturated frost zone". ASHRAE Transactions, Vol.107 (2), 2001, 753-767.

[7] Mago, P.J. and Sherif, S.A., "Modeling the cooling prCoess path of a dehumidifying coil under frosting conditions". ASME J of Heat Transfer, Vol. 124, 2002, 1182–1191.

[8] Cleland, D.J. and O'Hagan, A.N., "Performance of an air-cooling coil under frosting conditions". ASHRAE Transactions, Vol. 109 (2), 2003, 243-250.

[9] Cleland, D.J., "Implications of coil frosting on systems design for low temperature applications". ASHRAE Transactions, Vol. 111 (1), 2005, 336-345.

[10] Cleland, D.J., "Cold store and loading dCok design to minimize condensation and coil frosting problems". In CD of the International Congress of Refrigeration, Beijing, 2007, Paper No. ICR07-D1-409.

[11] Stoecker, W.F., *"Industrial Refrigeration Handbook"*. Business News Publishing Company, Michigan,1988.

[12] ASHRAE, *2004 "ASHRAE Handbook - Systems and Equipment"*, ch.S21 SI. American SCoiety of Heating, Refrigerating and Air-Conditioning Engineers. Atlanta, Georgia, 2004.

[13] ASHRAE, *2005 "ASHRAE Handbook – Fundamental"s*, ,ch.F06 SI. American SCoiety of Heating, Refrigerating and Air-Conditioning Engineers. Atlanta, Georgia,2005.

[14] Magnus, G., "Versuche über die Spannkräfte des Wasserdampfs". Annalen der Physik und Chemie, Vol. 61 No.2, 1844, 225-248.

[15] Sonntag, D., "New values for the thermodynamic parameters of water vapor". Izmeritel'naya Tekhnika, Vol. 9, 1982, 54-56.

[16] WMO, *"Measurement of Humidity"*, 2006, ch.4, In, *Guide to Meteorological Instruments and Methods of Observation*. Preliminary seventh edition. Geneva – Switzerland.

[17] Whiteman, C.D., De Wekker, S.F.J., and Haiden, T., "Effect of dewfall and frostfall on nighttime cooling in a small, closed basin". J. of Applied Meteorology and Climatology, Vol. 46, 2007, 3-13.

[18] [Ali, Ahmed HamzaH. and Ismail, Ibrahim M. "Evaporator airside fouling: Effect on performance of room air conditioners and impact on indoor air quality". Int J of HVAC&R Research, Vol. 14 No.2, 2008, 209-219.

[19] Libbrecht, K.G., "Morphogenesis on ice: The physics of snow crystals". Engineering & Science, Vol. 64,No.1, 2001, 10-19.

[20] Simkins, B., "Dehumidification approaches for cold storage loading dCoks". Presentation at ASHRAE Winter Meeting, Atlanta, GA, 2001.

JJMIE
Volume 2, Number 4, December. 2008
ISSN 1995-6665
Pages 209- 214
Jordan Journal of Mechanical and Industrial Engineering

Optimization of Surface Roughness in End Milling on Mould Aluminium Alloys (AA6061-T6) Using Response Surface Method and Radian Basis Function Network

K.Kadirgama[a], M.M.Noor[a], N.M.Zuki.N.M[a], M.M. Rahman[a], M.R.M. Rejab[a], R. Daud[a], K. A. Abou-El-Hossein[b]

[a] *Faculty of Mechanical Engineering, Universiti Malaysia Pahang, P. O. Box 12, 25000 Kuantan. Malaysia*

[b] *Mechanical Engineering Department, University of Pretoria, South Africa*

Abstract

This paper is concerned with optimization of the surface roughness when milling Mould Aluminium alloys (AA6061-T6) with carbide coated inserts. Optimization of milling is very useful to reduce cost and time for machining mould. The approach is based on Response Surface Method (RSM) and Radian Basis Function Network (RBFN). RBFN was successfully used by Tsoa and Hocheng in their recent research. They used this network to predict thrust force and surface roughness in drilling. In this work, the objectives are to find the optimized parameters, and to find out the most dominant variables (cutting speed, federate, axial depth and radial depth). The optimized value has been used to develop a blow mould. The first order model and RBFN indicates that the feedrate is the most significant factors effecting surface roughness. RBFN predict surface roughness more accurately compared to RSM.

Keywords: Response Surface Method, Radian Basis Function Network, Surface roughness, Optimized

1. Introduction

Roughness plays an important role in determining how a real object will interact with its environment. Rough surfaces usually wear more quickly and have higher friction coefficients than smooth surfaces do. Roughness is often a good predictor of the performance of a mechanical component since irregularities in the surface may form nucleation sites for cracks or corrosion. Although roughness is usually undesirable, it is difficult and expensive to control during manufacturing. Decreasing roughness of a surface will usually exponentially increase its manufacturing costs. This often results in a trade-off between the manufacturing cost of a component and its performance in application.

Recent investigation performed by Alauddin *et al.* [1] has revealed that when the cutting speed is increased, productivity can be maximised, and surface quality can be improved. According to Hasegawa *et al.* [2], surface finish can be characterised by various parameters such as average roughness (Ra), smoothening depth (Rp), root mean square (Rq), and maximum peak-to-valley height (Rt).

The Present study uses average roughness (Ra) for the characterisation of surface finish since it is widely used in industry. By using factors such as cutting speed, feed rate and depth of cut, Hashmi and his coworkers [3, 4] have developed surface roughness models and determined the cutting conditions for 190 BHN steel and Inconel 718. EI-Baradie [5] and Bandyopadhyay [6] have shown that by increasing cutting speed, the productivity can be maximised, and the surface quality can be improved simultaneously. According to Gorlenko [7] and Thomas [8], surface finish can be characterised by various parameters. Numerous roughness height parameters such as average roughness (Ra), smoothening depth (Rp), root mean square (Rq), and maximum peak-to-valley height (Rt) can be strongly correlated. Mital and Mehta [9] have conducted a survey of previously developed surface roughness prediction models and factors influencing the surface roughness. They have found that most of the surface roughness prediction models have been developed for steels. Koren *et al.* [10] have proposed a model-based approach to sense tool wear and breakage. Algorithms and on-line training of model-based approach, using artificial intelligence methods, have been suggested by Koren *et al.* [10]. Tarng and Lee [11] have proposed the use of average and median force of each tooth in the milling operation.

* *Corresponding author.; e-mail:* Kumaran@ump.edu.my,

Measured by sensors, the average and median forces of each tooth have been used as input values. An appropriate threshold has been subsequently built to analyse information and detect the tool conditions.

Ko *et al.* [12] have introduced an unsupervised and a self-organised neural network combined with an adaptive time-series AR modelling algorithm to monitor tool breakage in milling operations. The machining parameters and average peak force have been used to build the AR model and neural network. Lee and Lee [13] have used neural network-based approach to show that by using force ratio, flank wear can be predicted within 8% to 11.9% error and by using force increment; the prediction error can be kept within 10.3% of the actual wear. Choudhury *et al.* [14] have used an optical fibre to sense the dimensional changes of the work-piece and correlated it to the tool wear using neural network approach. Dimla and Lister [15] have acquired the data of cutting force, vibration, and measured wear during turning. And neural network has been trained to distinguish the tool state.

2. Response Surface Method and RBFN

The Box-Behnken Design is normally used when performing non-sequential experiments i.e. performing the experiment only once. These designs allow efficient estimation of the first and second–order coefficients. Because Box-Behnken design has fewer design points, they are less expensive to run than central composite designs with the same number of factors. Box-Behnken Design do not have axial points, thus we can be sure that all design points fall within the safe operating. Box-Behnken Design also ensures that all factors are never set at their high levels simultaneously [16 - 18].

Genetic Algorithm (GA) was used to find the optimum weight, momentum, and step size to be used in RBFN. Later the optimum weight would be fed to the RBFN. Then training would be needed until the R.M.S.E reaches a satisfactory value. The training data acquired from Response Surface Method to RBFN mode, and the epoch number was 10,000 [19]. After 1,000 iterations, the RBFN was better enough to produce acceptable results. Transfer function used as sigmoid, but the momentum used was 0.7.

3. Experimental Setup

The 27 experiments were carried out on Haans machining centre with 6-axis as shown in Figure 1.a, and 90^0 tool holder as shown in Figure 1.b. Water soluble coolant was used in these experiments. Each experiment was stopped after 90 mm cutting length.

For the surface roughness measurement, surface roughness tester was used. Each experiment was repeated three times using a new cutting edge every time to obtain accurate reading of surface roughness. The physical and mechanical properties of the workpiece are shown in Table 1 and Table 2. After the preliminary investigation, suitable levels of factors were used in the statistical software to deduce the design parameters for Aluminium Alloys (AA6061-T6) as shown in Table 3. The lower and higher speed values selected were 100 m/s and 180 m/s, respectively. For the feed, the lower value was 0.1 mm/rev and the higher value was 0.2 mm/rev. For the axial depth, the higher value was 0.2 mm, and the lower value was 0.1 mm. And for the radial depth, the higher value was 5 mm, and lower value was 2 mm.

(a)

(b)

Figure 1. (a) Haans CNC milling with 6-axis ,(b) 90^0 tool holder

Table 1: Physical properties of workpiece

Component	Mg	Mn	Si	Ti	Zn
Wt %	0.8-1.2	Max 0.15	0.4-0.8	Max 0.15	Max 0.25
Component	Mn	Si	Ti	Zn	
Wt %	Max 0.15	0.4-0.8	Max 0.15	Max 0.25	

Table 3: Design Parameters

Cutting speed (m/min)	Feedrate (mm/rev)	Axial depth (mm)	Radial depth (mm)
140	0.15	0.1	5
140	0.15	0.15	3.5
100	0.15	0.15	5
140	0.15	0.15	3.5
180	0.15	0.2	3.5
180	0.15	0.15	2
100	0.2	0.15	3.5
140	0.15	0.15	3.5
180	0.15	0.15	5
100	0.15	0.2	3.5
140	0.2	0.1	3.5
180	0.1	0.15	3.5
140	0.15	0.2	2
180	0.15	0.1	3.5
140	0.1	0.15	2
140	0.15	0.2	5
100	0.15	0.1	3.5
140	0.2	0.15	2
100	0.15	0.15	2
140	0.2	0.15	5
140	0.1	0.1	3.5
140	0.2	0.2	3.5
140	0.15	0.1	2
100	0.1	0.15	3.5
180	0.2	0.15	3.5
140	0.1	0.2	3.5
140	0.1	0.15	5

4. Results and Discussion

The first order linear equation for predicting temperature is expressed as:

$$y = 0.5764 + 0.0049x_1 - 3.5850x_2 + 1.5383x_3 - 0.016x_4 \quad (1)$$

Generally, reduction in cutting speed and axial depth of cut will cause the surface roughness to become larger. On the other hand, increase in feedrate and radial depth will slightly cause a reduction in surface roughness.

Table 2: Mechanical properties for workpiece

Hardness, Brinell	95
Hardness, Knoop	120
Hardness, Rockwell A	40
Hardness, Rockwell B	60
Hardness, Vickers	107
Ultimate Tensile Strength	310 MPa
Tensile Yield Strength	276 MPa
Elongation at Break	12 %
Elongation at Break	17 %
Modulus of Elasticity	68.9 GPa
Density	2.7 g/cc

The feedrate has the most dominant effect on the surface roughness followed by the axial depth, cutting speed, and radial depth. A better surface roughness is obtained with the combination of low cutting speed, axial depth, high federate, and radial depth. Figure 2 shows surface roughness values obtained by experimentation and values predicted by first order model and RBFN. It is obvious that the predicted values by RBFN are very close to the experimental readings. The adequacy of first order model is verified using analysis of variance (ANOVA). The model was checked for its adequacy at a 95% level of confidence.

Table 4 indicates that the model is adequate since *P* values of lack-of-fit are not significant and F-statistics is 2.27. This implies that the model could fit and that it is adequate. The optimum value for surface roughness is 0.4261 µm, which corresponds to design variables: Cutting speed (m/min) =100, Feed rate (mm/rev) = 0.2, Axial depth (mm) = 0.1 and Radial depth (mm) = 5.0. The cutting conditions of fine surface in Figure (2.a) are Cutting speed (m/min) =100, Feed rate (mm/rev) = 0.2, Axial depth (mm) = 0.1 and Radial depth (mm) = 5.0 .And the cutting conditions for rough surface in Figure 2.b are Cutting speed (m/min) =140, Feed rate (mm/rev) = 0.15, Axial depth (mm) = 0.15 and Radial depth (mm) = 3.5. The sensitivity test was performed to obtain the variables that affect the surface roughness as shown in Figure 3a. The test shows that federate is the main domain followed by axial depth, radial depth, and cutting speed. Feed rate is the velocity at which the cutter is fed, that is, advanced against the work piece. Surface plot shows the correlation between the variables and response in Figure 3.b. A blow mould has been developed according to optimized parameters. The final product of the blow mould has a surface roughness of 0.45µm as shown in Figure 4. Eventually the time of machining has been reduced with the optimized method.

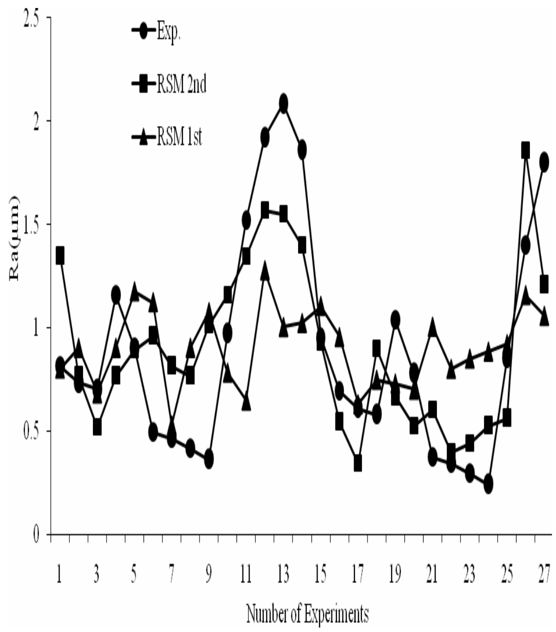

Figure 2: Comparison between experimental results and predicted results (First order & RBFN)

Table 4: ANOVA analysis

Source	DF	Seq SS	Adj SS	Adj MS	F	P
Regression	4	0.9309	0.9309	0.2327	0.78	0.552
Linear	4	0.9309	0.9309	0.2327	0.78	0.552
Residual Error	22	6.5937	6.5937	0.2997		
Lack-of-Fit	20	6.3151	6.3151	0.3158	2.27	0.351
Pure Error	2	0.2786	0.2786	0.1393		
Total	26	7.5246				

5. Conclusion

RBFN has been found to be the most successful technique to perform trend analysis of surface roughness with respect to various combinations of four cutting parameters (cutting speed, federate, axial depth, and radial depth). The models have been found to accurately represent surface roughness values with respect to experimental results.

Both RSM and RBFN model reveal that feedrate is the most significant design variable in determining surface roughness response as compared to others. With the model equations obtained, a designer can subsequently select the best combination of design variables for achieving optimum surface roughness. This eventually will reduce the machining time and save the cutting tools.

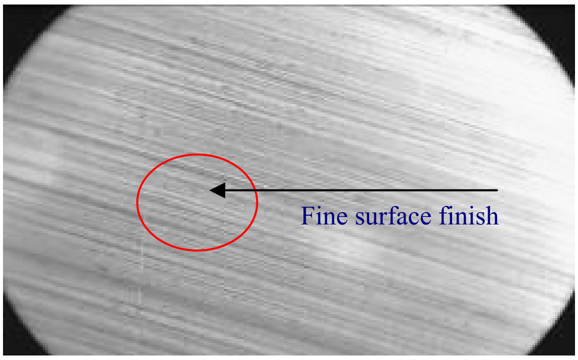

(a)

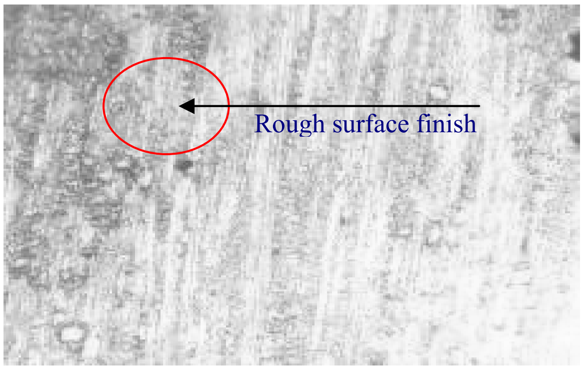

(b)

Figure 2. (a) Fine surface, (b) Rough surface.

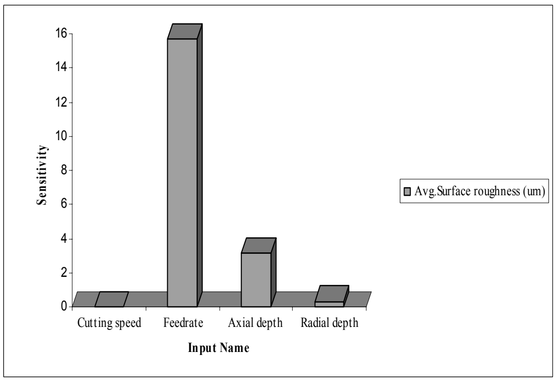

(a)

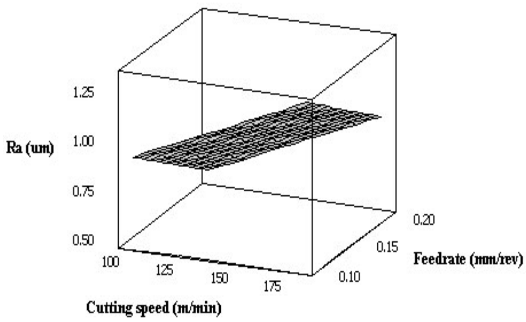

(b)

Figure 3: (a) Sensitivity Test ,(b) Surface plot.

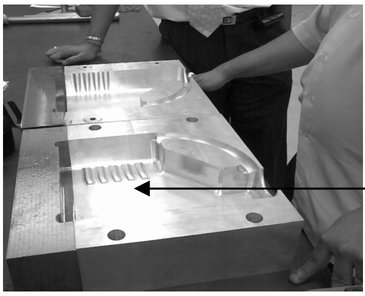

Figure 4: Blow mould

Acknowledgement

Financial support by University Malaysia Pahang is grateful acknowledged.

References

[1] M.Alauddin, M.A.EL Baradie, M.S.J.Hashmi,"Prediction of tool life in end milling by response surface methodology", Vol 71,1997, 456-465.

[2] M. Hasegawa, A. Seireg, R.A. Lindberg, "Surface roughness model for turning", Tribology International, December Vol,1976, 285–289.

[3] M. Alauddin, M.A. El Baradie, M.S.J. Hashmi, "Computer-aided analysis of a surface-roughness model for end milling", J. Mat. Proc. ,Vol .55,1995,123–127.

[4] M. Alauddin, M.A. El Baradie, M.S.J. Hashmi, "Optimization of surface finish in end milling Inconel 718", J. Mat. Proc. Vol . 56 ,1996,54–65.

[5] M.A. EI-Baradie, "Surface roughness model for turning grey cast iron 1154 BHN)", Proc. IMechE, 207 11993) 43-54.

[6] B.P. Bandyopadhyay and E.H. Teo, "Application of lactorial design of experiment in high speed turning", Proc. Mam~ll htt. Part 4, Adrances in Materials & Automation, Atlanta. GA, USA, ASME, NY, 1990, 3-8.

[7] O.A. Gorlenko, "Assessment of starface roughness parameters and their interdependence", Precis. Eng., 3 (1981)2.

[8] T.R. Thomas, "Characterisation of surface roughness", Precis. Eng., Vol. 3, 1981, 2-?.

[9] Mital, M. Mehta, "Surface roughness prediction models for fine turning", International Journal of Production Research, Vol. 26, 1988, 1861–1876.

[10] Y. Koren, et al,"Tool wear and breakage detection using a process model" Ann. CIRP, Vol. 35, 1986, 283–288.

[11] Y. S Tarng, B. Y,Lee,"A Sensor for the Detection of Tool Breakage in NC Milling", Journal of Materials Processing Technology, Vol. 36, 1995, 259-272.

[12] T. J .Ko, D. W Cho, M. Y. Jung,"On-line Monitoring of Tool Breakage in Face Milling: Using a Self-Organized Neural Network", Journal of Manufacturing systems, Vol. 14, 1998, 80-90.

[13] J.H. Lee, S.J. Lee,"One step ahead prediction of flank wear using cutting force", Int. J. Mach. Tools Manufact, Vol. 39, 1999, 1747–1760.

[14] S.K. Chaudhury, V.K. Jain, C.V.V. Rama Rao,"On-line monitoring of tool wear in turning using a neural network"; Int. J. Mach. Tools Manufact, Vol. 39, 1999, 489–504.

[15] D.E. Dimla, P.M. Lister,"On-line metal cutting tool condition monitoring. II: tool state classification using multi-layer perception neural network", Int. J. Mach. Tools Manufact, Vol. 40 ,2000, 769–781.

[16] N.R. Draper, H. Smith, "Applied Regression Analysis", Wiley, New York, 1981.

[17] G.E.P. Box and N.R. Draper. "Empirical model-building and response surfaces", New York, John Wiley & Sons, 1987.

[18] Box, G.E.P. & Behnken, D.W. 1960. "Some new three level designs for the study of quantitative variables". Technometrics Vol. 2,1960, 455-475.

[19] C.C. Tsao, H. Hocheng, "Evaluation of thrust force and surface roughness in drilling composite material using Taguchi analysis and neural network", Vol. 203, 2008, 342-348.

JJMIE

Volume 2, Number 4, December. 2008
ISSN 1995-6665
Pages 215 -226

Jordan Journal of Mechanical and Industrial Engineering

Quota Allocation to Distributors of the Supply Chain under Distributors' Uncertainty and Demand Uncertainty by Using Fuzzy Goal Programming

B.Chandra Mohana Reddy[a *], K. Hemachandra Reddy[b], C. Nadha Muni Reddy[c]
K.Vijaya Kumar Reddy[d]

[a,b] Mechanical Engineering Department., J.N.T.U . College of Engineering , Anantapur – 515002, AP. India

[c]S.V.P.C.E.T, Puttur, Chittur (dist), A.P. , India

[d] Mechanical Engineering Department, J.N.T. University., Hyderabad, A.P., India

Abstract

The supply chain consists of multiple components including suppliers, manufacturing centers, and distributors. The decision-making on quota allocation to distributors under Distributors' uncertainty and demand uncertainty are important parts of supply chain of many firms. In this paper, fuzzy goal programming approach is applied for quota allocation to distributors of the supply chain. Customers are assumed as a random variable, and distribution is continuous and normal. Due to surge effect, the demand through supply chain is varied, which is calculated for a particular inventory policy for reserve stock, and sudden rise and fall of demand to the Std limits of normal distribution. The maximum and minimum values of demand at the distributors' stage are considered for various Std limits. And they formulate a fuzzy goal programming by considering linear member ship function. Commercially available LINDO software is used to solve the fuzzy goal-programming problem for quota allocation to the distributors. From the results, it is found that maximized sales revenue, minimized transportation cost, minimized late deliveries, and minimized defective items are increased from maximum STD limit to the minimum STD limit. Change in minimized late deliveries and minimized defective items are negligible to consider. Moreover, difference of maximized sales revenue and minimized transportation cost is significant to consider, and it is increased from maximum STD limit to the minimum Std limit of demand. This means maximum difference can be obtained at low fluctuation of the demand than the high fluctuation of the demand. The formulated Fuzzy Goal Program can be used to solve actual problems.

Keywords: Normal continuous distribution, Linear membership function, Fuzzy goal programming, and Decision-making.

1. Introduction

Supply chain is a set of facilities, supplies, customers, products; and methods of controlling inventory, purchasing, and distribution. In a supply chain, flow of goods between a supplier and a customer passes through several echelons, and each echelon may consist of many facilities.

This paper focuses mainly on distribution performance and quota allocation to distributors and its selection under distributors' uncertainty and demand uncertainty. In designing a supply chain, a decision maker must consider decisions regarding the selection of the right distributors and their quota allocation. The choice of the right distributor is a crucial decision with extensive implications. By nature, distributor selection is a multi-criterion decision-making problem. A supply chain decision faces many constraints. Some of these are related to distributors' internal policy and externally imposed system requirements. In such decision making situations, high degree of fuzziness and uncertainties are involved. Fuzzy set theory provides a framework for handling the uncertainties of this type [6].

In this paper, a fuzzy goal programming approach is used to solve the multi-objective-optimization problems for quota allocation to the distributors in supply chain. Since crisp set assign a value of either 1 or 0. Whereas in fuzzy set is not assigned such a value. But the value of any set lies between 1 and 0. A function can be generalized such that the value assigned to the element of the universe set fall within specified range and indicated member ship grade of this element in the set. Such a function is called a

* Corresponding author. e-mail: cmr_b@yahoo.com.

fuzzy membership function, and set defined by it is called a fuzzy set [9].

Membership functions which can be used in fuzzy goal programming problem are linear membership functions or no linear member ship functions. Fuzzy mathematical programming which is defined by a non-linear membership function results in a non-linear programming. Usually a linear membership function is employed for linear programming in order to avoid non-linearity [7]. Therefore, in this paper, a linear membership function is employed for both objectives and constraints, which is having fuzziness.

The central four fuzzy goals considered in this paper are maximization of sales revenue, minimization of transportation cost, minimization of defective items rejected and minimization of late deliveries with constrain such as minimum and maximum capacity of distributors, maximum budget allocated to distributors, and maximum flexibility of distributors and maximum sales value of distributors. First, the problem is formulated as multi-objective linear programming, and then it is reformulated as fuggy goal programming by using variable λ. Commercial available LINDO software is used to solve the fuzzy goal-programming problem for quota allocation to distributors.

2. Review of Literature:

Complex and dynamic interactions between supply chain entities lead to considerable uncertainty in planning. Uncertainty tends to propagate the supply chain up and down. And it undergoes with surge or bullwhip effect [1]. Many proposed strategies for mitigating the bullwhip effect have a history of successful application [2]. This effect leads to inefficiencies in supply chains since it increases the cost for logistics, and it lowers its competitive ability. Particularly, the bullwhip effects negatively influence a supply chain in dimensioning of capacities, variation of demand, and high level of safety stock. Julija Petuhova and Yuri Merkuryev [8] carried out simulations to measure distributor's performance before and after applying the supply-side collaboration. Their results show that the supply-side collaboration can improve distributor's performance in terms of more accurate service level realization and better stabilizing effect.

Manoj Kumar , Prem Vrat and R.Shankar proposed a fuzzy multi-objective goal programming by using triangular membership function for allocating quantity to vendors; and solved this by LINDO software. The proposed approach has the capability to handle realistic situations in a fuzzy environment and provides a better decision tool for the vendor selection decision in a supply chain. Hasan Selim, Ceyhun Araz and Irem Ozkarahan[4] had developed a multi-objective production-distribution planning model in the fuzzy environment for to improve the supply chain performance. Pandian Vasant[7] attempted to model decision processes with multiple criteria in business and engineering leads to concepts of multi objective fuzzy linear programming. Hasan Selim and Irem Ozkarahan have developed a supply chain distribution network design model. The goal of the model is to select optimum numbers, locations, and capacity levels of plants and warehouses to deliver products to retailers at the least cost while satisfying desired service level. Maximal covering approach is employed in statement of service level [10].

3. Why is Simulation and Fuzzy Set Theory Used in Supply Chain?

Due to the Bullwhip effect, a poor plan can easily spread to the whole supply chain areas. The impact of a poor plan on the overall business is huge. It causes cycles of excessive inventory and severe backlogs, poor product forecasts, unbalanced capacities, poor customer service, uncertain production plans, and high backlog costs, or sometimes even lost sales. Simulation and fuzzy set theory permit the evaluation of operating performance prior to the implementation of a system and also these enable companies to perform powerfully if analyses lead them to better planning decisions.

4. A Mathematical Model to Calculate Output Required at Each Stage in The Supply Chain for Uncertainty Demand.

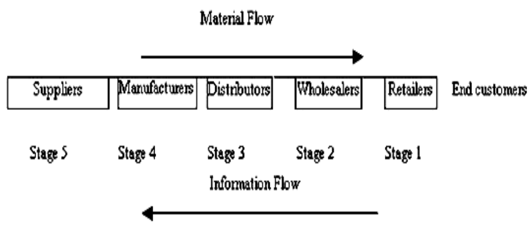

Figure 1: Five stages of simple supply chain

A mathematical model is shown below to calculate output required and safety stock required at each stage of the supply chain. For these typical five stages, simple supply chain is shown in Figure 1. The five stages are suppliers, manufacturers, distributors, wholesalers, and retailers. If the demand by End-customers is D, and the policy for reserve stock specifies that a portion (r) should be held constant, then (rD) is the safety stock for finished products at the retailer's stores. If there is a sudden rise or a sudden fall of demand at end-customers, then D (1+x) quantities of products are needed at the retailers, and also the safety stock required now should be rD (1+x). Here (x) is in terms of percentage of sudden rise or sudden fall of the demand [3]. The (x) in terms of percentage for 3Std limit of normal distribution is shown below

a.For sudden rise of the demand :

$$x = \frac{(D + 3\,Std) - D}{D} X\ 100$$

b.For a sudden fall of the demand

$$x = \frac{(D - 3\,Std) - D}{D} X\,100$$

Similarly x in terms of percentage can be shown for all other Std limits of normal distribution. Then the output required and safety stock required at each stage will be calculated by using the following equations.

Stage 1: Retailer

- Output required = D (1+x)
- Safety stock required = rD (1+x)

Stage 2: Wholesalers

- Output required = D (1+x) for the final stage + (rD (1+x) – rD) for the Safety stock at the final stage = D (1+x (1+r))
- Safety stock required = rD (1+x (1+r))

Stage 3: Distributors

- Output required = D (1+x (1+r)) for the 2 stage + (rD (1+x (1+r)) – rD) for the safety stock at the 2 stage= D (1+x (1+r) 2)
- Safety stock required = rD (1+x (1+r) 2)

Stage 4: Factories

- Output required = $D(1+x(1+r)^2)$for the 3 stage + $(rD(1+x(1+r)^2)$– rD) for the safety stock at the 3 stage= $D (1+x (1+r)^3)$
- Safety stock required = $rD (1+x (1+r)^3)$

Stage 5: Suppliers

- Output required = $D(1+x(1+r)^3)$for the 4 stage + $(rD(1+x(1+r)^3)$– rD) for the safety stock at the 4 stage= $D (1+x (1+r)^4)$
- Safety stock required = $rD (1+x (1+r)^4)$

And so on. It can be shown that the output required at the n^{th} stage is D_n then [3] $D_n/D = 1+x(1+r)^{n-1}$

5. Multi-Objective Distributor Model Under Distributors' Uncertainty and Demand Uncertainty

Four distributors and four main objectives are considered such as: maximizing sales revenue (Z_1), minimizing transportation cost (Z_2), minimizing defective items rejected (Z_3), and minimizing late deliveries (Z_4). Besides, the constraints considered for formulation of the problem are minimum and maximum selling capacity of the distributors, maximum budget allocation to distributors, flexibility of distributors, and sales value of distributors. By considering above information, the problem is formulated as multi objective linear program as shown below [5].

5.1. Decision Variable

x_i order quantity from the distributors I, where i=1,2…..N

5.2. Parameters

D Max. = Upper bound of aggregate demand of the item over a fixed planning period
D Min. = Lower bound of aggregate demand of the item over a fixed planning period
N = Number of distributors competing for selection
p_i = Price of a unit item at distributors i
t_i = Transportation cost of a unit item of the ordered quantity x_i for the distributors i
ld_i = Percentage of the late delivered units by the manufacturers to distributors i
C_i Max. = Upper bound of the quantity can be taken by distributors I
C_i Min. = lower bound of the quantity can be taken by distributors i
B_i = Budget allocated to each distributors
d_i = Percentage of rejected units delivered by distributors i
F_i = Supplier quota flexibility for distributors i
F Max = Upper bound of total flexibility in quota that a distributors should have
F Min = Lower bound of total flexibility in quota that a distributors should have
R_i = distributors rating value for distributors i
PV Max.= Upper bound to total purchasing value that a distributors should have
PV Min.= Lower bound to total purchasing value that a distributors should have:

Min. $Z = (Z_1, Z_2, Z_3, Z_4)$
Subjected to
$\sum x_i \le D$, D is varying form D min. to D max.
$x_i \le C_i$, C_i is varying form C_i min. to C_i max
$x_i \le B_i$

$\sum F_i x_i \ge F$, F is varying form F min. to F max
$\sum R_i x_i \ge P$, P is varying form P min. to P max
$x_i \ge 0$ and $Z_1 = \sum p_i x_i$, $Z_2 = \sum t_i x_i$, Z_3 $\sum d_i x_i$, $Z_4 = \sum ld_i x_i$

6. Fuzzy Multi-Objective Model

Consider the fowling linear multi-objective model,

Opt Z = CX
s.t. AX ≤ b

Where $Z = (z_1,z_2,\ldots\ldots\ldots z_k)$ is the vector of objectives, C is a K*N of constants, X is a an N*1 vector of the decision variables, A is an M*N matrix of constants and b is an M*1 vector of constants. This model can be applied to solve many real problems [4].To solve above problem a linear membership function can be used for each goal $\mu_{1k}(C_kX)$, where

$$\mu_{1k}(C_kX) = \begin{cases} 1 & \text{if } CkX >= Z_k \\ 1 - \dfrac{(Z_k - C_kX)}{dlk} & \text{if } Z_k - d_{1k} <= CkX <= Z_k \\ 0 & \text{if } CkX <= Z_k - d_{1k} \end{cases}$$

And another linear membership function is $\mu_{2i}(a_iX)$, for the i^{th} constraint in the system constraints AX ≤ b, where

$$\mu_{2i}(a_iX)) = \begin{cases} 1 & \text{if } a_iX <= b_k \\ 1 - \dfrac{(a_iX - b_k)}{d_{2i}} & \text{if } b_k <= a_iX <= b_i + d_{2i} \\ 0 & \text{if } a_iX >= b_i + d_{2i} \end{cases}$$

Figure 2: Membership function for maximization of fuzzy goal

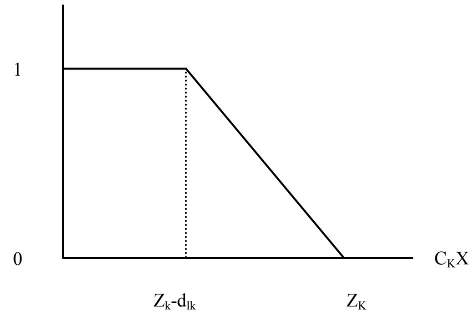

Figure 3: Membership function for minimization of fuzzy goal

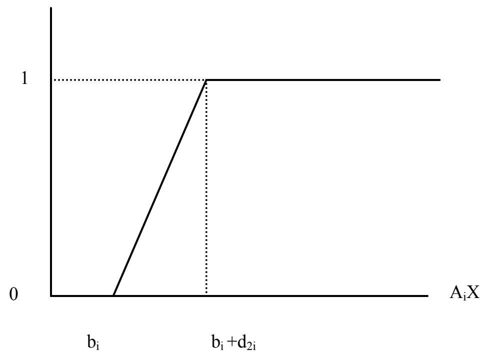

Figure 4: Membership function of fuzzy constraints

These membership functions are illustrated in Figure 2, Figure 3, and Figure 4 respectively. Where d_{1k} (k=1,2,….K) and d_{2i} (i=1,2,….M) are chosen constants of admissible violations, and a_i is the i^{th} row of matrix A. $\mu_{1k}(C_kX)$ and $\mu_{2i}(a_iX)$ denote to the degree of membership of goals and constraints respectively. Degree of membership of goals and constraints express satisfaction of the decision maker with the solution. So, values of membership functions must be maximized [4].

In one of the fuzzy set theorems, membership function of intersection of any two (or more) sets is the minimum membership function of these sets. After eliciting linear membership functions and by applying this theorem, objective function of multi-objective linear programming model incorporating the fuzzy goals and fuzzy constraints can be formulated as follows [4].

$\text{Max}_x \min(\mu_{11}(C_1X), \ldots, \mu_{1k}(C_kX), \mu_{21}(a_1X), \ldots, \mu_{2i}(a_iX))$

By introducing the auxiliary variable λ, this problem can be equivalently transformed as.

$\max \ \lambda$

$\mu_{1k}(C_kX) \geq \lambda$ k=1,2,….K

$\mu_{2i}(a_iX) \geq \lambda$ i=1,2,….M

According to above descriptions fuzzy linear program can be rewritten as following:

$\text{Max} \ \lambda$

$$\lambda \leq \frac{1-(Z_k - C_kX)}{d_{1k}} \quad k=1,2,\ldots K$$

$$\lambda \leq \frac{1-(a_iX - b_i)}{d_{2k}} \quad i=1,2,\ldots M$$

$0 \leq \lambda \leq 1$ and $X \geq 0$

7. Fuzzy Goal Programming

Fuzzy Goal programming is one of the most powerful multi-objective decision making approach. If there are no priorities and also no relative importance assigned to objectives, formulation of fuzzy goal-programming model is similar to formulation in general fuzzy linear programming model. The main difference between Fuzzy goal programming and fuzzy linear programming is that fuzzy linear programming uses definite intervals determined by solution of linear programming models. And accordingly, the solution does not change from decision maker to another decision maker. Whereas in fuzzy goal programming, aspiration levels are specified by decision maker and reflect relative flexibility [4].

8. Methodology

The following methodology is used in three steps for quota allocation to distributors of the supply chain under Distributors' uncertainty and demand uncertainty by using fuzzy goal programming. In the first step, demand at end customer is assumed as random variable and distributed as continuous normal distributed pattern. The Monte Carlo simulation method and Excel are used to simulate the demand for various random numbers. The 20 random numbers are generated by using Excel with command Rand ().The mean demand and standard deviation are calculated for demands of 20 random numbers.

In the second step, output required or demand for five stages of simple supply chain is simulated for various Std limits of normal distribution. Output required from down stream to up stream (stage-1 to stage-5) is increased for sudden raise of the demand and decreased for sudden fall of the demand at particular inventory policy for reserve stock r. Therefore, this variability of demand from stage -1 to stage-5 is called as surge effect. So that surge effect is simulated here for five stages supply chain.

In the third step, an illustration for quota allocation to distributors under distributors' uncertainty is taken, and maximum and minimum outputs required for all STD limits at the stage of distributor are taken for demand uncertainty at distributors. For this, first multi objective linear programming problem is formulated; and is solved for individual objectives. With these results of individual objectives, fuzzy aspiration levels are fixed. And finally fuzzy goal programming problem is formulated and solved by using commercial available software LINDO.

9. Simulation of Demand Uncertainty at End Customer

The demand at end customer is assumed as random variable and distributed as continuous normal distributed pattern. In simulation process, mean of demand is assumed as (500) units and standard deviation Std is assumed as (25) units. The demand is calculated for the normal distribution limits such as ±3Std, ±2Std, ± 1Std and ±0.67Std and cumulative probabilities are taken from normal distribution tables to the Z values such as –3, -2, -1, 0, 1, 2 and 3 [3]. A graph has been plotted is shown in Figure 5 for calculated values of demand and cumulative values of probability distribution.

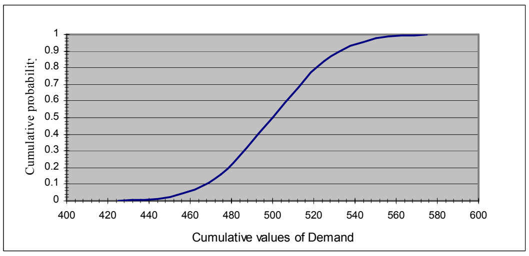

Figure 5: calculated values of demand and cumulative values of probability distribution.

The Monte Carlo simulation method Microsoft Excel is used to simulate the demand for various random numbers. The 20 random numbers are generated by the command Rand () and 20 numbers are considered as the probability of occurrence of the demand for 20 months. The value of demands for 20 months are taken from graph (From Figure 5) for corresponding random numbers and tabulated in Table 1. The mean and standard deviation are calculated for demands of 20 numbers.

10. Simulation of Surge Effect in Supply Chain

Surge effect in five stages supply chain is simulated for minimum and maximum fluctuation of the demand at end costumer. Five stages supply chain is shown in Figure1.

Here the demand is considered as two different cases for the limits of 0.67Std, 1Std, 2Std, 3Std of the normal distribution curve. In the first case, sudden rise of demand is considered from mean to upper limit of the demand. In the second case, sudden fall of demand is considered from mean to lower limit of demand. The (x) in terms of percentage for both the cases is calculated using the formulas, shown in the section-5.

Table 1: The value of demands for 20 months

Months	Random numbers	Simulated demand (X)	D - X	$(D-X)^2$
1	0.30236	485	16.2	262.44
2	0.99278	572	-70.8	5012.64
3	0.047325	455	46.2	2134.44
4	0.662034	510	-8.8	77.44
5	0.293601	480	21.2	449.44
6	0.901139	530	-28.8	829.44
7	0.125719	468	33.2	1102.24
8	0.749202	515	-13.8	190.44
9	0.694485	510	-8.8	77.44
10	0.184959	472	29.2	852.64
11	0.901331	530	-28.8	829.44
12	0.367548	490	11.2	125.44
13	0.459338	492	9.2	84.64
14	0.696288	512	-10.8	116.64
15	0.406118	490	11.2	125.44
16	0.619101	508	-6.8	46.24
17	0.566073	504	-2.8	7.84
18	0.188001	477	24.2	585.64
19	0.323692	490	11.2	125.44
20	0.263223	482	19.2	368.64
		9972	52	13404

*Mean (D)=498.6 Mean (D) = $\dfrac{\sum_{i}^{n} \text{Xi}}{n} = 498.6$

*Standard deviation (Std) = $\sqrt{\dfrac{\Sigma (D-X)^2}{n}} = 25.88822$

By using this (x) in terms of percentage and inventory policy for reserve stock (r) in terms of percentage, quantity required at various stages through supply chain from downstream to upstream is calculated by using equation presented in section-5. The results are tabulated in table-2 and a graph is drawn and shown in Figure 6 for policy decision r = 20% and x for sudden rise and for sudden fall of demand.

Table 2 : Quantity required at various stages in supply chain for sudden rise and sudden fall of demand and Inventory policy for reserve stock r =20%

	Upper standard limits			
	0.67std	1std	2std	3std
	X% of sudden rising			
	0.034788	0.051922	0.103844	0.155765
Retailers	515.9453	524.4883	550.3766	576.2644
Whole -salers	519.4144	529.666	560.7319	591.7973
Distributors	523.5772	535.8792	573.1583	610.4368
Factories	528.5727	543.335	588.07	632.8041
Suppliers	534.5672	552.282	605.964	659.645
	Lower standard limits			
	.0.67std	1std	2std	3std
	X% of sudden falling			
	0.034788	0.051922	0.103844	0.155765
Retailers	481.2547	472.7117	446.8234	420.9356
Whole -salers	477.7856	467.534	436.4681	405.4027
Distributors	473.6228	461.3208	424.0417	386.7632
Factories	468.6273	453.865	409.13	364.3959
Suppliers	462.6328	444.918	391.236	337.555

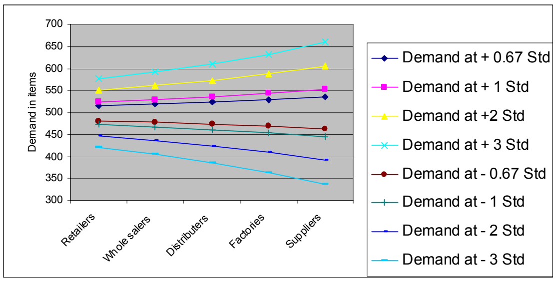

Figure 6: for policy decision r=20% and x for sudden rise and for sudden fall of demand.

11. Quota Allocation to Distributors Under Distributors' Uncertainty and Demand Uncertainty by Using Fuzzy Goal Programming Approach

11.1. Distributors' Uncertainty

Distributors' uncertainty is such that distributors con not take fixed quantity from manufacturers. Quantity taken by uncertain distributors is varying from time to time. Generally this type of distributors can give good performance in certain range of quantity taken from the manufacturers i.e. between minimum quantities which the distributors can receive to maximum quantity distributors can be received from manufactures or factories. When distributors get below minimum quantity, they cannot give good performance due to loss of their business. Besides, distributors cannot get beyond maximum quantity due to their maximum constraint.

11.2. Demand Uncertainty

Similarly, demand of any item at end customers is dynamics; and is not fixed to a certain value. This also varies from time to time. Demand is assumed as continuous random variable and distribution as continuous normal distribution at end customers. Plus and minus Std limits of normal distribution are considered for variable demand. By using this end customers demand, demand at the distributors stage is calculated for each Std limit. This calculated demand at distributors' stage is used in the multi objective linear program. The overall flexibility and overall purchase value rating variability are also considered for distributors of the supply chain.

Similarly, demand of any item at end customers is dynamics; and is not fixed to a certain value. This also varies from time to time. Demand is assumed as continuous random variable and distribution as continuous normal distribution at end customers. Plus and minus Std limits of normal distribution are considered for variable demand. By using this end customers demand, demand at the distributors stage is calculated for each Std limit. This calculated demand at distributors' stage is used in the multi objective linear program. The overall flexibility and overall purchase value rating variability are also considered for distributors of the supply chain.

11.3. Variability of The Demand

The variability of demands (i.e. $D_{min.}$ and $D_{max.}$) at stage of distributor in supply chain for all Std limits are taken form Table 2 and tabulate separately in the following Table 3.

Table 3 Variability of Demand for r=20%and Various Std Limits at Stage of Distributes in Supply Chain

STD limits of Normal distribution	Variability of demand at the stage of distributors ($D_{min.}$ - D_{max})
0.67 Std	474 - 524
1 Std	461 – 536
2 Std	424 – 573
3 Std	387 – 610

Table 4: Distributors Source Data of The Illustrative Example

Distributors No.	s_i Rs.	t_i Rs	d_i (%)	ld_i (%)	C_i Min. Units
1	100	15	3	2	50
2	300	10	4	3	15
3	250	5	2	9	25
4	350	20	7	5	30
Distributors No.	C_i Max. Units	B_i Rs	Fi (%)	R_i (%)	Distributors No.
1	200	20000	99.6	86	1
2	235	70500	99.9	92	2
3	225	56250	9.98	98	3
4	220	77000	9.97	88	4

11.4. An Illustration of Quota Allocation to Distributors

Distributors' source data of the illustrated example is prepared based on available data, where data is presented for the supplier selection problem [6]. Distributors source data of the illustrated example shown in Table 4[6] represents the data source for the sale price quoted (s_i in rupees per unit); transportation cost (t_i in rupees per unit); the percentage defective items rejections d_i; the percentage of late deliveries to distributors ldi; minimum distributors capacity limitations $C_{i;}$ min. units, maximum distributors capacity limitations $Ci_{;}$ max. units; the budget allocations for distributors B_i; distributors' quota flexibility F_i and distributors sales value rating R_i on a scale of 0–1. The least value of flexibility in distributors' quota and least total purchase value of distributors' items are policy decisions; and depend on the demand. The least and maximum value of flexibility in distributors' quota is given as $F = F_oD$, and the least and maximum total purchase value of distributed items is given as PV =RD: If overall least flexibility (F_o) is 0.05 and maximum flexibility (F_o) is 0.95 on the scale of 0–1, the overall least distributors' rating (R) is 0.10 and maximum rating (R) 0.90 on the scale of 0–1, and the mean demand (D) of normal distribution is 500. Then the least and maximum value of flexibility in distributors' quota (F) and the least and maximum total purchase value of distributed items (PV) are 25, 475, 50 and 450, respectively. By using variability demand from Table 4 and distributors' source data from Table 5, a multi-objective linear programming problem for quota allocation to distributors can be formulated as:

Maximize $Z_1 =100x_1 + 300x_2 + 250x_3 + 350x_4$
Minimize $Z_2 = 15x_1 + 10x_2 + 5x_3 + 1x_4$
Minimize $Z_3 = 0.03x_1 + 0.04 x_2 + 0.02 x_3 + 0.07 x_4$
Minimize $Z_4 = 0.02x_1 + 0.03x_2 + 0.09x_3 + 0.05x_4$
Subjected to
$474 \geq x_1 + x_2 + x_3 + x_4 \leq 524$ (0.67 Std)
$50 \geq x_1 \leq 200$, $15 \geq x_2 \leq 235$, $25 \geq x_3 \leq 225$, $30 \geq x_4 \leq 220$
$100x_1 \leq 20000$, $300x_2 \leq 70500$, $250x_3 \leq 56250$,
$350x_4 \leq 77000$
$25 \leq 0.996x_1 + 0.999 x_2 + 0.998 x_3 + 0.997 x_4 \geq 475$
$50 \leq 0.86x_1 + 0.92 x_2 + 0.98 x_3 + 0.88 x_4 \geq 450$
$x_1, x_2 ,x_3,x_4 \geq 0$

11.5. Aspiration Levels or Fuzzy Range:

In the Table 5, LPP Results of the individual objectives for minimum and maximum bound of constraints are shown for 0.67 Std limit.

Table 5: LPP Results of the Individual Objectives for Minimum and Maximum Bound of Constraints at 0.67 Std Limit

S. No	Objectives	Min. bound	Max bound	Difference	Max bound Moved to	Fuzzy range
1	Max. Sales revenue	26250.00	164750.0	138500	303250	277000
2	Min. transportation cost	150.4082	1735.217	1584.8088	3320.0258	3169.6176
3	Min. Defective items rejected	1.3895	13	12.389535	25.3895	24.3895
4	Min. Late deliveries	1.2283	14.5614	13.3331	27.8946	26.6662

In case of goal programming selection of aspiration levels or fuzzy range is most important. From Table 5 for maximization of sales revenue, the difference between 26250.00 and 164750.0 is 138500. Then the maximum bound is moved to the 164750.0 + 138500 = 3032350. Therefore, now the fuzzy range is 2 X 1385000 = 277000 to maximize the sales revenue. Similarly, fuzzy range for other objectives can be calculated.

11.6. Linear Membership Functions

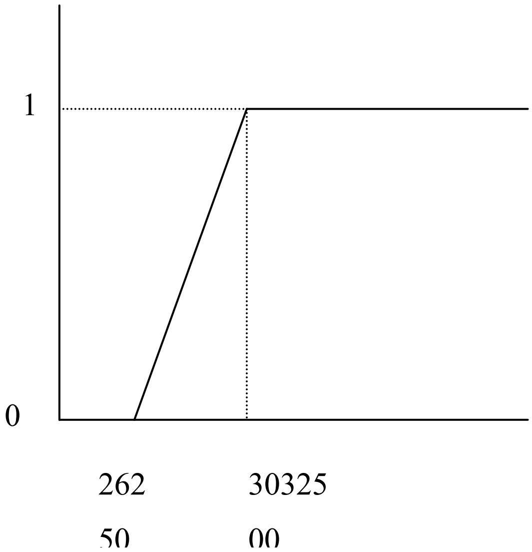

Figure 7: Linear membership function for sales revenue at 0.67 Std (Maximization)

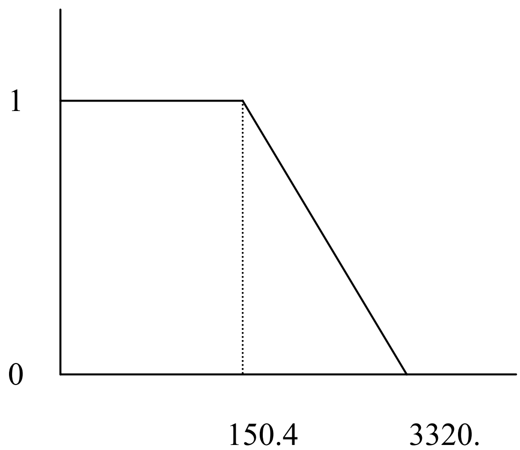

Figure 8: Linear membership function for transportation cost at 0.67 Std (Minimization)

Figure9: Linear membership function for demand variation at 0.67 Std

The Linear membership functions for other objectives like minimization of defective items rejected and minimization of late deliveries are same as Figure 8. Similarly the linear membership functions for other constraints like capacity limitation of distributors, flexibility of distributors and sales value of distributors are same as Figure 9.

11.7. Fuzzy Goal Programming

By using data from Table 6 and linear membership functions and introducing the auxiliary variable λ, the fuzzy goal programming problem can be written as follows for 0.67 Std limit.

Max λ

Subjected to

$$\lambda \le \frac{Z_1 - 2625}{277000}, \lambda \le \frac{3320.0258 - Z_2}{3169.6176}$$

$$\lambda \le \frac{25.3895 - Z_3}{24.3895}, \lambda \le \frac{27.8946 - Z_4}{26.6662}$$

$$\lambda \le \frac{x_1 + x_2 + x_3 + x_4 - 474}{50}, \lambda \le \frac{x_1 - 50}{150}$$

$$\lambda \le \frac{x_2 - 15}{220}, \lambda \le \frac{x_3 - 25}{200} \quad \lambda \le \frac{x_4 - 30}{190}$$

$$100x_1 \le 20000, 300x_2 \le 70500$$

$$250x_3 \le 56250, \ 350x_4 \le 77000$$

$$\lambda \le \frac{0.996x_1 + 0.999x_2 + 0.998x_3 + 0.997x_4 - 25}{450}$$

$$\lambda \le \frac{0.86x_1 + 0.92x_2 + 0.98x_3 + 0.88x_4 - 50}{400}$$

$x_1, x_2, x_3, x_4 \ge 0, \ 0 \le \lambda \le 1$

11.8. Results and Discussions:

Table 6: Allocation of items for four distributors by Fuzzy goal programming

Standard limits	x_1 in No. of items	x_2 in No. of items	x_3 in No. of items	x_4 in No. of items	λ	Total of x_1, x_2,x_3 & x_4 in No. of items	Variability of demand in No. of items
Mean 500 demand	74	109	141	176	0.16	500	No variability exactly =500
o.67 Std	70	109	119	183	0.126	481	474 - 524
1 Std	72	104	116	180	0.145	472	461 – 536
2 Std	78	86	111	177	0.182	452	424 – 573
3 Std	83	70	108	174	0.214	435	387 – 610

Table 7: Optimized values of the four objectives at various std Limits

Standard limits	Max. Sales revenue in Rs. (1)	Min. transportation cost in Rs. (2)	Total cost = diff. of (1) & (2)	Min. defective items rejected in No.s	Min. Late deliveries in No. s
Mean 500 demand	136950	3081	133869	22	27
0.67 Std	133500	2918	130582	22	25
1 Std	130400	2880	127520	22	24
2 Std	123300	2557	120743	21	23
3 Std	117200	2662	114538	20	23

Formulated above goal program is solved for various Std limits of normally distributed demand. The corresponding results are in Table 6 and Table 7. In Table 6, quantity allocated to four distributors and sum of allocated quantity of distributors are present. In Table 6, the total quantity is maintained within the range of variable demand of standard limits. In the Table 7, optimized values of all four objectives are present.

Optimized values of four objectives are decreased for varying from 0.67Std limit to 3Std limit. The effect of minimized defective items rejected and minimization of late deliveries are nominal. But effect of maximization sales revenue and minimization of transportation cost are significant. Both are decreased for varying from 0.67Std limit to 3Std limit. Therefore, the difference is more at minimum fluctuation of demand than maximum fluctuation of demand. Figure 10 shows the variation of maximized revenue, minimized transportation cost and difference of two for varying from 0.67Std limit to 3Std limit. Finally, this can be said that loss of business for any supply chain is more at maximum fluctuation of demand than minimum fluctuation of demand.

12. Conclusions:

- The surge effect in supply chain is simulated for uncertainty demand. The demand of the end customer is assumed as random demand of continuous normal distribution.
- From the simulation results, it is found that the quantity required at the stages through the supply chain from down stream to upstream is increased for sudden rise of demand of the end customers, and is decreased for the sudden fall of demand of the end customers.
- Fuzzy goal programming problem is successfully formulated for multi objectives of distributors and for demand varying from maximum limit to the minimum limit at the stage of the distributors.

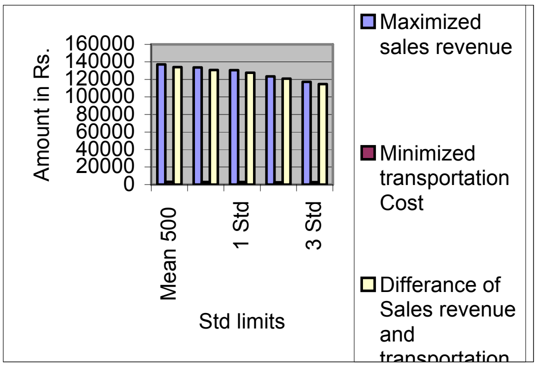

Figure 10: Sales revenue, Transportation cost and difference of two

- Neglecting the effect of optimized results of defective items rejected and late deliveries, the difference of maximization of sales revenue and minimization of transportation cost is more at minimum fluctuation of demand than the maximum fluctuation of demand.

- The total allocated items are also maintained within the range of the variable demand at the stage of distributors. At minimum fluctuation of demand, the items allocated to distributors are more, so that it has been given high difference.

References:

[1] Rohit Bhatnagar, Amrik S. Sohal, "Supply chain competitiveness: measuring the impact of location factors, uncertainty and manufacturing practices", Technovation, Elsevier (Available online www.elsevier.com/locate/technovation) 2003.

[2] Warburton Roger D. H., "An analytical investigation of the Bullwhip Effect", Production and Operations Management, 13(2),150–160, 2004.

[3] Samuel & Ellon, "Elements of production planning and control", second revised edition, Navaneethan prakashan Ltd, Bombay, 1994.

[4] Hasan Selim, Ceyhun Araz and Irem Ozkarahan"An integrated Multi_objective supply chain model in a Fuzzy environment" (www.mmo.org.tr), Endustri Muhendisiligi devgisi, Cillt:15,sayfa. pp 2-16, 2004.

[5] R.P.Mohanthy & S.G.Deshmukh, "Supply Chain Management – Theories & Practices" ,Indian text edition, Biztantra Information in management – an Imprint of Dreamtech press, Edition-2005.

[5] Manoj Kumar , Prem Vrat & R.Shankar, "A Fuzzy Goal Programming Approach For Vendor Selection Problem In A Supply Chain" , Computers & Industrial engineering, Published by Elsevier Ltd. (www.sciencedirect.com), September 2003.

[6] Pandian Vasant, "“Application Of Multi Objective Fuzzy Linear Programming In Supply Production Planning Problem", Senior Mathematics Lecturer, Department of Mathematics, American Degree Program, Nilai International College, 71800 Nilai, Malaysia, (Available at www.generation5.org), 2004.

[7] Julija Petuhova And Yuri Merkuryev, "Combining Analytical and Simulation Approaches to Quantification of the Bullwhip Effect", International Journal of Simulation Vol. 8 No 1, 16 – 24, 2006.

[8] George J. Klir and Bo. Yuan, "Fuzzy Sets and Fuzzy logic, Theory and Applications", Indian Reprint, Prentice Hall of India Pvt. Ltd., New Delhi –2005.

[9] Hasan Selim and Irem Ozkarahan, "Application of Fuzzy Multi-objective Programming Approach to Supply Chain Distribution Network Design Problem" Springer Berlin / Heidelberg, Vol. 4293,415-425, 2006.

المملكة الأردنية الهاشمية

الجامعة الهاشمية

المجلة الأردنية
للهندسة الميكانيكية والصناعية

JJMIE

مجلة علمية عالمية محكمة

http://jjmie.hu.edu.jo/

ISSN 1995-6665

المجلة الأردنية للهندسة الميكانيكية والصناعية
مجلة علمية عالمية محكمة

المجلة الأردنية للهندسة الميكانيكية والصناعية: مجلة علمية عالمية محكمة أسستها اللجنة العليا للبحث العلمي، وزارة التعليم العالي والبحث العلمي، الأردن، وتصدر عن عمادة البحث العلمي والدراسات العليا، الجامعة الهاشمية، الزرقاء، الأردن.

ترسل البحوث إلى العنوان التالي :

رئيس تحرير المجلة الأردنية للهندسة الميكانيكية والصناعية
عمادة البحث العلمي والدراسات العليا
الجامعة الهاشمية
الزرقاء - الأردن
هاتف : 3903333 5 00962 فرعي 4147
Email: jjmie@hu.edu.jo
Website: www.jjmie.hu.edu.jo